TISSUE-ENGINEERED SKIN GRAFTS PREVASCULARIZED WITH ADIPOSE-DERIVED CELLS

DISSERTATION

ZUR

ERLANGUNG DER NATURWISSENSCHAFTLICHEN DOKTORWÜRDE
(DR. SC. NAT.)

VORGELEGT DER

MATHEMATISCH-NATURWISSENSCHAFTLICHEN FAKULTÄT

DER

UNIVERSITÄT ZÜRICH

VON

AGNIESZKA KLAR

AUS

POLEN

PROMOTIONSKOMITEE

PROF. DR. BEAT SCHAEFER (VORSITZ)

PROF. DR. LUKAS SOMMER

PROF. DR. IVAN MARTIN

PROF. DR. ERNST REICHMANN (LEITUNG DER DISSERTATION)

ZÜRICH, 2014

This work has been performed under the supervision of Prof. Dr. Ernst Reichmann at the Tissue Biology Research Unit, Department of Surgery, University Children's Hospital Zurich, Zurich, Switzerland.

TABLE OF CONTENTS

1. SUMMARY

Survival of cells within a transplanted skin substitute is dependent on the diffusion of nutrients and oxygen from the underlying wound site. Thus, formation of mature capillary networks *in vitro* in the skin substitute, so called prevascularization, is a promising approach to overcome this limitation. For this purpose I investigated human adipose-derived stem cells as a novel cell source for the tissue-engineering of prevascularized skin substitutes.

The so called stromal-vascular fraction (SVF) isolated from adipose tissue is a heterogeneous cell population including mesenchymal and endothelial cells but is depleted from mature adipocytes. I observed that both endothelial and mesenchymal cells present in the SVF assembled into a dense, microvascular network when submerged within fibrin hydrogels [1]. I also found that human tissue-engineered capillaries were already stabilized *in vitro* by perivascular cells (pericytes) as illustrated by a staining for pericyte specific markers such as α-smooth muscle actin (αSMA) and neuron-glial antigen 2 (NG2).

Most importantly, I demonstrated that SVF-derived capillary networks present in the prevascularized skin substitutes had the potential to connect to the host vasculature (by inosculation) within 3-4 days after transplantation onto the backs of immuno-incompetent rats. In contrast, transplantation of non-prevascularized controls, lacking endothelial cells, resulted in a delayed ingrowth of rat vessels and graft perfusion, which was not observed before day 14 after transplantation. Moreover, I examined the effects associated with rapid graft perfusion *in vivo* regarding the regeneration of the dermal and epidermal skin compartment. Skin substitutes prevascularized by cells of the SVF demonstrated an increased graft size after transplantation, as well as an enhanced collagen type I deposition in the dermal compartment. Furthermore, I evaluated the expression of tissue homeostasis and wound healing markers in the epidermis. The staining for cytokeratin 16 and 17 (wound healing markers) revealed that the period of wound healing could be dramatically decreased in the prevascularized skin grafts. Expression of cytokeratin 19 (skin homeostasis marker) restricted to the basal keratinocyte layer rather than also expressed in several suprabasal layers, demonstrated that graft prevascularization contributed to a faster epidermal homeostasis.

In the second part of my work, I have characterized different features of tissue-engineered skin substitutes regarding our future clinical trial. In this regard, I was able to contribute to the optimization of the protocol for the production of skin substitutes to shorten their total culture time from 21 to 12 days [2]. I have also examined whether it is possible to integrate pigment producing melanocytes into the epidermis of tissue-engineered dermo-

epidermal skin grafts [3]. An important part of this study was to observe the function and behaviour of those melanocytes and their interactions with keratinocytes in short- and long-term *in vivo* experiments. In addition, I contributed to the investigation of the innervation of the afore-mentioned skin grafts *in vivo* [4-5].

2. ZUSAMMENFASSUNG

Das Überleben der Zellen innerhalb eines transplantierten Haut-Substituts ist abhängig von adäquater Diffusion von Nährstoffen, Sauerstoff, Wachstumsfaktoren, Zytokinen und Hormonen ausgehend vom darunter liegenden Wundbett. Deshalb ist die Bildung reifer Kapillarnetzwerke *in vitro* in dem Haut-Substitut (eine sogenannte Prä-Vaskularisierung) ein viel versprechender Ansatz, um diese Einschränkung zu überwinden. Zu diesem Zweck untersuchte ich die aus menschlichem Fettgewebe gewonnenen Stammzellen als eine neuartige Zellquelle für das Tissue-Engineering von Haut-Substituten.

Die stromal-vaskuläre-Zellfraktion (SVF) aus dem Fettgewebe ist eine heterogene Zellpopulation die sowohl Mesenchym- als auch Endothelzellen enthält, aber keine reifen Adipozyten mehr. Die hier dargestellte Arbeit zeigt folgende Befunde: Ich beobachtete erstens, dass die Mesenchymal- und Endothelzellen der SVF ein dichtes, miteinander kommunizierendes Kapillar-Netzwerk in Fibrin-Hydrogelen *in vitro* entwickelt haben [1]. Zweitens konnte ich demonstrieren, dass die menschlichen engineerten Kapillaren bereits *in vitro* durch perivaskuläre Zellen (Perizyten) stabilisiert wurden. Dies wurde durch eine Färbung mit Perizyt-spezifischen Markern wie α-Aktin der glatten Muskeln (αSMA) oder Neuron-Glia-Antigen 2 (NG2) nachgewiesen.

Nach der Transplantation auf immuno-inkompetente Ratten schlossen sich diese Kapillarnetzwerke in den prä-vaskularisierten Haut-Substituten an die Ratten-Blutgefässe innerhalb von 3-4 Tagen an (Inoskulation). Im Gegensatz dazu war das Einwachsen von Ratten-Blutgefässen in die nicht prä-vaskularisierten Kontroll-Substitute verzögert. Die Blutperfusion der gesamten Dermis wurde *in vivo* erst nach dem 14. Tag beobachtet. Im Übrigen untersuchte ich die Effekte der schnellen Blutperfusion der prä-vaskularisierten Haut-Substitute auf die epidermale und dermale Hautregeneration *in vivo*. Die prä-vaskularisierten Substitute zeigten *in vivo* eine grössere Fläche und eine verstärkte Kollagen Typ I-Ablagerung in der Dermis. Weiterhin analysierte ich die Expression von Homöostase- und Wundheilungs-Markern in der Epidermis. Die Färbung für Zytokeratine 16 und 17 ergab, dass die Wundheilungsperiode in den prä-vaskularisierten Haut-Substituten drastisch verringert war. Darüber hinaus zeigte eine verminderte Expression von Zytokeratin 19 in den Keratinozyten der Basalschicht, dass die Prä-Vaskularisierung ebenfalls zu einer schnelleren epidermalen Homöostase beitrug.

Im zweiten Teil meiner Arbeit habe ich verschiedene Merkmale der tissue-engineerten Haut-Substitute in Hinblick auf unsere zukünftige klinische Anwendung untersucht.

Diesbezüglich habe ich das Protokoll zur Herstellung unserer Haut-Substitute soweit optimiert, dass deren Produktion von 21 auf 12 Tage reduziert werden konnte [2]. Ich habe auch untersucht, ob es möglich ist, in unseren Haut-Substituten Pigment produzierende Zellen, sogenannte Melanozyten, in die Epidermis zu integrieren [3]. Ein wichtiger Teil dieser Studie war es die Funktion und das Verhalten der Melanozyten, sowie ihre Interaktionen mit den Keratinozyten in kurz- und langfristigen *in vivo* Versuchen, zu beobachten. Zudem wurden in diesen Substituten die Innervierung und das Einwachsen von Blut- und Lymphgefässen systematisch untersucht [4-5].

.

3. INTRODUCTION

3.1 Human skin

The skin is the largest organ of the body and consists of three main layers: the epidermis, dermis, and subcutaneous layer (hypodermis) making up 16% of body weight, with a surface area of 1.5 – 2 m^2 [6] (Fig. 1). The most important function of the skin is to form a physical protection barrier against micro-organisms, ultraviolet radiation, toxic agents as well as mechanical insults. Moreover, skin mediates inflammatory responses and perception by sensory nerves. The thickness of human skin may vary between 1.5 and 4 mm depending on the different anatomical site, age, race and gender. Hairs, nails, sebaceous, sweat, and apocrine glands are regarded as skin appendages (Fig. 1).

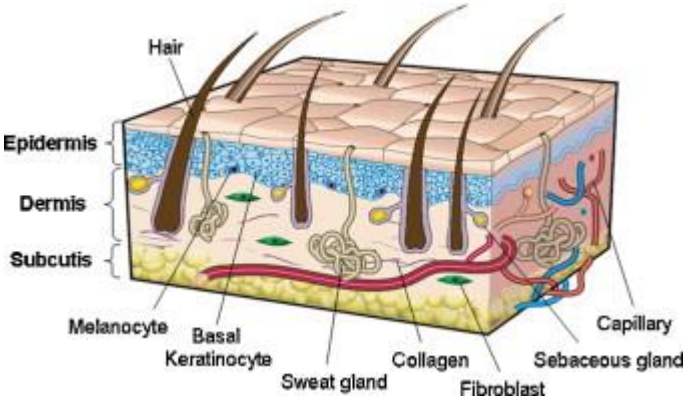

Figure 1. Schematic view of the composition of human skin. Human skin is composed of three layers: the epidermis, dermis and subcutis (hypodermis), as well as the most important skin appendages such as hairs, sebaceous, and sweat glands. The epidermis is a stratified squamous epithelium composed mainly of keratinocytes and melanocytes. The major cellular component of the dermis are fibroblasts, producing extracellular matrix like collagen fibers. The dermis has a rich vascular network whereas the epidermis does not contain any blood and lymphatic capillaries (non-vascular) [6].

3.1.1 Epidermis

Structure and function

A stratified squamous epidermis is the outermost surface of human skin. Its thickness varies between 0.05 mm on the eyelids to 0.8 ± 1.5 mm on the soles and palms. ***Keratinocytes*** are

the main cells of the epidermis; other cells are melanocytes, Langerhans, and Merkel cells (Fig. 1) [7].

In humans, ***melanocytes*** of the epidermis are located in the basal layer at a ratio one melanocyte to five keratinocytes [8]. In the hair follicle melanocytes are residing in the bulge and above the dermal papillae. They synthesize and transfer melanosomes containing melanin granules via dendritic protrusions to the keratinocytes giving color to the skin, hair, and parts of the eye to protect from UV irradiation [9-10]. Melanocytes are derived from precursor cells called melanoblasts that originate from the neural crest. Both light- and dark-skinned people have the same number of melanocytes, however they differ in the amount, type, and distribution of melanin that each melanocyte produces [11]. Melanin pigment occurs in two types: black to brown eumelanin and yellow to reddish pheomelanin [11]. High eumelanin content is found in dark-skinned people, who are better protected from UV radiation. In contrast, in albinos melanin synthesis is impaired and they often have very low or no pigment in their skin, hairs, and eyes.

Langerhans cells are dendritic cells distributed in all suprabasal layers of the epidermis, mostly in the spinous layer [12]. They can be identified by the expression of a specific protein, named CD1a and make up 2-8% of all epidermal cells. Langerhans cells protect skin from infections by the recognition, uptake, processing, and presentation of antigens to T lymphocytes [7].

Merkel cells were first described by Friedrich S. Merkel in 1875 as touch cells with a sensory touch function. They can be specifically identified by the expression of cytokeratin 20. In humans, Merkel cells are scattered along the dermo-epidermal junction, in eccrine glandular ridges of glabrous skin, within the hair follicles of hairy skin, and in certain mucosal tissues. As skin sensory receptors, Merkel cells stay in close contact with dermal sensory nerve endings. They may contribute to the development of the nerve plexus in the upper dermis, ecrine sweat glands, the hair follicle, and nails [7, 13].

Keratinocytes form four separate layers which can be distinguished by the different stages of keratin maturation:

– stratum basale (basal or germinativum cell layer)

– stratum spinosum (spinous or prickle cell layer)

– stratum granulosum (granular cell layer)

– stratum corneum (horny layer)

In addition, the stratum lucidum represents a thin layer of translucent cells present at the border between the stratum granulosum and stratum corneum. The stratum lucidum is mostly seen at body sites covered by a relatively thick epidermis.

Epidermal stratification is characterized by the graded distribution of specific cytoskeletal and junction components, including specific keratins (Ks), desmogleins (DSGs), and cadherins as demonstrated in Fig. 2 (right part).

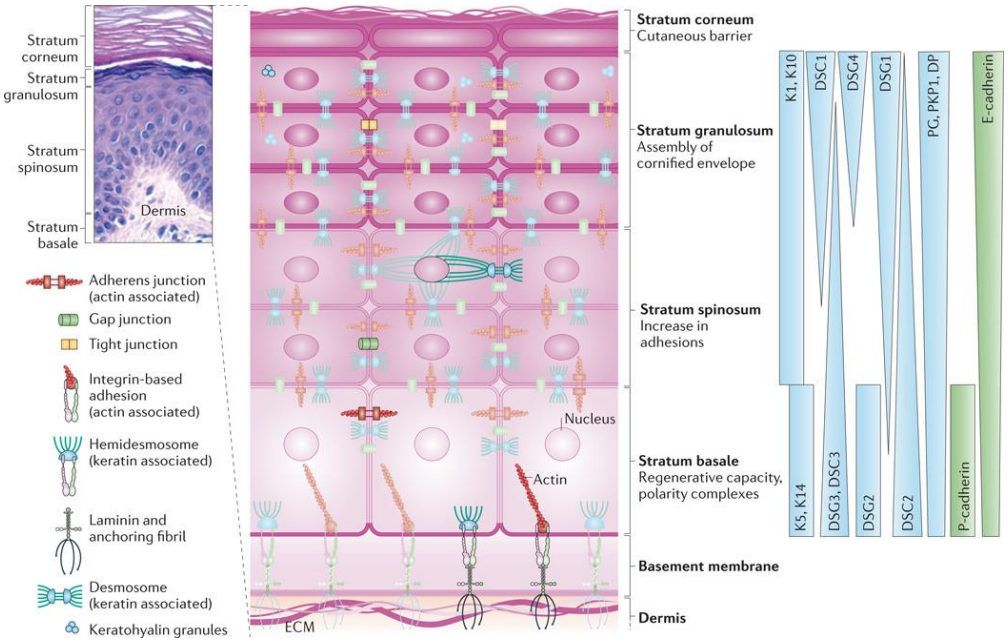

Figure 2. Schematic view of human interfollicullar epidermis. The epidermis is composed of stratified cell layers, which differentiate to allow a constant renewal of the skin. A hematoxylin- and eosin-staining (left, above) and an accompanying scheme (middle) illustrate four main skin layers: stratum basale, stratum spinosum, stratum granulosum, and stratum corneum. Epidermal stratification is characterized by the graded distribution of specific cytoskeletal and junction components, including specific keratins (Ks), desmogleins (DSGs), and cadherins. Abbreviations: DP, desmoplakin; DSC, desmocollin; E-cadherin, epithelial cadherin; P-cadherin, placental cadherin; PG, plakoglobin; PKP1, plakophilin 1 [14].

Organization of the stratified epidermis

Keratinocytes within the epidermis show apical-basal axis of polarity. In the basal layer keratinocytes are anchored to the basement membrane by integrins (Fig. 2). These heterodimeric transmembrane receptors consist of α- and β-subunits and bind specific extracellular matrix (ECM) components via their extracellular domains [15]. Integrin α6β4 has a crucial role in the formation of the hemidesmosome complex that contributes to the anchoring of basal keratinocytes to the underlying basement membrane (Fig. 3). An inherited

defect in this anchorage leads to epidermolysis bullosa (EB), a severe skin disorder causing skin blisters and fragility.

As a very dynamic organ, skin possesses a high regenerative potential and is in a constant state of change [16]. One epidermal keratinocyte stem cell may be able to give rise to enough cells to cover the body surface [17-18]. Keratinocyte stem cells reside in the basal layer of the epidermis and divide to give rise to transient amplifying cells, which can further divide or exit the cell cycle to differentiate [19]. Once keratinocytes start to differentiate, they detach from the basement membrane by losing their hemidesmosome anchorage and move upwards in the epidermis. First they enter the spinous cell layer, then move into the granular layer, and eventually enter the outer cornified layer of the epidermis. Whereas basal, spinous and granular cells are alive, the terminally differentiated cells of the stratum corneum are dead and constitute the outer protective cell layer.

Epidermal keratinocytes are linked through protein bridges called desmosomes or macula adherens (Latin for adhering spot), which provide strong mechanical cell-cell cohesion [20] (Fig. 3). Desmosomes from neighboring cells are connected by members of the cadherin family, called desmogleins and desmocollins, situated between two cells. On the cytoplasmic side of each cell membrane these cadherin-type proteins inset into a dense complex of anchoring proteins (plakophilin, plakoglobin, and desmoplakin) via armadillo proteins [14]. Desmosomes bind to intracellular keratin cytoskeletal filaments (tonofilaments) providing a strong cell-cell junction [21]. The disruption of this desmosome-keratin filament complex leads to a breakdown of cell adhesion causing the symptoms of the blistering skin disease (Pemphigus vulgaris and foliaceus). The patients suffering from this disease produce auto-antibodies directed against desmoglein 3 and desmoglein 1 [22].

Adherens junctions are a second family of cadherin-based junctions in the epidermis. They are composed of the classic cadherins - E-cadherin (epithelial) and P-cadherin (also known as cadherin 3) forming an adhesion between the neighboring cells through homophilic, calcium-dependent interactions (Fig. 3). An ablation of both cadherins causes lethal blistering [23]. The cytoplasmic domains of these cadherins are associated with important signaling proteins such as p120 catenin and β-catenin. β-catenin binds via armadillo repeat domains to α-catenin, an actin-binding protein [14].

Tight junctions appear at the apical side of keratinocytes in the stratum granulosum preventing fluid loss and protecting against pathogens (Fig. 3) [21, 24]. Tight junctions are composed of transmembrane proteins (claudins and occludins) linked to the actin cytoskeleton [25]. Other interaction partners of claudins are: the zona occludens (ZO) proteins

ZO-1, ZO-2, ZO-3, and multi-PDZ domain protein-1 [26]. Tight junctions, adherens junctions, and desmosomes constitute the intercellular junctional complex in mammals (Fig. 3).

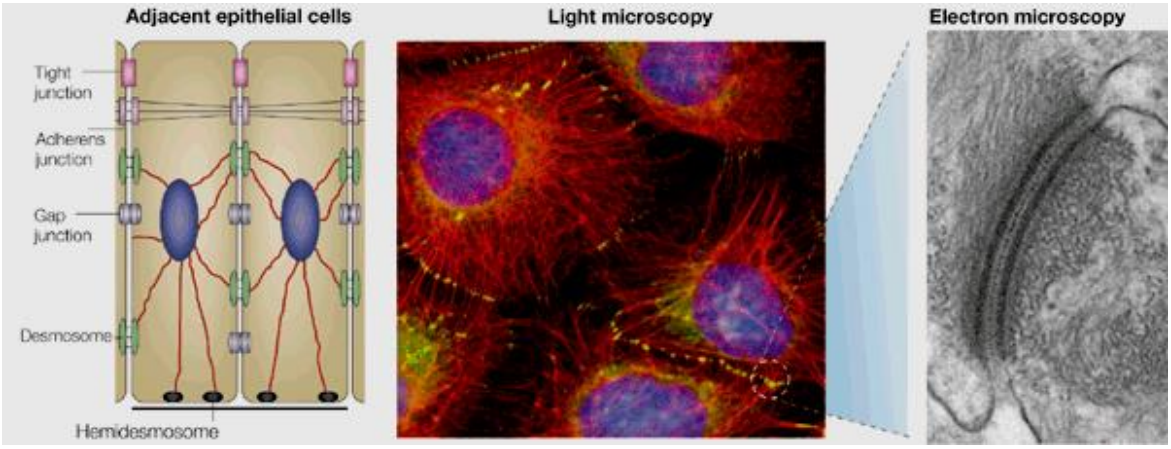

Figure 3. Organization of the junctional complex of epithelial cells. Tight junctions are present in the later spinous layers of the epidermis at the most apical position and maintain the epithelial barrier function beneath the stratum corneum. Adherens junctions organize cortical actin, and together with desmosomes attach epithelial cells together. Tight junctions, adherens junctions, and desmosomes form the "junctional complex". Gap junctions form patch-like lateral connections between the cells and form channels for the transport of small molecules between neighboring cells. Hemidesmosomes are integrins which anchor the cells to the basal lamina. In the light microscopy picture keratin tonofilaments of epithelial cells (in red) are associated with desmosomes, which are shown by a desmoplakin staining (in green). At the ultrastructural level desmosomes appear as bilaterally symmetrical structures with a zipper-like midline as a central core region that spans the intercellular space between opposing cells [21].

Cytoskeletal proteins

There are three main classes of filaments in eukaryotic cells: microtubules, actin filaments (microfilaments or F-actin), and intermediate filaments (Fig. 4) [27]. Microtubules have a diameter of 20-25 nm and consist of two different globular protein subunits such as alpha-tubulin and beta-tubulin, which form together long, hollow cylinders. Actin filaments are helical polymers formed by globular actin monomers, called G-actin. They are the smallest components of the cytoskeleton with a diameter of about 7-9 nm. Intermediate filaments are of about 8-12 nm in diameter and provide strong mechanical stability to the cell.

Keratins (previously also called cytokeratins) are filament-forming proteins (tonofilants) of epithelial cells and are essential for normal structure and function of the

epidermis [27]. Accordingly to their biochemical properties, keratins are classified into two groups: type I or acidic and type II or basic epithelial keratins [28].

There are also other types of intermediate filaments such as type III: desmin, vimentin, glial fibrillary acidic protein (GFAP), type IV: nestin, and type V: lamin A.

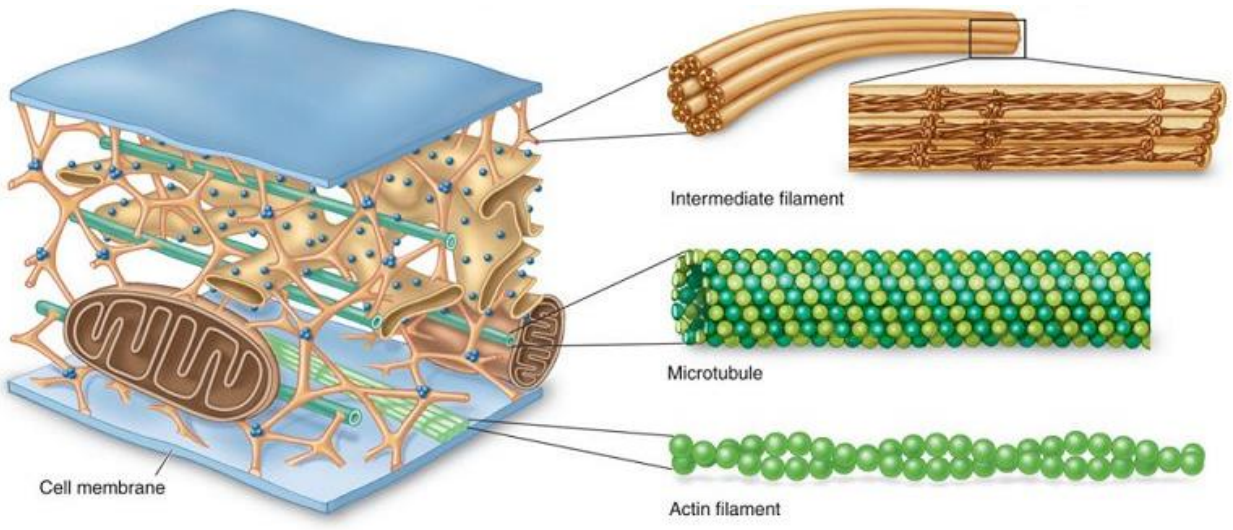

Figure 4. Structural organization of microtubules, microfilaments, and intermediate filaments in a cell [29].

3.1.2 Dermis

The dermis contains nerve endings, blood and lymphatic vessels, as well as skin appendages such as hair follicles, sweat, and sebaceous glands often reaching into the hypodermis [30]. The dermis comprises two layers, a thin papillary and thicker reticular layer. The upper papillary dermis gives shape to the stratum basale of the epidermis through finger-like protrusions called dermal papillae (Fig. 5). The papillary layer contains loosely arranged collagen fibres, whereas in the deeper reticular layer bundles of collagen are thicker and appear as reticulated (net-like) structures (Fig. 5).

The dermis is populated by fibroblasts which deposit collagen, elastin fibers, and structural glycosaminoglycans [7]. Collagen fibers make up 75% of the dermis providing mainly structural and mechanical strength to the skin. The most abundant type of collagen in this layer is type I (89-90%) and type III (8-12%) collagen. Elastin maintains normal skin elasticity and flexibility, whereas glycosaminoglycans keep the optimal level of hydration.

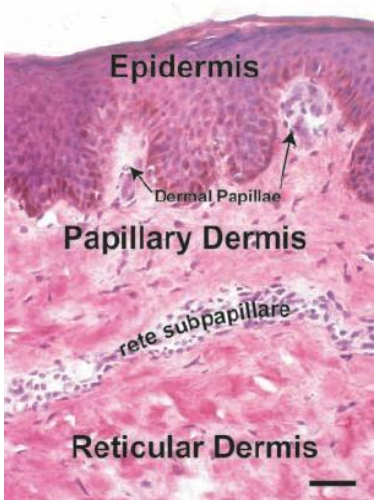

Figure 5. Hematoxylin- and eosin staining of normal human skin showing the two components of the dermis - the papillary and the reticular layer. The dermal papillae protruding into the epidermis belong to the papillary layer, characterized by a fine network of collagen fibrils. In contrast, the underlying reticular layer appears reticulated (net-like) due to a dense and tight collagen bundle meshwork. Rete subpappillare separate these two layers [30].

Basement membrane (BM)

The epidermis is separated from the underlying dermis by the complex basement membrane (BM), deposited by both keratinocytes and fibroblasts [31-32]. Fibroblasts deposit laminin-1, nidogen-1/2, collagen type IV and VII, whereas keratinocytes produce laminin-332 (laminin-5), perlecan, and also collagen IV and VII [32-34].

The BM is composed of a set of distinct glycoproteins and proteoglycans to form anchoring complexes and provide an adhesive and dynamic interface (Fig. 6) [31, 35-36]. These complexes are composed of the hemidesmosomes, anchoring filaments, and anchoring fibrils. Anchoring filaments extend from the basal cell membrane into the lamina lucida, connecting hemidesmosomes with the lamina densa, containing collagen type IV fibrils coated with perlecan. The lamina lucida with the lamina densa make up the basal lamina. Further, the anchoring complex - BP180, plectin, laminin - interacts with transmembrane alpha6beta4 (α6β4) integrin. During BM assembly α6β4 becomes integrated into hemidesmosome complexes and connected to the keratin network via the β4 subunit. Moreover, α6β4 binds to laminin-332 (laminin-5) [37].

Anchoring fibrils, formed by collagen type VII, extend from the lamina densa into the papillary dermis and connect the lamina densa to interstitial collagen fibrils. Thus, the BM

connects the complex basal keratinocyte cytoskeletal framework with the abundant network of interstitial collagen bundles in the dermis.

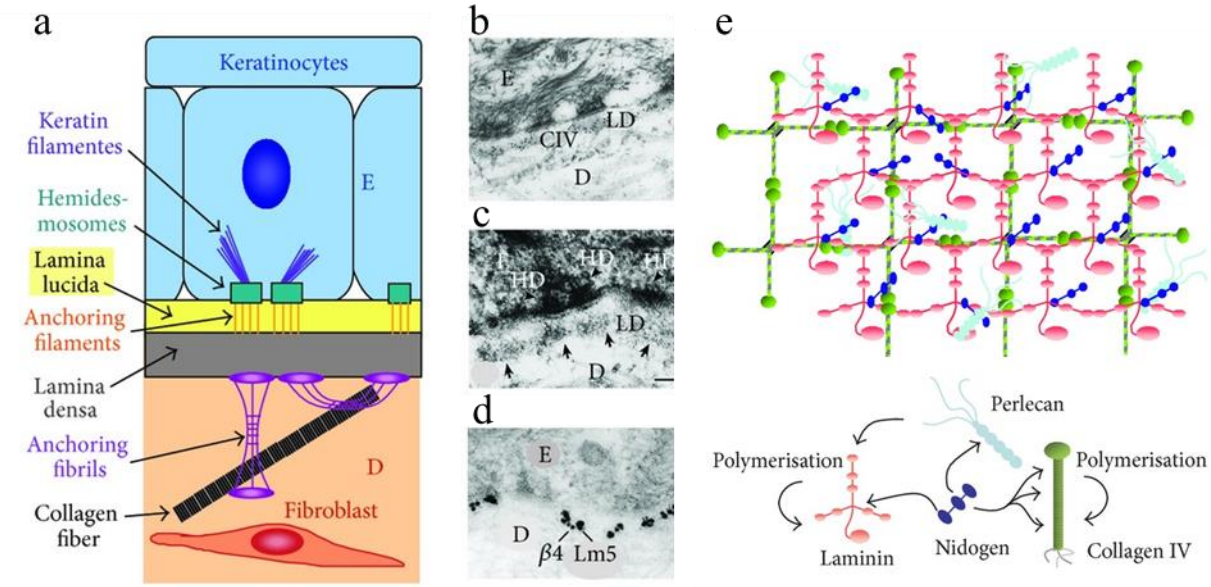

Figure 6. Ultrastructural characterization of the basement membrane (BM) of skin. (a) The anchoring complexes between epidermis (E) and dermis (D) form the dermo-epidermal junction. (b) The collagen-epidermal interface of a 3D co-culture of keratinocytes with fibroblasts similar to normal skin. (c) Immuno-electron microscopy indicating the alignment of collagen IV with the lamina densa (LD) and (d) colocalization of integrin α6β4 with laminin-332 (laminin-5; Lm5) (small/large gold particles staining). (e) Schematic representation of the BM. The mat-like BM structure develops through the interactions between the four major BM components. Abbreviations: CIV, collagen IV; LD, lamina densa; HD, hemidesmosomes [31].

Blood and lymphatic vessels

The dermis is rich in blood vessels. They provide nutrients to the skin and regulate body temperature. The dermal vasculature consists of both a superficial and a deep plexus of arterioles and venules being connected by communicating vessels that arise from arteries and lead eventually to veins that reside within septa of the subcutaneous fat (Fig. 7) [7]. The superficial plexus also called the "subpapillary plexus" is formed just beneath the epidermis and consists of finger-like capillary loops projecting into the dermal papillae, whereas the deep plexus is positioned in the lower part of the reticular dermis (Fig. 7) [38]. Both plexuses are connected by communicating blood vessels that are oriented perpendicular to those plexuses. From the superficial plexus, a branch of capillaries loops into each dermal papilla

with a single loop of capillary vessels, one arterial and one venous. Dilatation or constriction of these capillary loops plays a direct role in the thermoregulation of skin.

The lymphatic system of skin develops through lymphangiogenesis in parallel with the blood vascular system. Interestingly, lymphatic vessels are normally absent in avascular structures such as epidermis, hair, nails, cartilage, cornea, and in some organs such as brain and retina. Abundant lymphatic networks in the dermis form superficial and deep plexuses corresponding to those of the blood vascular system. The main function of the skin lymphatic system is to collect the lymph and drain it into regional lymph nodes.

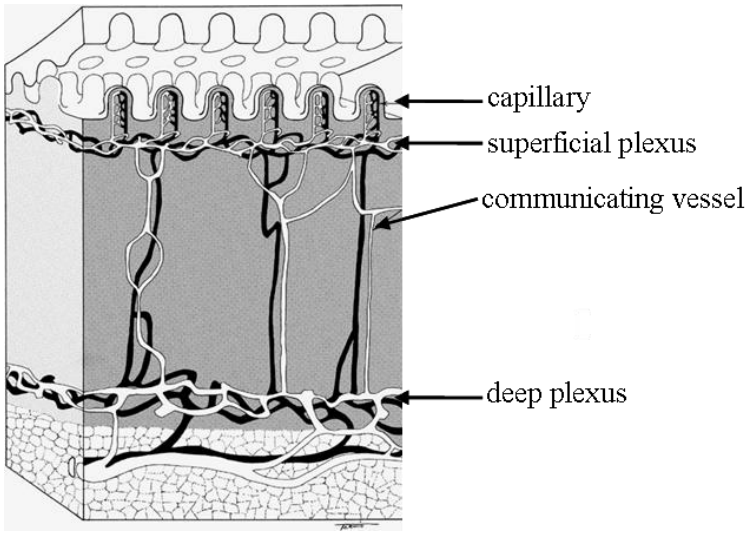

Figure 7. The dermal vasculature consists of a network of two plexuses that parallel the skin surface. The superficial plexus (subpapillary plexus) is situated in the upper part of the dermis, whereas the deep plexus is positioned in the lower part of the reticular dermis. Both plexuses are connected by communicating blood vessels that are oriented perpendicular to those plexuses. Capillaries emanate from the vascular plexuses to supply the papillary-periadnexal (adventitial) dermis and the epithelial and non-epithelial structures of adnexa housed in the reticular dermis [38].

The process of new blood and lymphatic vessel formation in skin transplants, especially in human tissue-engineered skin substitutes, remains poorly understood. I have therefore investigated the kinetics of host vessel ingrowth within those skin substitutes [4].

The adequate and rapid revascularization of skin transplants is crucial for the initial take, survival, and incorporation into the recipient's tissue. Studies on full-thickness skin, containing blood vessels and capillaries, demonstrated the fusion of host and graft capillaries (inosculation) three days after transplantation [39-40]. These studies used either intravenous injection with radioisotopes [39] or India ink [40], and the reestablishment of blood flow in

transplant vessels was observed at two or four days, respectively. Finally, the group of Zarem *et al.* established a modified transparent skin chamber in the mouse and demonstrated that revascularization of full-thickness skin grafts occurs through both vascular ingrowth from the recipient wound site and inosculation [41]. Furthermore, skin graft revascularization also involves vascular regression and replacement of graft endothelial cells through angiogenesis and reconnection (inosculation) [42].

As far as lymphatic regeneration after skin transplantation is concerned, very few studies have been performed. A study of Yan *et al.* in mouse suggested that lymphatic regeneration after skin tissue transfer starts at the peripheral edges of the graft and occurs by ingrowth of lymphatic vessels and spontaneous re-connection with the existing lymphatics [43]. However, the ingrowth of blood vessels into skin wounds precedes formation of new lymphatic vessels [44]. Nogami *et al.* followed the recovery of lymphatic vessels in rat skin incision wounds up to 12 weeks and found that lymphatic vessels were not present in the wound area, but only in the surrounding intact tissue [45]. This impairment of lymphatic regeneration is linked to lymphedema, fibrosis, and scar formation [46-47].

Innervation and nerve endings of the skin

As skin is an important sensory organ, it has a rich nerve supply containing nerve endings of different types (Fig. 8).

The skin's afferent nervous system consists of both myelinated and non-myelinated fibres, which transmit impulses from the various nerve endings, and are therefore responsible for cutaneous sensation. The skin sensory nerve endings consist not only of free nerve endings, but can also appear as specialized "encapsulated" nerve endings such as Meissner's, Pacinian, and Ruffini's corpuscles [48].

The skin's efferent nervous system comprises non-myelinated fibres from the sympathetic nervous system, which are in contact with blood vessels and the skin appendages, for example with arrector pili muscles and eccrine sweat glands.

After severe skin injuries such as third-degree burns, there is no sensation in the burned area as all nerve endings are destroyed. The grafted skin will have little or no sensation directly after transplantation, but will slowly regain it by the regeneration of nerve endings. However, the mechanism of reinnervation is still poorly understood. Interestingly, nerves are often aligned with blood vessels and show similar patterns in the development and regeneration after injuries [49-54].

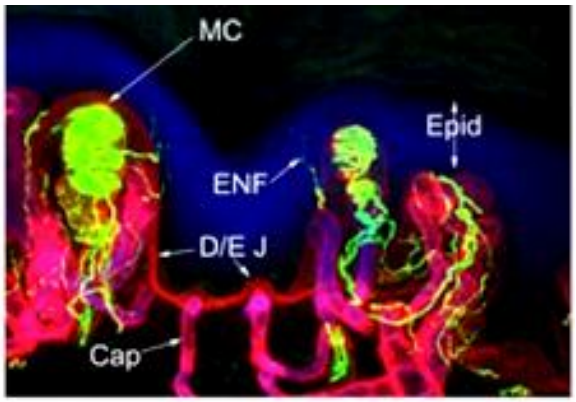

Figure 8. The innervation of skin. Green fibers stained for pan-neuronal protein PGP9.5 show the typical innervation of the fingertip skin. Blood capillaries are stained using an antibody to collagen type IV (red), and the epidermis with ulex (blue). Two encapsulated Meissner's corpuscles can be observed near to the dermo-epidermal junction. Abbreviations: ENF, epidermal nerve fibers; D/E J, dermal-epidermal junction; Epid, epidermis; Cap, capillaries; MC, Meissner's corpuscles. Image courtesy of Dr. Patrick Dougherty at M. D. Anderson Cancer Center, Houston.

It has been postulated that blood vessels serve as guiding instances for nerve outgrowth by the secretion of specific factors. Several molecules with attractive and repulsive properties have been identified regulating the proper path finding and guidance of nerves. These include the netrins, the semaphorins, the slits, and their receptors. Moreover, other factors including a glial-derived neurotrophic factor (GDNF) family member called artemin, and others such as endothelin-3, have been described [55-56]. These factors are released by smooth muscle cells surrounding arteries. They direct the growth of sympathetic nerves along these vessels to the end organs [57]. Vascular endothelial growth factor (VEGF-A) also controls axon cone growth and sprouting along arterial networks [58-59].

3.1.3 Hypodermis

The hypodermis (also called subcutis or the subcutaneous fat layer or superficial fascia) is a layer between the dermis and the underlying fascia of muscles [7]. It is, like the dermis, derived embryologically from mesenchyme and consists of well-vascularized, loose, areolar connective tissue and adipose tissue. The main function of it is fat storage as well as insulation and cushioning of the integument. Fat-storing cells, called adipocytes, synthesize and store lipids in their cytoplasm, thereby appearing as large clear cells with the nucleus close to the plasma membrane at its border or not visible at all (Fig. 9A). Adipose tissue is highly vascularized with each adipocyte being in contact with at least one capillary (Fig. 9B).

This rich blood supply provides sufficient support for the active metabolism, which occurs in the thin rim of cytoplasm surrounding the lipid droplet.

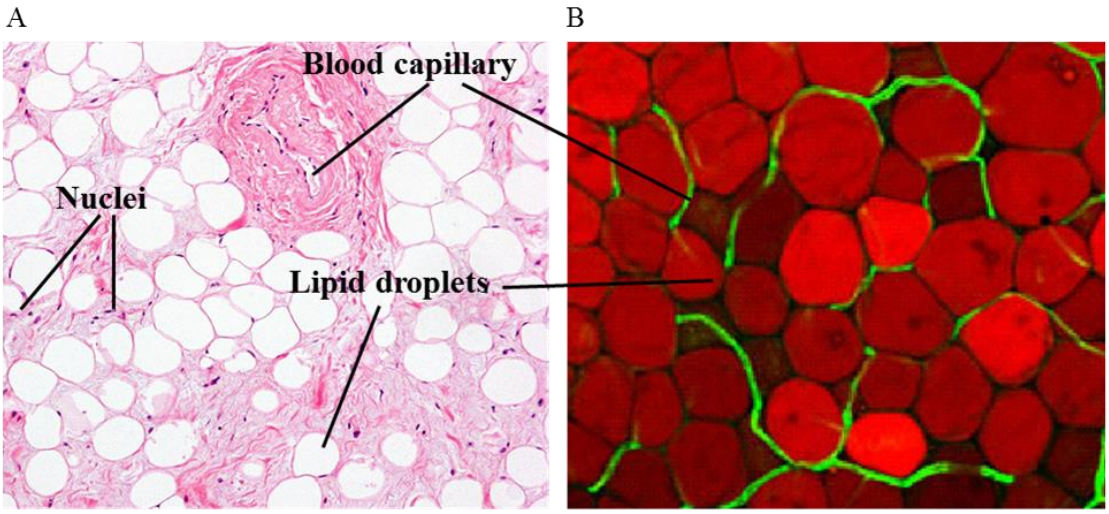

Figure 9. Adipose tissue. A. Hematoxylin- and eosin staining showing lipid drops in adipocytes, nuclei and blood capillaries (magnification 100x). B. Specific staining for adipocytes (in red), which are encircled by blood capillaries stained in green (magnification 160x). Image courtesy of David Burk, Pennington Biomedical Research Center

Cell isolation from adipose tissue is performed under local anesthesia using simple procedures such as liposuction. The so-called stromal-vascular fraction (SVF) can be isolated in large quantities and represents an attractive cell source for regenerative medicine [60-61]. I routinely isolated 1.6 – 0.9 x 10^5 nucleated cells from 1 ml of a fat liposuction biopsy and 1 – 0.55 x 10^5 nucleated cells from 1 gram of an excision biopsy [62]. Figure 10 illustrates the different steps of the isolation and distinct applications of adipose-derived stem cell. For this procedure the liposuctioned fat is washed and treated with collagenase II to release single cells from the fat tissue.

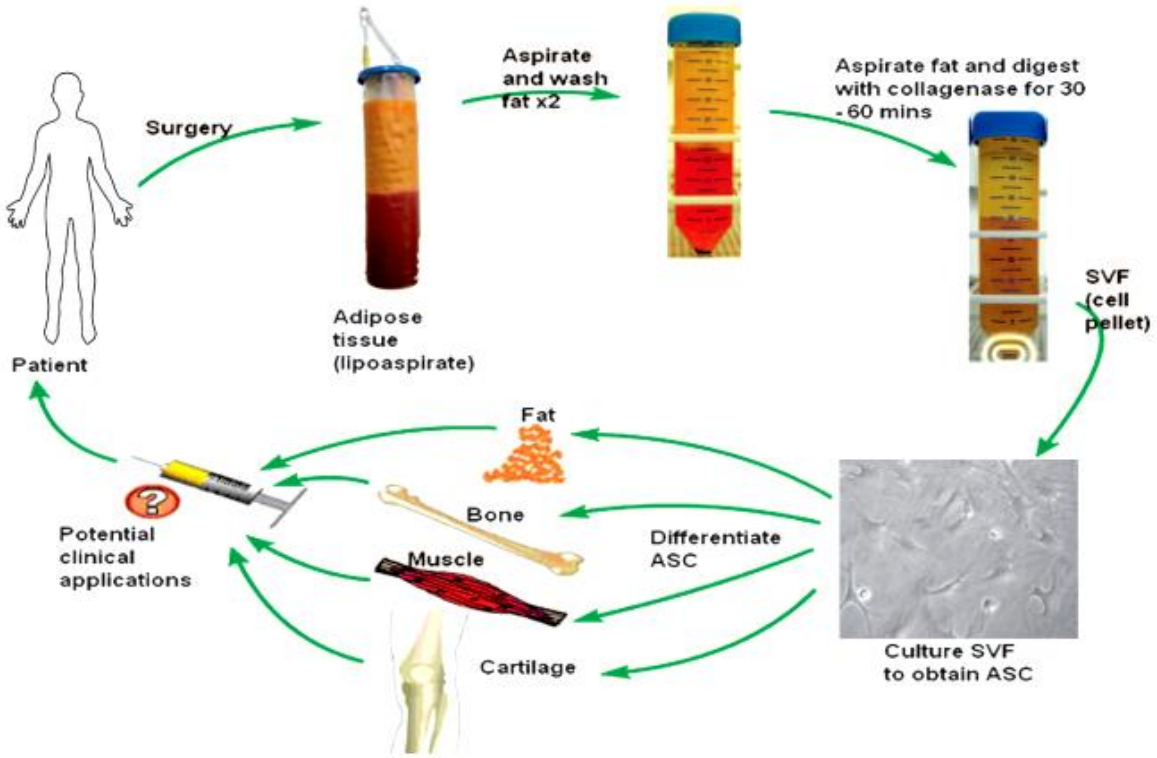

Figure 10. Scheme of human adipose-derived stem cell (ASC) isolation and differentiation for potential clinical applications. Abbreviations: SVF, stromal vascular cell fraction [61].

After enzyme inactivation, the so called SVF is pelleted after centrifugation. The SVF is a heterogeneous cell population composed of mature cells such as endothelial cells, adipose stromal cells (ASC), as well as distinct progenitor/stem cell populations [61] (Fig. 11).

Upon expansion in monolayer cultures on tissue culture plastic, the SVF yields an adherent stromal cell population, termed adipose stromal cells (ASC) [63-64]. ASC are characterized by the expression of typical mesenchymal/stromal markers such as CD90 and CD73 and completely lack other cell types [64]. ASC demonstrate a higher proliferation potential and higher number of stem cells in comparison to bone marrow stem cells (BMSC) and obtaining them is less invasive as compared to bone marrow isolation. ASC have potential therapeutic implications for clinical practice as they can be easily induced to the osteogenic, chondrogenic, and adipogenic lineage *in vitro*, and injected back to the patient's damaged organ (Fig. 10).

Due to the shortage of autologous skin cells in severely burned patients, other non-skin cell sources such as adipose-derived cells have been explored for skin tissue engineering. I characterized the cells of the human SVF and succeeded in using them to reconstruct the prevascularized dermal compartment of a full-thickness skin substitute. I demonstrated that endothelial and stromal cells both derived from the SVF, assemble into mature vascular

structures *in vitro*, thus actively contributing to the prevascularization of tissue-engineered skin grafts and stimulating their engraftment *in vivo* [1].

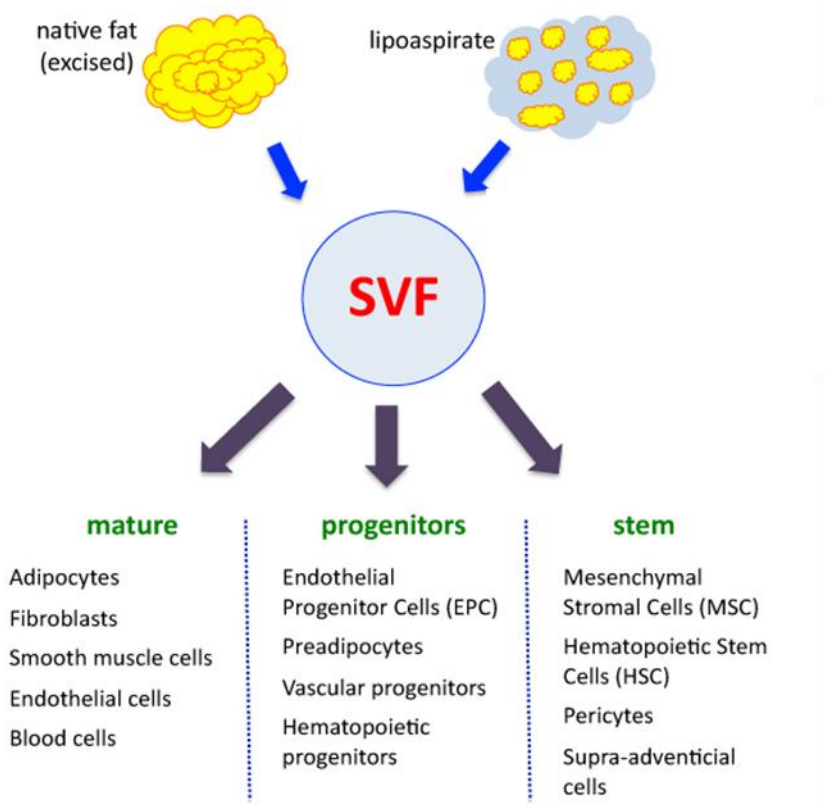

Figure 11. Cellular composition of the stromal vascular fraction (SVF) of adipose tissue. SVF isolated from an excised or lipoaspirate fat biopsy comprises distinct mature, progenitor, and stem cell types. Depending on the donor differences and adipose tissue processing method, the cell composition of the SVF can vary significantly (modified from "Breaking down fat: Composition of stromal vascular fraction", A. Bersenev, 2013).

3.2 Skin injuries and wound healing

3.2.1 Skin injuries

Thermal injuries, such as scalds and burns, are one of the most devastating conditions encountered in medicine. A burn is primarily caused by heat or due to radiation, radioactivity, electricity, friction or contact with chemicals. WHO estimated that 322.000 deaths every year are caused worldwide by fire burns only - the vast majority occur in low- and middle- income countries [65-66]. These severe injuries impair all aspects of the patient's life, from the physical to the psychological and pose difficult and unique medical challenges. Tragically, children under 5 years and the elderly (aged over 70 years) have the highest fire-related burn

mortality rates worldwide. In addition to those who die, millions are left with lifelong disabilities and scars.

3.2.2 Wound healing

Immediately after an injury, a synchronized wound healing process with multiple biological pathways becomes activated [67] (Fig. 12).

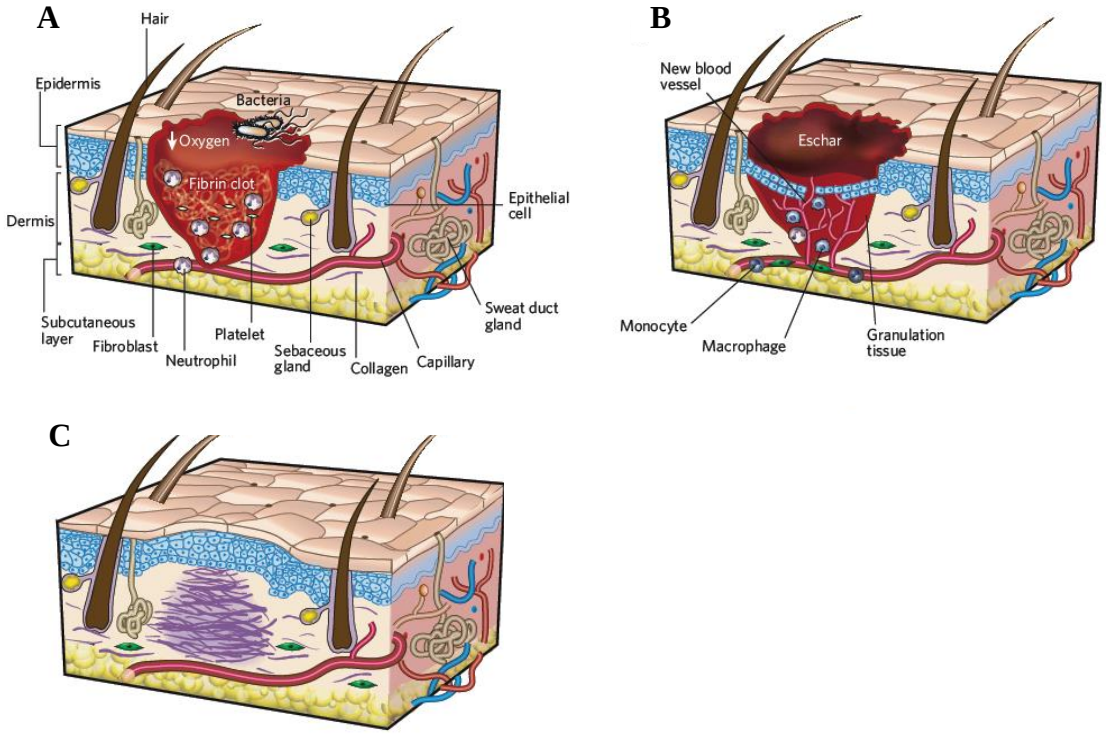

Figure 12. Schematic representation of the three wound healing stages. a) During the first phase - inflammation - a fibrin clot is formed and neutrophils are recruited to the wound to remove bacteria and damaged tissue. b) During proliferation phase an eschar is formed and cells such as keratinocytes and fibroblasts migrate into the wound to close the wound and form granulation tissue, respectively. c) During the third phase, tissue maturation and remodeling occurs. Parallel collagen fibers (violet) are deposited by fibroblasts and a scar tissue is formed [67].

The normal healing process following an injury of the skin starts when platelets form a fibrin clot to stop bleeding. Subsequently, neutrophils enter the wound site and begin the removal of bacteria and damaged tissue during the inflammatory phase. This triggers migration of other cells such as fibroblasts to the wound site and as a result a simple

granulation tissue is formed. The subsequent proliferative phase is characterized by extensive growth of epithelial cells, fibroblast deposition of collagen fibers in a disorganized pattern, and ingrowth of blood vessels. Finally, during the maturation/remodeling phase, these collagen fibers become more organized, the number of blood vessels is normalized, and the epidermis is restored to normal thickness. The newly developed tissue fills the area of injury, however, forming a fibrotic tissue called scar.

Wound healing is substantially delayed in patients suffering from diabetes or after radiation exposure. By contrast, an excessive wound response may lead to hypertrophic scars and keloids characterized by the deposition of large amounts of extracellular matrix, impaired vascularization, and cell proliferation. These frequently occur after major skin injuries such as burns [67].

3.3 Skin replacement therapies

The loss of skin occurs very often due to burns, trauma, congenital abnormalities, disease, or chronic, non-healing ulcers in elderly people [68-69] (Fig. 13). These skin defects can lead to skin necrosis and thus represent a challenging problem for public health [70-71]. Hence, the main aims of burn care are to restore skin, its function, and appearance.

Skin wounds measuring more than 4 cm in diameter will not heal spontaneously and need to be closed by skin graft transplantation [72]. After the early debridement of the damaged tissue, an autologous split-thickness skin graft harvested from an uninjured skin site is transplanted to cover the skin defect [71] [73]. This treatment method is used as the today's "gold standard", however it usually leads to disfiguring hypertrophic or keloid scars if transplanted without any dermal matrix [74-75].

In comparison, autologous full-thickness skin transplantation can be performed only for patients with skin injuries smaller than 1-2% of the Total Body Surface Area (TBSA) [68]. The major problem is the lack of a functional dermis, especially in large skin wounds over 70% of the TBSA with only 30% of remaining normal skin which is insufficient for harvesting [76]. Hence, its frequent wide use is limited by donor site availability.

Figure 13. The need of tissue-engineered skin. Left: Acute wounded patient suffering from a large burn after escharatomy. Because of the large Total Body Surface Area (TBSA) affected, not enough healthy skin is available for a split-thickness skin graft. Right: The elective situation. Patient suffering from a giant congenital melanocytic nevus in the elbow area. After resection, the best medical treatment would be the application of a tissue-engineered skin substitute to match skin color and texture as closely as possible [68].

3.3.1 Tissue engineering of skin

Tissue engineering of skin substitutes in the laboratory represents an advanced therapy for acute and chronic skin wounds. In the past, autologous cultured epidermal autografts (CEA) were used for burn and reconstructive surgery, however this mostly did not result in a satisfactory and esthetic skin replacement [77-78]. Therefore, the ultimate goal of the Tissue Biology Research Unit (TBRU) was to tissue engineer a novel human dermo-epidermal full thickness skin substitute for clinical use. Using this approach only a small patient' biopsy is harvested, and after subsequent cell isolation and expansion *in vitro*, autologous skin substitutes are produced. They show many features of an "ideal" skin regarding the anatomy, physiology, biological stability, and cosmetic properties [2, 79-80]. The dermal compartment is reconstructed using a collagen type I hydrogel containing autologous fibroblasts and with autologous keratinocytes on the top of it to form the epidermal coverage [79] (Fig. 11). These substitutes represent an optimal skin replacement for deep wounds as they provide both skin layers as for long-term wound coverage with reduced or no scarring.

To further improve the skin grafts properties, and to achieve skin pigmentation for sufficient protection against UV-radiation, we developed tissue engineered autologous dermo-epidermal substitutes with integrated melanocytes. Our *in vivo* pre-clinical studies

demonstrated that we were able to reconstruct the patient's own skin color [68]. This technique also holds a great promise to treat hypo- or hyperpigmentation skin disorders such as melanocytic nevus and vitiligo [81].

However, successful transplantation of tissue engineered skin substitutes thicker than 400μm depends on the rapid onset of blood perfusion. This ensures adequate supply of oxygen and nutrients, cell survival, and function of the transplanted skin grafts [82-84]. Whereas autologous full-thickness skin grafts become perfused within days by inosculation of its pre-existing blood vessels with those of the patient, avascular skin substitutes are totally dependant on neovascularization from the wound bed. This process can take up to 14 days or even longer in patients with compromised angiogenesis (e.g., diabetes or the aged) [85]. Therefore, the incorporation of microvascular networks into the tissue-engineered skin graft before its transplantation, hence pre-vascularization, considerably accelerates its blood perfusion, integration, and remodeling of the transplant.

We succeeded in developing a plexus of highly organotypic, branching, lumen-forming capillaries in engineered skin substitutes. After transplantation onto immuno-incompetent rats, human capillaries rapidly connected to the vasculature of the recipient's animal [1, 86-87].

4. RESULTS

4.1 Tissue-engineered dermo-epidermal skin grafts prevascularized with adipose-derived cells

Agnieszka S. Klar[1], Sinan Güven[2], Thomas Biedermann[1], Joachim Luginbühl[1], Sophie Böttcher-Haberzeth[1], Claudia Meuli-Simmen[4], Martin Meuli[3], Ivan Martin[2], Arnaud Scherberich[2*], and Ernst Reichmann[1*]

[1]Tissue Biology Research Unit, Department of Surgery, University Children's Hospital Zurich, Zurich, Switzerland.

[2]Department of Biomedicine, University Hospital of Basel, University of Basel, Basel, Switzerland.

[3]Department of Surgery, University Children's Hospital Zurich, Zurich, Switzerland.

[4]Department of Plastic, Reconstructive, Esthetical and Hand Surgery, Kantonsspital Aarau, Aarau, Switzerland.

[*]Corresponding authors: Prof. Dr. Ernst Reichmann, Tissue Biology Research Unit, August Forel Str. 7, CH-8008 Zurich, Switzerland, Email: Ernst.Reichmann@kispi.uzh.ch;
PD. Dr. Arnaud Scherberich, Department of Biomedicine, University Hospital of Basel, University of Basel, Basel, Switzerland, Email: Arnaud.Scherberich@usb.ch

Published in:

Biomaterials, 2014, 35(19):5065-5078
Impact factor 8.3

Abstract

The major problem in skin grafting is that tissue-engineered skin grafts after their transplantation are initially entirely dependent on diffusion. Since this process is slow and inefficient, nutrients, growth factors, and oxygen will insufficiently be supplied and the regenerating graft will undergo a physiological crisis, resulting in scar-like dermal structures and shrinkage. The tissue-engineering of a vascular network in human dermo-epidermal skin substitutes (DESS) is a promising approach to overcome this limitation. Here we report, for the first time, on the use of the adipose stromal vascular fraction (SVF)-derived endothelial cell population to tissue-engineer DESS containing a highly efficient capillary plexus. To develop vascular networks *in vitro*, we employed optimized 3D fibrin or collagen type I hydrogel systems. Upon transplantation onto immune-deficient rats, these preformed vascular networks anastomosed to the recipient's vasculature within only four days. As a consequence, the neo-epidermis efficiently established tissue homeostasis, the dermis underwent almost no contraction, and showed sustained epidermal coverage *in vivo*. Overall, the here described rapid and efficient perfusion of SVF-based skin grafts opens new perspectives for the treatment of hitherto unmet clinical needs in burn/plastic surgery and dermatology.

Keywords

Fibrin; Collagen; Skin tissue-engineering; Angiogenesis; Adipose tissue; Endothelial cell

Introduction

Skin defects caused by burns, trauma, or non-healing chronic wounds are frequent and often cause severe clinical problems [1]. Recently, a tissue-engineered dermo-epidermal full-thickness skin substitute (DESS) [2-6] has been proposed as an alternative to autologous split-thickness skin grafting, which represents the current clinical gold-standard, yet is limited by donor-site shortage, propensity to contraction, shrinkage and scarring [7-8]. Despite its innovative clinical potential, the major challenge associated with the above mentioned DESS might be insufficient initial vascularization, resulting in some kind of nutritional crisis early after transplantation, and impaired regeneration due to the initial lack of oxygen and nutrients. Notably, this crisis can not be avoided by any kind of the presently used skin grafts with the exception of full-thickness skin. This graft is prevascularized and gets rapidly perfused (by inosculation) after transplantation. However, full-thickness skin grafts can only be used to cover relatively small surfaces, due to the severe trauma that goes along with its preparation.

Numerous strategies to enhance vascularization of autologous grafts were suggested [9-11]. A promising approach is the generation of prevascularized grafts harboring a vascular network, able to rapidly anastomose with the blood vessels of the host site upon transplantation, thereby promoting cell survival, differentiation, and physiological integration of the engineered tissue [12-14]. Such a self-assembly of organotypic capillary networks can be achieved *in vitro* by co-culture of primary endothelial cells (EC) and stromal cells (e.g. mesenchymal stem cells, dermal fibroblasts) in three-dimensional (3D) cultures. Certain stromal cells may differentiate into perivascular cells (pericytes), which are involved in the development and remodelling of blood capillaries by stabilizing and guiding EC and by releasing pro-angiogenic growth factors, such as angiopoietin, FGF, VEGF, and TGF [15-16]. Several attempts aimed to develop a vascularized dermal equivalent by using human dermal fibroblasts (HDF) and EC, such as human dermal microvascular endothelial cells (HDMEC) [17-18], human umbilical vein endothelial cells (HUVEC) [19-21], or human blood outgrowth endothelial cells (HBOEC) [22]. However, many of these approaches are based on dermal stromal and other vasculogenic cells which are difficult to obtain in sufficient numbers. Therefore, their clinical application is difficult to envision.

The disadvantage of using autologous dermal fibroblasts in combination with HDMEC is their cumbersome and time-consuming isolation and culture procedure. Other EC, like HUVEC and HBOEC are derived from sources such as umbilical cord and cord blood, which are both allogeneic to the patient and potentially immune-reactive. Application of

peripheral blood-derived HBOEC is limited due to their low precursor frequency, long *in vitro* cell differentiation, and prolonged expansion time. Furthermore, the *in vivo* vasculogenic capacity of HBOEC declines rapidly with time in cell culture [23]. Other investigators using HUVEC reported their impaired survival and *in vivo* skin engraftment unless the cells were transduced with an anti-apoptotic Bcl-2 gene [24].

The ideal clinical approach to create a prevascularized dermal equivalent should use abundant autologous cells, derived from a single-cell source, and easy harvested from the patient with minimal donor-site morbidity. Therefore, the stromal vascular fraction (SVF) of human adipose tissue is a promising option since it perfectly corresponds to the above-mentioned profile [25]. The SVF is known as a heterogeneous population of multipotent stem and progenitor cells, including EC, stromal cells, pericytes, preadipocytes, as well as hematopoietic cells [26-30].

The advantages of the SVF are the following: First, one-single SVF biopsy delivers autologous stromal, vasculogenic and pericytic cells in an ideal ratio. Second, unlike other cell types, such as skin-derived fibroblasts and EC, SVF cells reveal a high vasculogenic potential across all age groups, even in elderly patients or with burns [31-32]. Third, cells of the SVF can be isolated in a fully automated procedure [33], in large quantities so that they do not require *in vitro* expansion, and can be used freshly, e.g. for direct intraoperative use [34]. SVF-seeded constructs have been shown to improve heart function and sustain microvascular perfusion and function in the infarct area [35-36]. Moreover, it has been demonstrated that if cultured within 3D scaffolds, the combination of endothelial and stromal cells both derived from the SVF assemble into vascular structures, thus actively contributing to the vascularization of tissue-engineered bone grafts, and stimulating their engraftment *in vivo* [37-38].

Upon expansion in standard monolayer cultures on tissue culture plastic, the SVF yields a homogeneous, plastic-adherent stromal cell population expressing typical mesenchymal/stromal markers, termed adipose stromal cells (ASC) [39-40]. Lu *et al.* provided direct evidence that the combination of two mesenchymal cell populations, namely ASC and dermal fibroblast can significantly improve epidermal morphogenesis *in vitro* [41]. ASC combined with an acellular dermal matrix (ADM) were also successfully used to accelerate wound healing of full-thickness cutaneous wounds in a murine model. In this model ASC promoted retention and neovascularization of the scaffold [42].

In the present study, we aimed at using the SVF to generate skin grafts containing their own intrinsic microvascular plexus as a nutritional support for both, the dermal and the

epidermal compartment. We found that SVF cells developing into a functional capillary plexus prior to transplantation markedly enhanced graft take and remodeling upon rapid graft perfusion four days after transplantation, thereby supporting survival, and triggering functionality of the transplanted graft.

Materials and Methods

Cell isolation and culture

Human subcutaneous adipose tissue samples were obtained either from lipoaspirates or fat excisions from healthy human donors (between 18 and 68 years of age), female or male, mostly from abdominal body location, all of them undergoing a surgical fat liposuction or excision operation. All donors gave their informed consent and the study protocol was approved by the local ethical committee (EKBB, Ref. 78/07). Lipoaspirates or excised fat samples were minced into small pieces and digested with 0.075% (W/V) type II collagenase (355 U/mg, Worthington, Lakewood, NJ, USA) for 60 min at 37°C under shaking. After centrifugation at 200 g for 10 min, the oil and aqueous layers were discarded. The resulting pellet was washed in phosphate buffered solution (PBS, Gibco, Invitrogen, Carlsbad, CA, USA) and passed through a 100 µm and 40 µm strainer. Red blood cells were lyzed by incubation for 2 min with a buffer containing 0.15 M/l ammonium chloride, 1.0 mM/l potassium bicarbonate (both Merck, Darmstadt, Germany), and 0.1 mM/l Na-EDTA (Fluka Analytical, Sigma-Aldrich Chemie GmbH, Buchs, Switzerland). After centrifugation and washing in PBS, the SVF cell pellet was resuspended in a complete medium (CM) consisting of α-Modified Eagle's Medium (α-MEM, Gibco) supplemented with 10% fetal bovine serum (FBS), 1% hepes, 1% sodium pyruvate and 1% penicillin-streptomycin-glutamin (100x) solution (all from Gibco), stained with crystal violet (Sigma) and counted by using a Neubauer chamber. We routinely isolated $1.6 – 0.9x10^5$ nucleated cells from 1 ml of a fat liposuction biopsy and $1 – 0.55x10^5$ nucleated cells from 1 gram of an excision biopsy [33].

For monolayer expansion, SVF cells were seeded at a density of $2×10^3$ cells/cm^2 onto tissue culture plates, cultured in CM supplemented additionally with 5 ng/ml FGF-2 (R&D Systems) and passaged at a density of $3×10^3$ cells/cm^2 when confluent. The donor-matched, monolayer-expanded adipose-derived cells will be thereafter referred to as adipose stromal cells (ASC), to distinguish them from the population of freshly isolated SVF cells. Human

skin-derived dermal fibroblasts (HDF) and keratinocytes (KC) were isolated and expanded from foreskin (males between 2 and 18 years of age) as previously described [2].

Cell characterization

The phenotype of freshly isolated SVF cells was determined by flow cytometry analysis. Cells were incubated for 30 min at 4°C in CM with different fluorochrome-conjugated antibodies against human CD31, CD34, CD73, CD90, CD146 (all from BD Bioscience, Franklin Lakes, NJ, USA) or CD105 (Serotec, Oxford, United Kingdom). Isotype IgGs were used as controls (all from BD Biosciences). After washing, cells were resuspended in FACS buffer (0.5% human serum albumin, 0.5 mM EDTA in PBS) and analyzed with a FACSCalibur flow cytometer (BD Biosciences).

Preparation of vascDESS, non-vascDESS, and HDF-DESS

Fibrin hydrogels were prepared using fibrinogen from bovine plasma (Sigma-Aldrich) reconstituted in 0.9% NaCl at a final concentration of 10 mg/ml. To achieve a comparable cell seeding inside the hydrogel, we seeded 3×10^5 SVF cells, 7.5×10^4 ASC, or 7.5×10^4 HDF per 3 ml gel. The concentration of SVF cells was optimized with respect to generating a functional and homogeneous dermal capillary plexus prior to transplantation. The corresponding prevascularized grafts started to be efficiently perfused 3-4 days after transplantation. The SVF contained 26±4% of mesenchymal and 28±9% of endothelial cells, whereas HDF or ASC-seeded gels contained 100% of stromal HDF or ASC cells, respectively. The table below demonstrates a comparison of cell population content between SVF, HDF, and ASC used for DESS transplantation experiment.

% of cells	**SVF**	**HDF**	**ASC**
stromal cells	26±4	100	100
endothelial cells	28±9	0	0

The seeding density of the cells was normalized according to the number of mesenchymal cells, which were approximately four times higher in ASC than in the SVF. We seeded 1×10^5 SVF cells per 1 ml of hydrogel to reconstitute the dermal skin compartment [2-3, 43].

Cells were centrifuged, resuspended in 100 µl EGM-2MV medium (Lonza, Basel, Switzerland) and mixed with 3 ml of the fibrinogen solution. The gels were placed in 6 well cell culture inserts with membranes of 3.0 µm pore-size (BD Falcon, Germany).

Polymerization was initiated by adding 33 µl of thrombin (Sigma Aldrich, 100 U/mL) and the gels were kept for 10 min at room temperature following by 1 h at 37°C in a humidified incubator containing 5% CO_2. To prepare collagen hydrogels, rat collagen type I (BD Bioscience, Franklin Lakes, NJ, USA) was mixed with 0.2 ml neutralization buffer containing 0.15 M NaOH [2-5]. After polymerization period, EGM-2MV was added to the upper and lower chambers of fibrin/collagen hydrogels, they were incubated for one or three weeks and analyzed for vascular network formation. To prepare dermo-epidermal skin substitutes (DESS) for transplantation, cells were cultured for two weeks in fibrin/collagen hydrogels in EGM-2MV medium, subsequently covered by keratinocytes (7.5×10^4/gel), cultured for additional one week, and transplanted onto the immuno-incompetent rats (Supplementary Figure 1) [2]. Stromal cells (with or without EC) formed the dermal compartment, whereas keratinocytes constituted the dominating cell type in the epidermal compartment of DESS. As the dermal compartment of vascDESS was prevascularized *in vitro*, it contained already a mature network of human engineered capillaries.

Transplantation of tissue-engineered skin substitutes

The surgical protocol was approved by the local Committee for Experimental Animal Research (permission number 76/2011). Immuno-incompetent female nu/nu rats, eight to ten weeks old (Harlan Laboratories, Netherlands), were prepared and anesthetized as previously described (three independent donors for SVF (n=6 per condition; 18 rats) and ASC (n=6 per condition; 18 rats), and four for HDF (n=4 per condition; 12 rats) (in total 48 rats) [44]. DESS were transplanted onto full-thickness skin defects created surgically on the backs of the rats.

To protect the transplants and to prevent wound closure from surrounding rat skin, custom made steel rings (diameter 2.6 cm) were sutured into full-thickness skin defects created on the backs of the rats, using non-absorbable polyester sutures (Ethibond®, Ethicon, USA). The transplants were then covered with a silicone foil (Silon-SES, BMS, USA), a polyurethane sponge (Ligasano, Ligamed, Austria), a cohesive conforming bandage (Sincohaft, Theo Frey AG, Switzerland), and tape as wound dressing. By these means the bandaged site was fully protected and the rat could not scratch the transplant. Dressing changes and photographic documentations were performed once per week. After 4, 7, and 14 days the transplanted skin analogs were excised *in toto* and processed for cryo- and paraffin sections, and electron microscopy.

Macroscopic assessment of the epidermal coverage area

On day 4, 7, and 14 following surgery, the skin grafted areas were macroscopically assessed using planimetry [44]. Transplanted skin regions with whitish, smooth appearance were considered to be healthy epidermis, and calculated in all skin grafts: vascDESS (SVF) (n=6), non-vascDESS (ASC) (n=6), and HDF-DESS (HDF) (n=4) using computer software (NIH ImageJ) (http://rsb.info.nih.gov/ij/).

Histological analysis

Paraffin sections (5 µm) were stained with hematoxylin and eosin (Sigma-Aldrich) to assess the histological morphology in the transplanted DESS.

Immunohistochemical staining

Immunofluorescence staining was performed as described in Biedermann *et al.* and Montano *et al*. [3, 17]. Briefly, cells cultured on tissue culture plastic or cryosections were fixed and permeabilized in acetone for 5 min at -20°C, air dried, washed three times in PBS, and blocked with 2% BSA in PBS (Sigma-Aldrich) for 30 min. Incubation with the diluted antibodies was performed in blocking buffer for 1 h at room temperature. Slides were washed three times for 5 min in PBS and blocked for an additional 15 min before the second antibody was added. Finally, the slides were incubated for 5 min in PBS containing 1 µg/ml DAPI (Sigma-Aldrich), washed twice for 5 min in PBS, and mounted in Dako mounting solution (Dako, Baar, Switzerland). Sections of transplanted paraffin-embedded skin grafts were deparafinized (xylol, 3×10 min), dehydrated (ethanol 100–96–80–70–50%, 2 min each), and washed in PBS (3×5 min). The sections were boiled in citric buffer for antigen retrieval and incubated for 30 min in 0.1% Triton X-100 (Sigma Aldrich) and blocked in 10% BSA in PBS (Sigma-Aldrich) for 30 min. Immunostaining was performed using a primary antibody, or control IgG, followed by FITC or TRITC-conjugated secondary antibody (Dako, Switzerland). Pictures of immunofluorescence stainings were taken with a DXM1200F digital camera connected to a Nikon Eclipse TE2000-U inverted microscope. The device is equipped with DAPI-, FITC-, and TRITC-filter sets (Nikon AG, Switzerland; Software: Nikon ACT-1 version 2.70). Images were processed with Photoshop 7.0 (Adobe Systems Inc, Germany).

Antibodies

For immunofluorescence the following antibodies were used - from Abcam (Cambridge, UK): collagen type I (clone: ab6308, 1:100), NG2 (clone: ab83508, 1:100); from BD Pharmingen (Basel, Switzerland): Ki-67 (clone B56, 1:200), CD31 (clone TDL-3A12, 1:50); from Progen (Heidelberg, Germany): CK16 (clone LL025, 1:100), CK17 (clone: 61036, 1:50); from Dako: CK19 (clone RCK108, 1:100), CD31 (clone JC7I, 1:150), αSMA (clone: M0851, 1:100); from R&D Systems Inc. (Minneapolis, USA): VE-cadherin-PE (clone: 123413, 1:50); from Dianova (Germany): CD90 (clone AS02, 1:50); from Santa Cruz (Labforce AG, Nunningen, Switzerland): laminin 5 (clone P3H9-2, 1:100). As a secondary antibody we used FITC or TRITC-conjugated immunoglobulins (Dako). For double immunofluorescence, some of the primary antibodies were pre-labeled with Alexa 488 or 555-conjugated polyclonal goat F(ab′)2 fragments, according to the manufacturer's instructions (Zenon Mouse IgG Labeling Kit, Molecular Probes, Invitrogen).

Whole-mount staining

Fibrin/collagen hydrogels cultured with the SVF or ASC for one or three weeks in vitro were fixed in 4% PFA and analyzed for capillary network formation (n=9 samples; from three independent donors/experiments). Gels were blocked for unspecific binding and permeabilized with 0.1% Triton X-100/10% FBS for 1 h at room temperature, and incubated with rabbit anti-CD31, mouse anti-αSMA, mouse anti-VE-cadherin, mouse anti-NG2 antibodies, and AlexaFluor 488 and 555-conjugated secondary antibodies (Invitrogen). Tissues were mounted in Dako mounting solution (Dako, Baar, Switzerland) for confocal imaging using a Leica SP1 confocal laser scanning microscope (Leica, Heerbrugg, Switzerland). Images were processed with Imaris 5.0.1 (Bitplane AG, Zurich, Switzerland).

Electron microscopy

For transmission electron microscopy analyses, fibrin hydrogels (samples of approximately $1mm^3$) were prefixed in 0.1 M cacodylate buffer (Merck, Germany) (pH=7.3) containing 2.5% glutaraldehyde for two hours, washed in cacodylate buffer, post-fixed with an aqueous solution of 1% OsO_4 and 1.5% $K_4Fe(CN)_6$ for one hour, dehydrated, and finally embedded in EPON 812 (Catalys AG, Switzerland). Ultrathin sections (approximately 50-70 nm) were collected on copper grids, contrasted with 4% uranyl acetate and 3% lead citrate, and

examined with a CM 100 transmission electron microscope (Philips, The Netherlands). All reagents were from Sigma unless mentioned otherwise.

Quantification of human capillary networks *in vitro* and *in vivo*

Whole-mounted fibrin/collagen hydrogels or transplanted skin graft sections were imaged by the confocal microscope. Distinct vascular parameters (number of capillaries, branch points, average and total capillary length, capillary maturity level, perfused capillaries) were quantified per mm^2 of hydrogel or transplant section using immunofluorescence staining against anti-human/rat CD31/αSMA antibody (n=6 per condition; from 3-4 independent donors/experiments). 3D confocal projection images were subjected to a series of image analyses (NIH ImageJ) allowing quantification of distinct parameters.

The number of human erythrocyte-perfused $CD31^+$ capillaries (auto-fluorescence of erythrocytes) was counted manually.

Quantification of collagen content *in vivo*

Deposition of collagen type I in the transplanted fibrin-derived skin grafts was visualized using anti-collagen type I immunofluorescence staining. For each sample, five sections (×10 magnification were captured to quantify relative collagen deposition (n=4-6 per condition; from three/four independent donors/experiments). The positively stained area was measured using the same macroscopic settings and quantified using NIH ImageJ software.

Quantification of neo-dermis thickness *in vivo*

Sections stained with human specific CD90 antibody were captured using the same macroscopic settings (n=6 per condition; from three independent donors/experiments). The thickness of the neo-dermis (hCD90-positive region) was measured using ImageJ software-based analysis.

Quantification of number of proliferating cells in vivo

Transplanted skin grafts were stained for Ki-67, and the ratio of proliferating nuclei (positive for Ki-67) over total nuclei (positive for DAPI) was quantified using ×20 magnification. In order to examine the proliferation rate of human EC, sections were co-stained for Ki67 and

hCD31$^+$, and Ki67$^+$hCD31$^+$ cells were quantified over total hCD31$^+$ cells. Six microscopic fields at ×20 magnification were used in each group (n=4-6 per condition; from three/four independent donors/experiments).

Statistical analysis

All results are reported as mean ±SD. Statistical analysis was performed with GraphPad Prism 4.0 (Graph Pad software, La Jolla, CA, USA). Comparison between two groups was performed using the unpaired Student's t test.

Results

Characterization of the SVF and expanded ASC

Distinct human SVF, harvested from five donors, consisted of a heterogeneous cell population (Fig. 1). Two different cell fractions were identified by cytofluorimetry: an endothelial (CD31+CD34+) one and a mesenchymal (CD73+CD90+) one (Fig. 1A, B). These findings confirm previously published data [37].

The CD31$^+$CD34$^+$ co-expression on the endothelial cell fraction was detected on approximately 28±9% of the whole SVF-population (n=5) (Fig. 1A). This CD31$^+$CD34$^+$ endothelial cell fraction was further characterized by quantifying the co-expression of other markers, including CD90 (Thy-1) (85±8%) and CD105 (endoglin) (91±9%) - markers expressed both by stem/progenitor and endothelial cells, and CD146 (S-Endo-1/MCAM) (68±8%) - a cell marker expressed among others on mature endothelial cells (e.g. HDMECs).

To further evaluate the phenotype, morphology, and adherence to cell culture plastic of cell types present in the SVF, we grew them on tissue culture plastic overnight and performed analyses for lineage-specific markers (Fig. 1C-F). Phase contrast data shown in Fig. 1C illustrate a characteristic colony of cells containing both, epithelioid and spindle-shaped cells. The colonies were typically surrounded by single spindle-shaped cells (white arrows). The colonies obviously consisted of CD31-positive cells and of cells positive for the stem/progenitor cell marker CD34, whereas only some of the single surrounding cells were CD34-positive and all were negative for CD31 (Fig. 1D). Figures 1E and F show that the colonies, in addition to vWF/CD31$^+$ endothelial cells contain cells positive for

mesenchymal/pericyte markers such as alpha-smooth muscle actin (αSMA) (Fig. 1E) and CD90 (Fig. 1F).

In vitro expansion of the SVF resulted in an adherent, homogeneous cell population that neither expressed CD31 nor CD34, hence the endothelial cell fraction was lost upon culturing. Instead all these cells co-expressed CD90 and CD73 (Fig. 1G, H). These data were confirmed by phase contrast microscopy (Fig. 1I) and immunofluorescence stainings revealing that the remaining population consisted of αSMA^+ (Fig. 1K) and $CD90^+$ (Fig. 1L) fibroblastic cells. These are commonly referred to as adipose-derived stromal cells (ASC) [37].

Vascular network formation in a 3D hydrogel *in vitro*

The 3D cellular microenvironment is known to have a strong impact on stem cell differentiation and functionality [45-46]. Either the freshly isolated SVF or donor-matched adipose stromal cells (ASC) were submerged into 3D fibrin and collagen type I hydrogels and cultured for one, or for three weeks *in vitro*, respectively. The ability of fibrin and collagen scaffolds to support the spontaneous formation of a vascular network *in vitro* was evaluated (Fig. 2). We did not detect any differences in the morphology and capillary network characteristics using these two types of scaffolds (data not shown).

After three weeks, confocal microscopy revealed branching capillaries in SVF-seeded fibrin hydrogels (Fig. 2A-D). In contrast, no microvascular structures were observed in the control group seeded with ASC. The specific staining for human endothelial markers, such as CD34, vascular endothelial cadherin (VE-cadherin), and CD31 confirmed that the EC population was not only retained within the 3D hydrogel, but also developed into capillaries (Fig. 2A-D, respectively). $CD34^+$ EC arranged into branching lumenized networks of microvessels occasionally originating from the centre (white star) of a given capillary arrangement (Fig. 2A). VE-cadherin expression was frequently detected in EC lining those capillaries (Fig. 2B). The lumen of the capillaries is marked in Fig.2 A and B by white arrows.

As the development of true capillaries involves not only lumen formation, but also their stabilization by pericytes, we performed co-staining for pericyte- (αSMA, neuron/glia-type 2 antigen (NG2)) and endothelial-specific marker (CD31), respectively (Fig. 2C, D). We found αSMA-positive cells (white arrows) closely associated with $CD31^+$ capillaries (Fig. 2C). However, αSMA-expressing cells were detected also at a distance from the capillaries

(Fig. 2C, white arrowheads). Pericyte-like cells expressing NG2 were wrapped around $CD31^+$ capillaries (Fig. 2D, white arrows) and were found exclusively at this perivascular location.

The formation of highly organized and mature capillaries *in vitro* was further confirmed by transmission electron microscopy (TEM) (Fig. 2E-G). A representative capillary cross-section in Fig. 2E shows several EC interconnected by intercellular junctions (green dotted lines), desmosomes (green arrowheads), and organized around a lumen [47-49].

The presence of characteristic endothelial structures including caveolae (special type of lipid rafts; small invaginations of the plasma membrane) [50], pinocytic vesicles, as well as pseudopodia [51], were also observed (Fig. 2E, G). At the basal site of EC and pericytes, a basal lamina was deposited as demonstrated by yellow arrows (Fig. 2E, F). Pericytes appeared as polymorphic cells in a close contact with EC. Notably, characteristic contacts between endothelial and pericytic cells formed by cytoplasmic invaginations and interruptions in the capillary basement membrane, known as "peg-and-socket" junctions, were observed (Fig. 2E, F) [52].

To determine whether there was a significant difference in branching and capillary interconnections, EC-harboring fibrin hydrogels were examined either at one, or at three weeks after cell seeding (Fig. 3). Using immunofluorescence stainings for human CD31, four different quantitative parameters characterizing the extent of capillary formation and ramification, namely the number of vascular structures per mm^2, branch points, as well as the total and average capillary length, were evaluated (n=9, from three independent donors). All parameters were significantly higher at three weeks as compared to one week, except the average capillary length (Fig. 3C-F). Consequently, the cells in fibrin hydrogels were cultured for three weeks before they were used for pre-clinical transplantation experiments.

Engineered human blood capillaries are functional *in vivo*

To demonstrate functionality of the human capillary plexus *in vivo*, hydrogels prevascularized by cells of the SVF were covered with human primary keratinocytes, now referred to as prevascularized dermo-epidermal skin substitutes (vascDESS), and transplanted onto the backs of immune-compromised rats (Supplementary Figure 1). Skin grafts containing donor-matched adipose stromal cells (ASC) were used as a non-vascularized control (non-vascDESS). The skin grafts were retrieved and examined at various time-points, namely 4, 7, and 14 days after transplantation (n=6 per condition, from three independent donors for both SVF and ASC).

Hematoxylin/eosin stainings of the sections of vascDESS revealed blood perfused capillaries as early as four days after transplantation (Fig 4A). There was a surprisingly high number of perfused capillaries at 7 and 14 days after transplantation (Fig. 4B, C), thus underlining the efficacy of the method. In contrast, non-vascDESS (control) did not contain any perfused capillaries at any time point (Fig. 4D-F). Already 4 days after transplantation, some human $CD31^+$ capillaries were closely associated with rat $CD31^+$ blood vessels (Fig. 4G, a higher magnification is shown in Supplementary Figure 2). Human-rat chimeric vessels were even more apparent at day 7 and 14 after transplantation (Fig. 4H, I, respectively). In contrast, non-vascDESS, did not contain any human CD31-expressing capillaries at any time-point (Fig. 4J-L), whereas ingrowing capillaries of rat origin were observed at 14 days after transplantation (Fig. 4L). Apparently these rat capillaries were not yet perfused at this time point since they did not contain erythrocytes.

The dynamics of blood perfusion in capillaries formed by human EC in the transplanted vascDESS was evaluated. Sections of grafts from all independent studies (n=6 per condition, three independent donors) were assessed by staining for human CD31 and subsequently quantified. At day 4 after transplantation, the total number of human capillaries per mm^2 was significantly lower (13±4) than after 7 days (25±10), however the highest number was found 14 days after transplantation (45±12) (Fig. 4M and Supplementary Table 1). Perfusion of the pre-existing human capillaries was analyzed based on the auto-fluorescence of rat erythrocytes in human CD31-positive capillaries. At day 4 only about 29±15% of all tissue-engineered capillaries were blood-perfused. The number of perfused capillaries increased to 82±20% at day 7, and to 89±10% at day 14 (Fig. 4M and Supplementary Table 1).

Maturation of tissue-engineered capillary networks *in vivo*

To assess the maturation of tissue-engineered human capillaries *in vivo*, sections of grafts 7 and 14 days after transplantation, were co-stained for the human endothelial marker (hCD31) and the pericyte marker (αSMA). The latter antibody recognized both human and rat αSMA (Fig. 5A-C and Supplementary Table 2). These analyses revealed that at day four after transplantation of vascDESS approximately 50±21% of human $CD31^+$ capillaries were already associated with pericytes (Fig. 5C). At day seven, 80±6% of human capillaries were supported by αSMA-positive pericytes (Fig. 5A, C), and almost all human capillaries (96±5%) showed double-staining for CD31 and αSMA at day 14 (Fig. 5B, C).

The proliferation rate of EC in human capillaries *in vivo* was analyzed by using an antibody to Ki67, a nuclear protein expressed in cycling cells [53] (Fig. 5D-F). This antibody did not discriminate between human and rat Ki67-positive cells. Double-staining for hCD31 and Ki67 showed an intensive phase of proliferation between day 4 and day 7, followed by a decrease at day 14 (Fig. 5D-F).

Epidermal regeneration in vascDESS *in vivo*

We hypothesized that increased neovascularization of vascDESS promotes epidermal development and functionality of the grafts *in vivo*. To prove this hypothesis, we macroscopically assessed the graft size *in vivo* by planimetry (Fig. 6A). Fig. 6A represents a macroscopic examination of vascDESS at day four after transplantation. Skin grafts containing ASC or human dermal fibroblasts (HDF) were used as a control (non/vascDESS and HDF-DESS, respectively) (n=6, from 3-4 independent donors). ASC and HDF-seeded gels contained only ASC or HDF cells, respectively, lacking endothelial cells. Engraftment was considered successful when the human epidermis on the graft was continuous, whitish, and smooth in appearance (Fig. 6A). By these criteria a complete take of all skin grafts was observed four days after transplantation within all the three groups containing SVF (vascDESS), ASC (non-vascDESS), or dermal fibroblasts (HDF-DESS). However, the planimetric analysis demonstrated that the graft size of the vascDESS group was significantly larger at day 4, day 7, and day 14, as compared to the non-vascDESS transplants (Fig. 6B) [54]. These results demonstrate that SVF-based prevascularization not only supported epidermal coverage, similar to HDF at day 4 and 7 following transplantation, but also reduced graft contraction as seen at day 14 (n=4-6 per condition).

Dermal SVF, ASC, or dermal fibroblasts clearly promoted the stratification of keratinocytes, resulting in the formation of a multilayered epidermis containing a basal layer (Fig. 6C-K). However, differences in the morphogenesis and homeostasis of the *in vivo* regenerated epidermis were observed, suggesting that keratinocytes were affected by these three mesenchymal cell types. We evaluated the formation of a basement membrane at the dermo-epidermal junction by the presence of human specific laminin 5, and confirmed its expression in all three types of skin grafts (day 14 *in vivo*) (Fig. 6F-K, respectively).

Additionally, the wound healing and homeostasis markers were analyzed in the newly formed epidermis *in vivo*. Normal, homeostatic interfollicular epidermis lacks the expression of both cytokeratins (CK) 16 and 17 [3, 55-56]. They are, however, induced in suprabasal

keratinocytes in wound situations, including epidermal regeneration after transplantation. The staining for CK16 and 17 revealed that the period of wound healing was dramatically decreased in vascDESS (Fig. 6C, F), as compared to both control groups: non-vascDESS (Fig. 6D, G) and HDF-DESS (Fig. 6E, H). As for the duration of the wound healing status of the tested grafts this finding points to a significant difference between vascDESS and HDF-DESS.

A major difference in the expression pattern of the skin homeostasis marker CK19 was observed among the three skin transplant groups (Fig. 6I-K). In normal interfollicular epidermis of young children (up to 18 months in age), and in a certain state of our transplanted skin grafts, CK19-positive keratinocytes are clustered in the stratum basale, while in older children and adults these $CK19^{+}$ cell clusters disappear completely [2]. In vascDESS (Fig. 6I) and HDF-DESS (Fig. 6K), the expression of CK19 was indeed confined to the epidermal basal cells, demonstrating a certain "intermediate" state of homeostasis, whereas in non-vascDESS (Fig. 6J), CK19-positive keratinocytes were still distributed in all suprabasal layers indicating that in these grafts tissue homeostasis was still far from being established [2].

Dermal remodelling of vascDESS *in vivo*

To gain information on both the dimensions of the human neo-dermis in vascDESS, and the capillaries in it after transplantation, sections of transplanted vascDESS were stained for the human specific CD90 antigen (Fig. 7A). As demonstrated in Fig. 7A, engineered hCD31-positive capillaries were abundant in the $CD90^{+}$ neo-dermis of transplanted vascDESS.

In the following, we examined, whether the rapid vascularization of vascDESS had an effect on the thickness of the regenerating neo-dermis *in vivo* (Fig. 7B). Quantitative analyses revealed that the thickness doubled in vascDESS between day 4 and 7, and further increased at day 14. In comparison, the dermal regeneration process of non-vascDESS was delayed and led to a significantly thinner neo-dermis (n=6 per condition) (Fig. 7B).

The content of collagen type I was further evaluated in the grafts by immunostaining. Comparing the deposition of collagen I in vascDESS, non-vascDESS and HDF-DESS correspondingly *in vivo*, we consistently found the highest collagen content in vascDESS at all time points investigated (Fig. 7C). Of note, ASC cells in non-vascDESS showed a significantly higher capacity of collagen type I deposition during dermal wound healing than HDF.

As we observed a rapid and efficient vascularization and perfusion of vascDESS after its transplantation, we set out to determine a possible effect of this rapid nutrition on epidermal/dermal cell proliferation. For that the expression of Ki67 in the three types of skin grafts was investigated. These analyses revealed a significantly increased percentage of cycling, Ki67-expressing cells in both the epidermal and dermal compartment of vascDESS as compared to the two control groups (Fig. 7D). Taken together, these data are in line with the conclusion that the rapid perfusion of the tissue-engineered capillary plexus in vascDESS has clear positive effects on the reconstitution process of the respective transplanted skin grafts.

Discussion

The absence of functional vascular structures is still one of central hurdles in tissue engineering and regenerative medicine. Tissue-engineered dermo-epidermal skin grafts (DESS), let alone any off-the-shelf products, although only still rarely applied in the clinic, are usually not prevascularized. As a consequence, even these very promising grafts, representing a surgical option at the forefront of plastic and burn surgery, are still dependent on diffusion (imbibition) in the first weeks upon transplantation until vascular ingrowth from the host site occurs. Accordingly, they experience a physiological crisis because of impaired nutrition, oxygen and growth factor supply in the initial 2-3 weeks after transplantation. This may well result in an expanded and somewhat misdirected phase of regeneration followed by fibrosis and other scar-like formations.

The goal of this study was to introduce a prevascularized, dermo-epidermal skin graft to be used clinically in an autologous and permanent fashion. The starting cell population was derived from the SVF isolated from human adipose tissue. There are several lines of evidence showing that cells from the SVF can spontaneously develop a microvasculature *in vitro* and *in vivo* [37, 57-58]. However, the mechanism of how SVF cells assemble into a capillary plexus, still remains unclear. Although endothelial cells play a crucial role in this process, they are not sufficient to establish a mature vascular network either *in vitro* [59] or *in vivo* [60]. As demonstrated in our study, and by others, at least a second (mesenchymal) cell type is necessary to foster the formation of stable and functional vascular networks [59, 61]. We show in this study that it is a peculiar and very convenient feature of the SVF that the ratio of cell types involved in capillary formation is intrinsically optimal and constant, ideally

supporting the development of capillary networks in fibrin or collagen hydrogels. This is in contrast to human dermal microvascular endothelial cells, HDMEC, which develop into capillaries when co-seeded with human dermal fibroblasts in a ratio of 1:1 within fibrin hydrogels [17]. Adjusting and maintaining the ratio of 1:1 is a labour-intensive process, and in contrast to the well balanced ratio of vasculogenic cell types of the SVF, this ratio can not be easily maintained in culture. Consequently, the dermal fibroblasts overgrow and dominate the graft. This may largely interfere with the development of capillary networks.

We show here that the optimal vasculogenic properties of the SVF were an exclusive feature of fresh SVF isolates and that culturing has a negative impact on the initial characteristics of SVF cells. This was indicated not only by the significantly impaired capillary formation, but also by the position of the cells in the *de novo* formed vasculature. Endothelial and perivascular cells were derived from fresh SVF isolates, whereas mostly perivascular cells were derived from cultured SVF. Flow cytometry of select markers revealed high expression of CD31 and CD34 in cells of fresh SVF isolates. However, both markers were rapidly downregulated upon 2D culture, suggesting a loss of endothelial cells as previously observed [37]. This reduction resulted in a lower density of newly formed capillaries by the cultured SVF cells *in vivo* and is consistent with the idea that the endothelial cells present in SVF cell isolates are required for capillary formation [57]. As pointed out by Traktuev *et al.* and Lin *et al.* the proportion of cells exhibiting a perivascular phenotype (αSMA^+ cells) does not change with culture [62-63]. This is again consistent with the finding that cultured SVF, hence ASC, preferentially incorporate as mural cells into angiogenic neovessels [63].

As already mentioned above, the endothelial cell fraction is usually rapidly lost in 2D cultures. We managed to expand and maintain the endothelial cell fraction of the SVF, by integrating it into a previously developed tissue-engineered, hydrogel-based, 3D dermo-epidermal skin graft [2, 5, 64]. In such a permissive environment, SVF cells formed spontaneously and *de novo* a mature microvascular plexus, which thereafter became denser and more ramified. Interestingly, the histological composition of these capillaries was similar to the composition of normal human capillaries, exhibiting normal sized lumina, pericyte coverage and organotypic microstructures, such as a basal lamina, "peg-and-socket" junctions, pseudopodia, caveolae, pinocytotic vesicles, and complex intercellular junctions. Of note, these specific features confirmed ultrastructurally the presence and interaction of EC and pericytes in the engineered vascular structures

Importantly, the tissue-engineered capillary plexus served as a functional (dermal) vascular interface between the recipient's circulation and the epidermis (the epithelium) of the DESS. Notably, the connection between the rat microvascular system and the human tissue-engineered vascular plexus occurred as early as 3-4 days after transplantation of the DESS. This rapid perfusion resulted in several positive effects (in comparison to non-vascDESS), which were: a) the significant increase of the transplanted dermo-epidermal area, indicative of the absence of shrinkage, most likely due to the efficient blood supply, b) increased collagen type I deposition, c) increased cell proliferation of both dermis and epidermis, hence an increased thickness of both tissues, d) reduced and shorter expression of typical wound healing markers, such as CK16 and CK17, e) significantly faster establishment of epidermal homeostasis. All these positive effects are important prerequisites for the clinical use of the SVF. In particular, the significantly reduced contraction of vascDESS may mean a major clinical improvement [65]. Contraction is especially dramatic in young patients, namely in the areas of the joints, which forces these patients to undergo repetitive, painful surgeries, and long hospitalization time.

In addition, the SVF is relatively abundant and accessible in comparison to other adult autologous cell sources and can be used directly after tissue harvest and cell isolation, without *in vitro* expansion. Furthermore, multiple Phase I clinical trials using adipose-derived SVF are suggesting that these cells are safe and can be efficiently transplanted in either an autologous or allogeneic manner [66-67]. Given these facts together with the notion that a single-cell source can give rise to efficient vascularization of a tissue-engineered graft makes this approach practical and clinically very attractive.

Conclusions

Our study provides a key improvement in maintaining the endothelial cell population of the stromal vascular fraction (SVF) in 3D hydrogels, which is otherwise rapidly lost in 2D culture. We present a detailed analysis of the *de novo* formation of SVF-based microvascular networks, their maturation, and integration into dermo-epidermal skin grafts. After transplantation, these preformed capillaries prove to be a key stimulator of rapid blood perfusion and dermo-epidermal regeneration. We conclude that the adipose-derived SVF represents a convenient source of endothelial cells and pericytes. Submerged within an appropriate 3D environment, these cells allow the *in vitro* prevascularization of human autologous dermo-epidermal skin grafts, which are a great promise for clinical use.

Conflict of interest

The authors have declared that no conflict of interest exists.

Acknowledgments

We acknowledge Gery Barmettler (University of Zurich, Switzerland) for the TEM image acquisition and analysis services, as well as his technical assistance. Moreover, we would like to thank Prof. Dr. Peter Wild (University of Zurich, Switzerland) for general advice and help with the interpretation of the TEM pictures. This work was financially supported by the Clinical Research Priority Program (CRPP) of the Faculty of Medicine of the University of Zurich to E.R., by the EU-FP7 project EuroSkinGraft (FP7/2007-2013: grant agreement No. 279024 to E.R.), by the EU-FP7 (MultiTERM, grant agreement No. 238551 to E.R.), and by the Swiss National Science Foundation (Grant No. 310030-120432 and 310030-138519 to A.S.). We are particularly grateful to the Foundation Gaydoul and the sponsors of "DonaTissue" (Thérèse Meier, Robert Zingg) for their generous financial support and interest in our work.

Appendix. Supplementary material

Supplementary Figure 1. Experimental study design.

Supplementary Figure 2. Confocal image of anastomosis in vascDESS *in vivo*.

Supplementary Table S1. Quantification of total and perfused human capillaries in vascDESS *in vivo*.

Supplementary Table S2. Quantification of total ($hCD31^+$) and mature ($hCD31^+\alpha SMA^+$) human capillaries in vascDESS *in vivo*.

References

[1] Sen CK, Gordillo GM, Roy S, Kirsner R, Lambert L, Hunt TK, et al. Human skin wounds: a major and snowballing threat to public health and the economy. Wound Repair Regen. 2009;17:763-71.

[2] Pontiggia L, Biedermann T, Meuli M, Widmer D, Bottcher-Haberzeth S, Schiestl C, et al. Markers to evaluate the quality and self-renewing potential of engineered human skin substitutes *in vitro* and after transplantation. J Invest Dermatol. 2009;129:480-90.

[3] Biedermann T, Pontiggia L, Bottcher-Haberzeth S, Tharakan S, Braziulis E, Schiestl C, et al. Human eccrine sweat gland cells can reconstitute a stratified epidermis. J Invest Dermatol. 2010;130:1996-2009.

[4] Bottcher-Haberzeth S, Klar AS, Biedermann T, Schiestl C, Meuli-Simmen C, Reichmann E, et al. "Trooping the color": restoring the original donor skin color by addition of melanocytes to bioengineered skin analogs. Pediatric Surgery International. 2013;29:239-47.

[5] Pontiggia L, Klar A, Bottcher-Haberzeth S, Biedermann T, Meuli M, Reichmann E. Optimizing *in vitro* culture conditions leads to a significantly shorter production time of human dermo-epidermal skin substitutes. Pediatr Surg Int. 2013;29:249-56.

[6] Klar AS, Bottcher-Haberzeth S, Biedermann T, Schiestl C, Reichmann E, Meuli M. Analysis of blood and lymph vascularization patterns in tissue-engineered human dermo-epidermal skin analogs of different pigmentation. Pediatr Surg Int. 2014;30:223-31.

[7] Tremblay PL, Hudon V, Berthod F, Germain L, Auger FA. Inosculation of tissue-engineered capillaries with the host's vasculature in a reconstructed skin transplanted on mice. Am J Transplant. 2005;5:1002-10.

[8] MacNeil S. Progress and opportunities for tissue-engineered skin. Nature. 2007;445:874-80.

[9] Ko HC, Milthorpe BK, McFarland CD. Engineering thick tissues-the vascularisation problem. Eur Cell Mater. 2007;14:1-18.

[10] Rivron NC, Liu JJ, Rouwkema J, de Boer J, van Blitterswijk CA. Engineering vascularised tissues *in vitro*. Eur Cell Mater. 2008;15:27-40.

[11] Scherberich A, Muller AM, Schafer DJ, Banfi A, Martin I. Adipose tissue-derived progenitors for engineering osteogenic and vasculogenic grafts. J Cell Physiol. 2010;225:348-53.

[12] Kaully T, Kaufman-Francis K, Lesman A, Levenberg S. Vascularization-the conduit to viable engineered tissues. Tissue Eng Part B Rev. 2009;15:159-69.

[13] Baranski JD, Chaturvedi RR, Stevens KR, Eyckmans J, Carvalho B, Solorzano RD, et al. Geometric control of vascular networks to enhance engineered tissue integration and function. Proc Natl Acad Sci U S A. 2013;110:7586-91.

[14] Frerich B, Winter K, Scheller K, Braumann UD. Comparison of different fabrication techniques for human adipose tissue engineering in severe combined immunodeficient mice. Artif Organs. 2012;36:227-37.

[15] Bergers G, Song S. The role of pericytes in blood-vessel formation and maintenance. Neuro Oncol. 2005;7:452-64.

[16] Jain RK. Molecular regulation of vessel maturation. Nat Med. 2003;9:685-93.

[17] Montano I, Schiestl C, Schneider J, Pontiggia L, Luginbuhl J, Biedermann T, et al. Formation of human capillaries *in vitro*: the engineering of prevascularized matrices. Tissue Eng Part A. 2010;16:269-82.

[18] Supp DM, Wilson-Landy K, Boyce ST. Human dermal microvascular endothelial cells form vascular analogs in cultured skin substitutes after grafting to athymic mice. Faseb J. 2002;16:797-804.

[19] Black AF, Berthod F, L'Heureux N, Germain L, Auger FA. *In vitro* reconstruction of a human capillary-like network in a tissue-engineered skin equivalent. Faseb J. 1998;12:1331-40.

[20] Hudon V, Berthod F, Black AF, Damour O, Germain L, Auger FA. A tissue-engineered endothelialized dermis to study the modulation of angiogenic and angiostatic molecules on capillary-like tube formation *in vitro*. Br J Dermatol. 2003;148:1094-104.

[21] Tonello C, Zavan B, Cortivo R, Brun P, Panfilo S, Abatangelo G. *In vitro* reconstruction of human dermal equivalent enriched with endothelial cells. Biomaterials. 2003;24:1205-11.

[22] Hendrickx B, Verdonck K, Van den Berge S, Dickens S, Eriksson E, Vranckx JJ, et al. Integration of blood outgrowth endothelial cells in dermal fibroblast sheets promotes full thickness wound healing. Stem Cells. 2010;28:1165-77.

[23] Melero-Martin JM, Khan ZA, Picard A, Wu X, Paruchuri S, Bischoff J. *In vivo* vasculogenic potential of human blood-derived endothelial progenitor cells. Blood. 2007;109:4761-8.

[24] Schechner JS, Crane SK, Wang F, Szeglin AM, Tellides G, Lorber MI, et al. Engraftment of a vascularized human skin equivalent. Faseb J. 2003;17:2250-6.

[25] Williams SK, Jarrell BE. Cells derived from omental fat tissue and used for seeding vascular prostheses are not endothelial in origin. Journal of Vascular Surgery. 1992;15:457-8.

[26] Baer PC, Kuci S, Krause M, Kuci Z, Zielen S, Geiger H, et al. Comprehensive phenotypic characterization of human adipose-derived stromal/stem cells and their subsets by a high throughput technology. Stem Cells and Development. 2013;22:330-9.

[27] Varma MJ, Breuls RG, Schouten TE, Jurgens WJ, Bontkes HJ, Schuurhuis GJ, et al. Phenotypical and functional characterization of freshly isolated adipose tissue-derived stem cells. Stem Cells and Development. 2007;16:91-104.

[28] Yoshimura K, Shigeura T, Matsumoto D, Sato T, Takaki Y, Aiba-Kojima E, et al. Characterization of freshly isolated and cultured cells derived from the fatty and fluid portions of liposuction aspirates. J Cell Physiol. 2006;208:64-76.

[29] Zimmerlin L, Donnenberg VS, Pfeifer ME, Meyer EM, Peault B, Rubin JP, et al. Stromal vascular progenitors in adult human adipose tissue. Cytometry A. 2010;77:22-30.

[30] Bourin P, Bunnell BA, Casteilla L, Dominici M, Katz AJ, March KL, et al. Stromal cells from the adipose tissue-derived stromal vascular fraction and culture expanded adipose tissue-derived stromal/stem cells: a joint statement of the International Federation for Adipose Therapeutics and Science (IFATS) and the International Society for Cellular Therapy (ISCT). Cytotherapy. 2013;15:641-8.

[31] Natesan S, Wrice NL, Baer DG, Christy RJ. Debrided skin as a source of autologous stem cells for wound repair. Stem Cells. 2011;29:1219-30.

[32] Natesan S, Zamora DO, Wrice NL, Baer DG, Christy RJ. Bilayer hydrogel with autologous stem cells derived from debrided human burn skin for improved skin regeneration. J Burn Care Res. 2013;34:18-30.

[33] Guven S, Karagianni M, Schwalbe M, Schreiner S, Farhadi J, Bula S, et al. Validation of an automated procedure to isolate human adipose tissue-derived cells by using the Sepax® technology. Tissue Eng Part C Methods. 2012;18:575-82.

[34] Doi K, Tanaka S, Iida H, Eto H, Kato H, Aoi N, et al. Stromal vascular fraction isolated from lipo-aspirates using an automated processing system: bench and bed analysis. J Tissue Eng Regen M. 2013;7:864-70.

[35] LeBlanc AJ, Touroo JS, Hoying JB, Williams SK. Adipose stromal vascular fraction cell construct sustains coronary microvascular function after acute myocardial infarction. Am J Physiol-Heart C. 2012;302:H973-H82.

[36] LeBlanc AJ, Nguyen QT, Touroo JS, Aird AL, Chang RC, Ng CK, et al. Adipose-derived cell construct stabilizes heart function and increases microvascular perfusion in an established infarct. Stem Cell Transl Med. 2013;2:896-905.

[37] Guven S, Mehrkens A, Saxer F, Schaefer DJ, Martinetti R, Martin I, et al. Engineering of large osteogenic grafts with rapid engraftment capacity using mesenchymal and endothelial progenitors from human adipose tissue. Biomaterials. 2011;32:5801-9.

[38] Scherberich A, Galli R, Jaquiery C, Farhadi J, Martin I. Three-dimensional perfusion culture of human adipose tissue-derived endothelial and osteoblastic progenitors generates osteogenic constructs with intrinsic vascularization capacity. Stem Cells. 2007;25:1823-9.

[39] Gimble JM, Katz AJ, Bunnell BA. Adipose-derived stem cells for regenerative medicine. Circ Res. 2007;100:1249-60.

[40] Mitchell JB, McIntosh K, Zvonic S, Garrett S, Floyd ZE, Kloster A, et al. Immunophenotype of human adipose-derived cells: temporal changes in stromal-associated and stem cell-associated markers. Stem Cells. 2006;24:376-85.

[41] Lu W, Yu J, Zhang Y, Ji K, Zhou Y, Li Y, et al. Mixture of fibroblasts and adipose tissue-derived stem cells can improve epidermal morphogenesis of tissue-engineered skin. Cells Tissues Organs. 2012;195:197-206.

[42] Huang SP, Hsu CC, Chang SC, Wang CH, Deng SC, Dai NT, et al. Adipose-derived stem cells seeded on acellular dermal matrix grafts enhance wound healing in a murine model of a full-thickness defect. Ann Plast Surg. 2012;69:656-62.

[43] Bottcher-Haberzeth S, Biedermann T, Pontiggia L, Braziulis E, Schiestl C, Hendriks B, et al. Human eccrine sweat gland cells turn into melanin-uptaking keratinocytes in dermo-epidermal skin substitutes. Journal of Investigative Dermatology. 2013;133:316-24.

[44] Schneider J, Biedermann T, Widmer D, Montano I, Meuli M, Reichmann E, et al. Matriderm versus Integra: a comparative experimental study. Burns. 2009;35:51-7.

[45] Abbott A. Cell culture: biology's new dimension. Nature. 2003;424:870-2.

[46] Burdick JA, Vunjak-Novakovic G. Engineered microenvironments for controlled stem cell differentiation. Tissue Eng Part A. 2009;15:205-19.

[47] Miranville A, Heeschen C, Sengenes C, Curat CA, Busse R, Bouloumie A. Improvement of postnatal neovascularization by human adipose tissue-derived stem cells. Circulation. 2004;110:349-55.

[48] Rehman J, Traktuev D, Li J, Merfeld-Clauss S, Temm-Grove CJ, Bovenkerk JE, et al. Secretion of angiogenic and antiapoptotic factors by human adipose stromal cells. Circulation. 2004;109:1292-8.

[49] Planat-Benard V, Silvestre JS, Cousin B, Andre M, Nibbelink M, Tamarat R, et al. Plasticity of human adipose lineage cells toward endothelial cells: physiological and therapeutic perspectives. Circulation. 2004;109:656-63.

[50] Frank PG, Woodman SE, Park DS, Lisanti MP. Caveolin, caveolae, and endothelial cell function. Arterioscler Thromb Vasc Biol. 2003;23:1161-8.

[51] Hueck IS, Rossiter K, Artmann GM, Schmid-Schonbein GW. Fluid shear attenuates endothelial pseudopodia formation into the capillary lumen. Microcirculation. 2008;15:531-42.

[52] Armulik A, Abramsson A, Betsholtz C. Endothelial/pericyte interactions. Circ Res. 2005;97:512-23.

[53] Scholzen T, Gerdes J. The Ki-67 protein: from the known and the unknown. J Cell Physiol. 2000;182:311-22.

[54] El-Ghalbzouri A, Van Den Bogaerdt AJ, Kempenaar J, Ponec M. Human adipose tissue-derived cells delay re-epithelialization in comparison with skin fibroblasts in organotypic skin culture. Br J Dermatol. 2004;150:444-54.

[55] Moll R, Krepler R, Franke WW. Complex cytokeratin polypeptide patterns observed in certain human carcinomas. Differentiation. 1983;23:256-69.

[56] Troyanovsky SM, Guelstein VI, Tchipysheva TA, Krutovskikh VA, Bannikov GA. Patterns of expression of keratin 17 in human epithelia: dependency on cell position. J Cell Sci. 1989;93 (Pt 3):419-26.

[57] Koh YJ, Koh BI, Kim H, Joo HJ, Jin HK, Jeon J, et al. Stromal vascular fraction from adipose tissue forms profound vascular network through the dynamic reassembly of blood endothelial cells. Arterioscl Throm Vas. 2011;31:1141-U539.

[58] Muller AM, Mehrkens A, Schafer DJ, Jaquiery C, Guven S, Lehmicke M, et al. Towards an intraoperative engineering of osteogenic and vasculogenic grafts from the stromal vascular fraction of human adipose tissue. Eur Cell Mater. 2010;19:127-35.

[59] Boyd NL, Nunes SS, Krishnan L, Jokinen JD, Ramakrishnan VM, Bugg AR, et al. Dissecting the role of human embryonic stem cell-derived mesenchymal cells in human umbilical vein endothelial cell network stabilization in three-dimensional environments. Tissue Eng Pt A. 2013;19:211-23.

[60] Koike N, Fukumura D, Gralla O, Au P, Schechner JS, Jain RK. Tissue engineering: creation of long-lasting blood vessels. Nature. 2004;428:138-9.

[61] Stratman AN, Malotte KM, Mahan RD, Davis MJ, Davis GE. Pericyte recruitment during vasculogenic tube assembly stimulates endothelial basement membrane matrix formation. Blood. 2009;114:5091-101.

[62] Lin G, Garcia M, Ning H, Banie L, Guo YL, Lue TF, et al. Defining stem and progenitor cells within adipose tissue. Stem Cells and Development. 2008;17:1053-63.

[63] Traktuev DO, Prater DN, Merfeld-Clauss S, Sanjeevaiah AR, Saadatzadeh MR, Murphy M, et al. Robust functional vascular network formation *in vivo* by cooperation of adipose progenitor and endothelial cells. Circ Res. 2009;104:1410-20.

[64] Biedermann T, Bottcher-Haberzeth S, Klar AS, Pontiggia L, Schiestl C, Meuli-Simmen C, et al. Rebuild, restore, reinnervate: do human tissue engineered dermo-epidermal skin analogs attract host nerve fibers for innervation? Pediatric Surgery International. 2013;29:71-8.

[65] Gauglitz GG, Korting HC, Pavicic T, Ruzicka T, Jeschke MG. Hypertrophic scarring and keloids: pathomechanisms and current and emerging treatment strategies. Mol Med. 2011;17:113-25.

[66] Mizuno H. Adipose-derived stem and stromal cells for cell-based therapy: current status of preclinical studies and clinical trials. Current Opinion in Molecular Therapeutics. 2010;12:442-9.

[67] Mizuno H, Tobita M, Uysal AC. Concise review: adipose-derived stem cells as a novel tool for future regenerative medicine. Stem Cells. 2012;30:804-10.

Figures and Tables

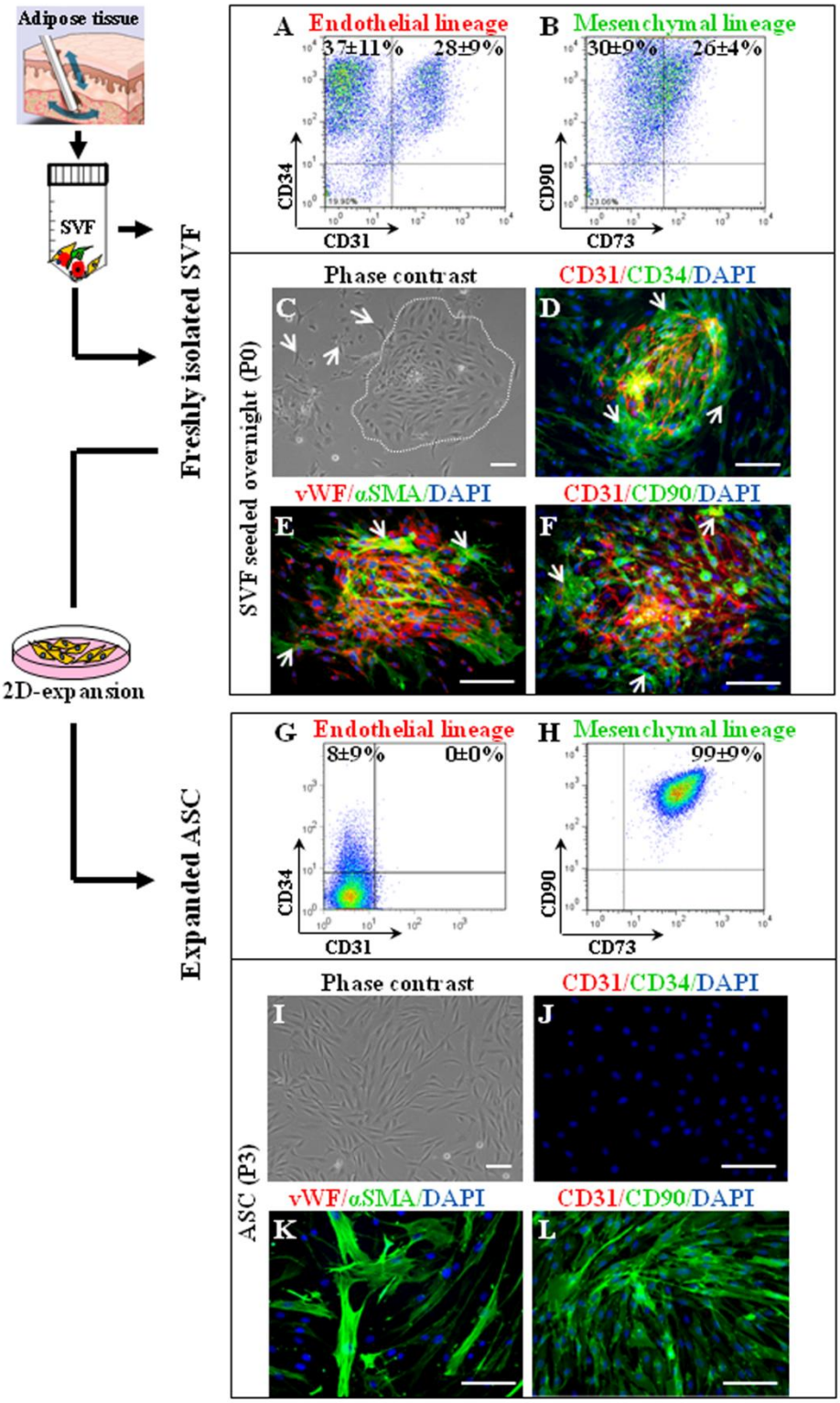

Figure 1. Characterization of the SVF and expanded ASC. (A, B) Freshly isolated SVF cells were co-stained for endothelial (CD31, CD34) (A) and mesenchymal (CD90, CD73) markers (B), and analyzed by flow cytometry. (C) Representative phase-contrast image of freshly isolated SVF cells seeded on tissue culture plastic. The white dotted line indicates an endothelial cell colony. White arrows mark spindle-shaped cells that surround this

colony. (D-F) Representative merged fluorescence images of CD31 and CD34 expressing cells (D), vWF and αSMA (E), as well as CD31 and CD90 (F). (G, H) Monolayer-expansion of SVF cells resulted in a homogenous, adherent population composed of adipose stromal cells (ASC) negative for the endothelial markers: CD31 and CD34 (G), and positive for the mesenchymal markers: CD90 and CD73 (H) as revealed by flow cytometry. (I) Phase-contrast micrograph of ASC at passage three expanded on cell culture plastic. (J-L) Merged fluorescence images of ASC expressing CD31 and CD34 (J), vWF and αSMA (K), and CD31 and CD90 (L). For (A, B) and (G, H) dot plot analyses represent the average values (±SD) of the gated populations calculated from five independent donors. DAPI stains the nuclei in blue. Abbreviations: ASC: adipose stromal cells; αSMA: alpha-smooth muscle actin (pericyte marker); vWF: von Willebrand factor (endothelial marker). Scale bars=100µm.

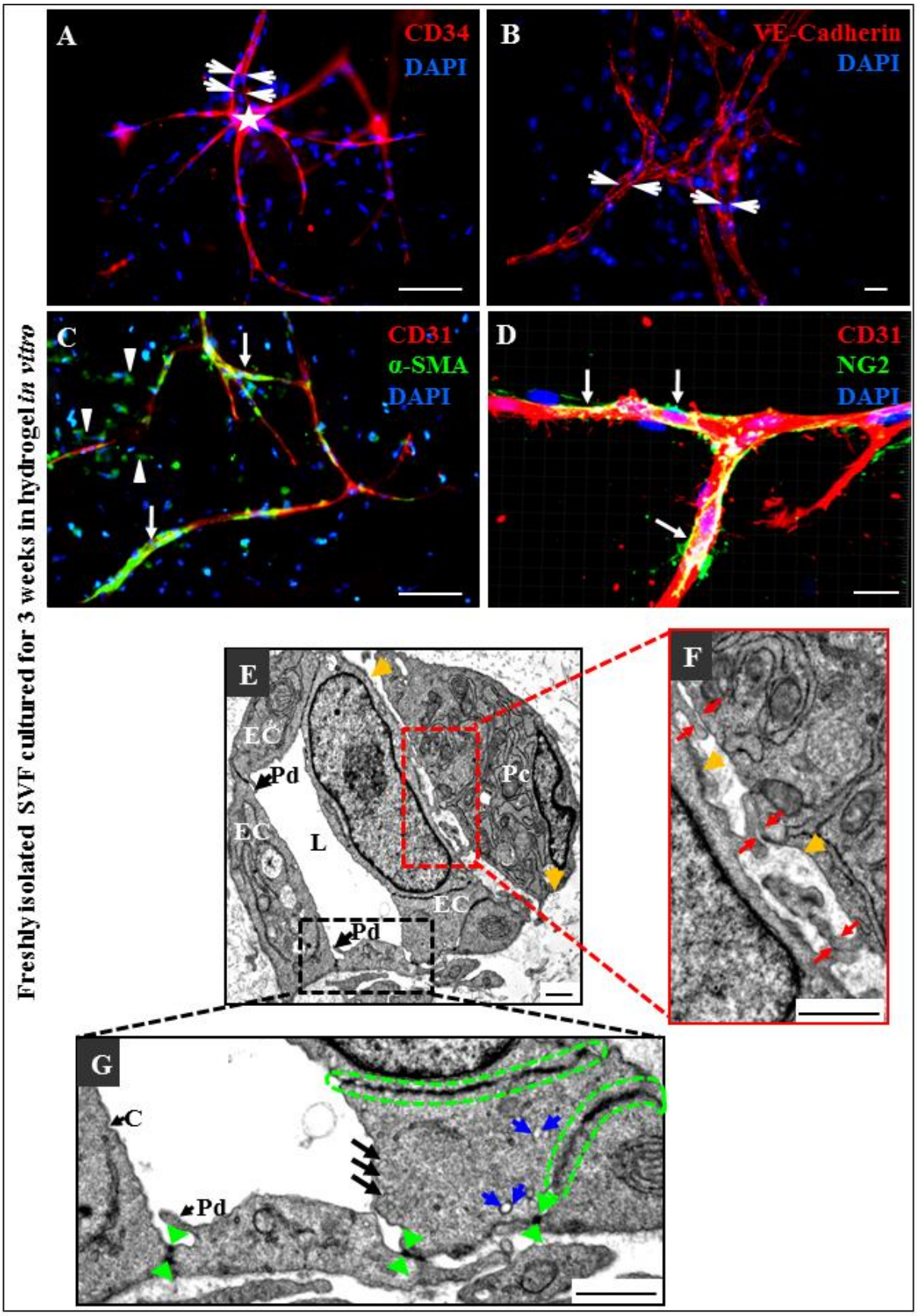

Figure 2. Cells of the SVF form complex vascular networks *in vitro*. (A, B) Confocal images of human SVF-derived capillaries cultured three weeks *in vitro* in a 3D fibrin hydrogel, and stained for endothelial-specific markers such as CD34 (A) and VE-cadherin (B). Arrows indicate lumenized capillaries (A, B). The white star in

(A) marks the center of a stellate-shaped capillary formation. (C, D) Pericytes are associated with endothelial cells as demonstrated by double-labeling for CD31 and αSMA (C) and CD31 and NG2 (D). White arrows indicate αSMA+/NG2+ cells directly associated with capillaries, whereas arrowheads mark αSMA+ cells which are not capillary-associated. DAPI stains the nuclei in blue. (E-G) Representative TEM micrograph of a mature capillary generated by cells of the SVF *in vitro*. (E) Cross-section through a capillary formed by several endothelial cells (EC) building an uninterrupted, complete endothelial lining around a lumen (L) covered by a pericyte (Pc), and basal lamina (yellow arrowheads). (F) and (G) are enlargements of the areas delineated in (E). (F) The pericyte forms extended, finger-like cytoplasmic processes interdigitating with the adjacent EC to form specific contacts termed "peg-and-socket" junctions (PS) indicated by red double arrows. (G) Black arrows mark characteristic endothelial structures including pseudopodia (Pd), caveolae (C) and pinocytotic (surface) vesicles. Blue arrows indicate vesicles which occur freely in the cytoplasm. Green dotted circles mark complex intercellular junctions that connect neighbouring endothelial cells and green double arrowheads desmosomes. Abbreviations: αSMA: alpha smooth muscle actin (pericyte marker); NG2: neuron/glia-type 2 antigen (pericyte marker); VE-cadherin: vascular endothelial cadherin (marker of endothelial adherens junctions); Nc: cell nucleus; TEM: transmission electron microscopy. Scale bars=100µm (A, C), 20µm (B, D), and 1µm (E, G).

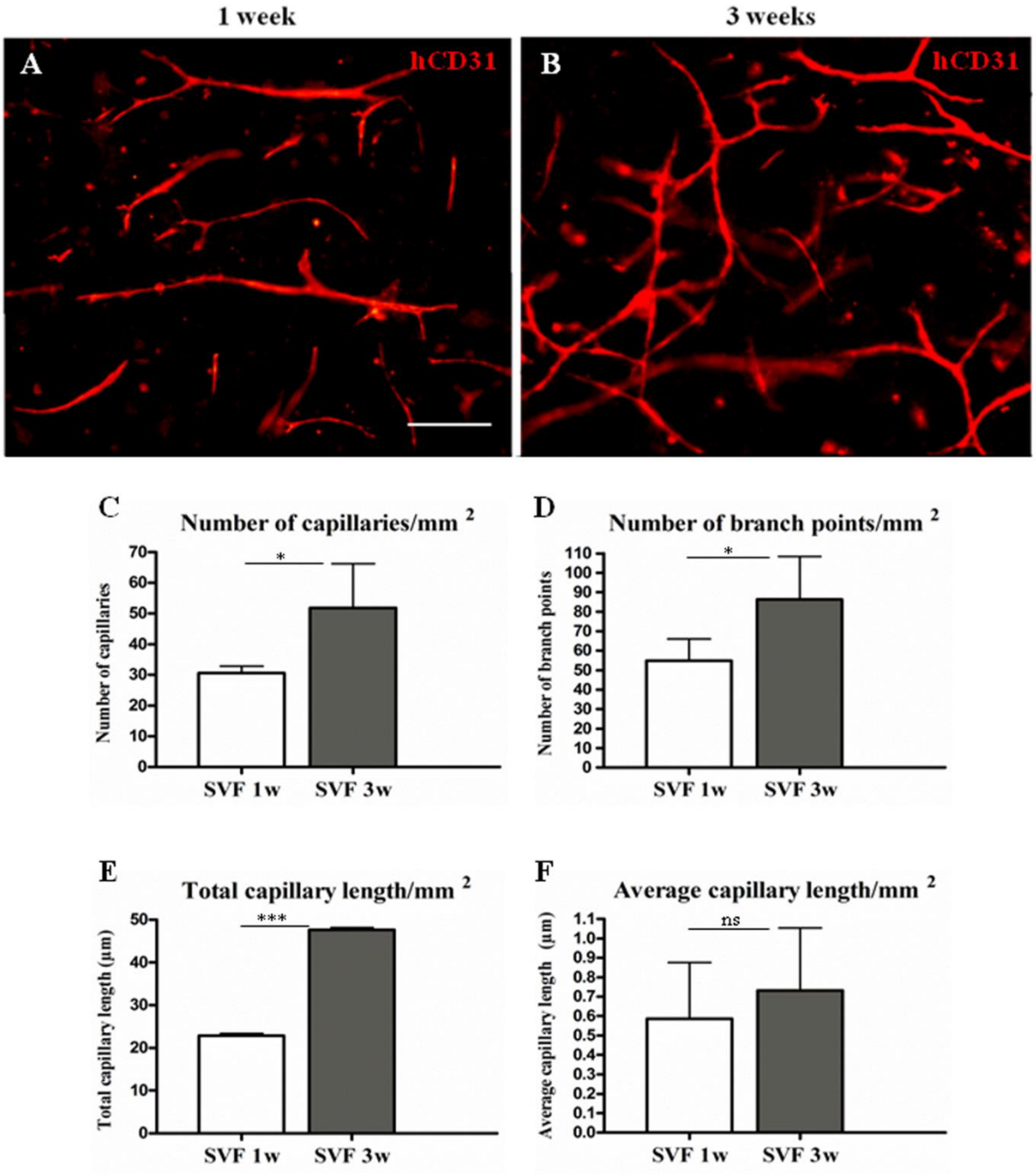

Figure 3. Optimization of vascular network formation *in vitro*. (A, B) To determine the optimal culture time for maximal *in vitro* capillary network formation, fibrin hydrogels containing the freshly isolated SVF were stained using a human specific CD31 antibody at one (A) and three (B) weeks of culture. (C-F) Quantitative analyses of vascular structures determining the number of capillaries/mm2 (C), the number of branch points/mm2 (D), the total length of capillaries/mm2 (E), and the average capillary length/mm2 (F). All data are representative of three independent donors (n=9 per condition). Scale bars=100µm.

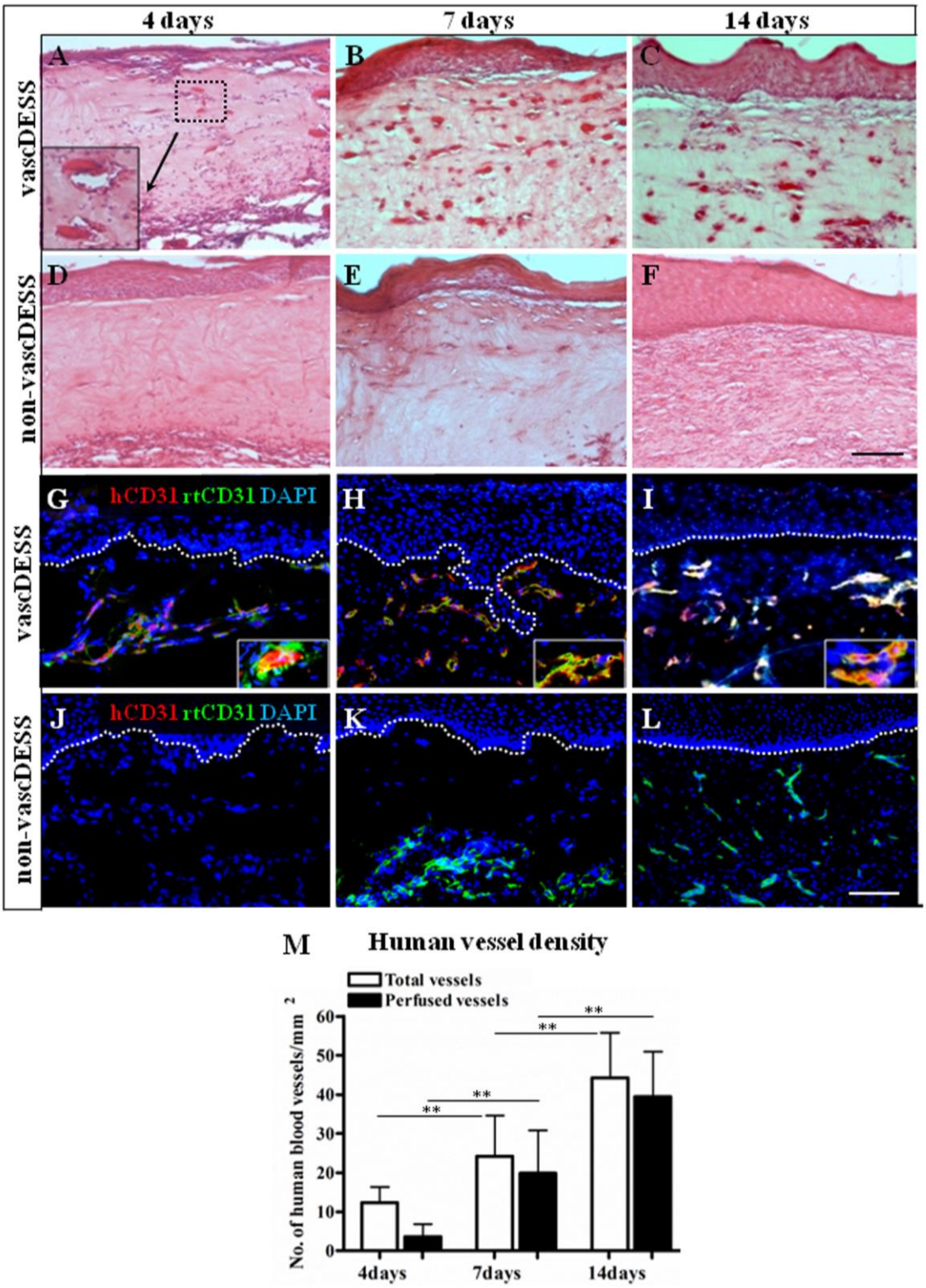

Figure 4. SVF-generated capillaries boost revascularization of vascDESS *in vivo*. (A-F) Hematoxylin/eosin stainings of vascDESS (containing cells of the SVF) and non-vascDESS (containing ASC) excised at 4 (A, D), 7 (B, E), and 14 (C, F) days after transplantation (a.T). Note the presence of perfused vessels (erythrocytes are obvious in their lumen) exclusively in vascDESS, already at day four a.T. (inset in A). (G-I) Some of the tissue-engineered human CD31-positive capillaries anastomosed as early as four days a.T. with the rat CD31-positive capillaries of the wound bed (G). By day 7 (H), the robust and lumenized human capillaries frequently

incorporated rat endothelial cells forming hybrid human/rat capillaries, which were colonized by rat vasculature at day 14 (I). Insets represent a high magnification view underlining the hybrid character of the capillaries. (J-L) Non-vascDESS did not stimulate ingrowth of rat vasculature before day 7 *in vivo* (J, K). Their neo-dermis was reasonably vascularized only 14 days a.T. (L). (M) Quantification of total and perfused human CD31 capillaries formed by the SVF at day 4, 7, and 14 a.T. in vascDESS. For (M) data are representative of three donors for SVF and ASC (n=6 per condition). White dotted lines indicate the dermo-epidermal junction (G-L). DAPI stains the nuclei in blue. Scale bars=100µm.

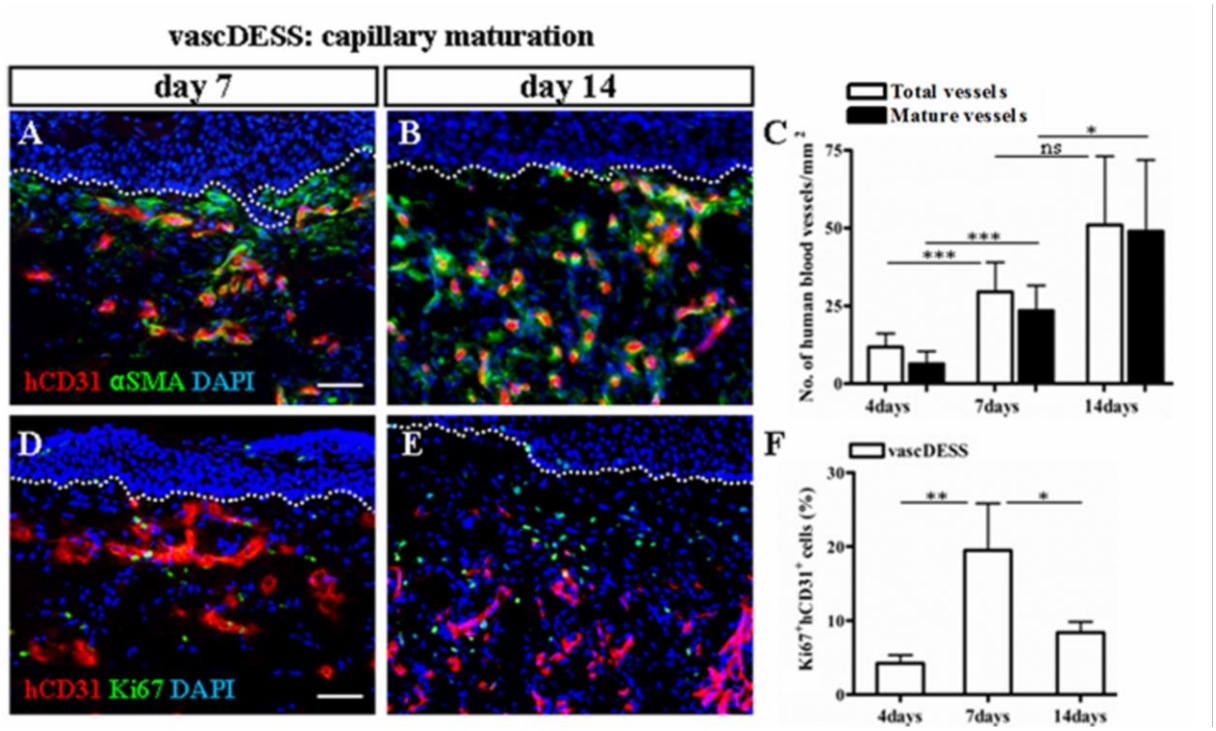

Figure 5. *In vitro* pre-formed SVF-capillaries organize into robust and mature capillary networks *in vivo*. (A, B) Immunofluorescence determination of human capillary maturation by co-staining for human CD31 and αSMA in vascDESS at day 7 (A) and 14 (B) a.T. (C) Quantification of total and mature (pericyte-associated) human CD31+ capillaries *in vivo*. (D-E) Immunostaining of human CD31-positive capillaries co-stained for the proliferation marker Ki67 in vascDESS. (F) Quantification of proliferating human endothelial cells (Ki67+ and hCD31+) in vascDESS *in vivo*. For (C, F) data are representative of three donors for SVF (n=6 per condition). DAPI stains the nuclei in blue. White dotted lines indicate the dermo-epidermal junction. Scale bars=50µm.

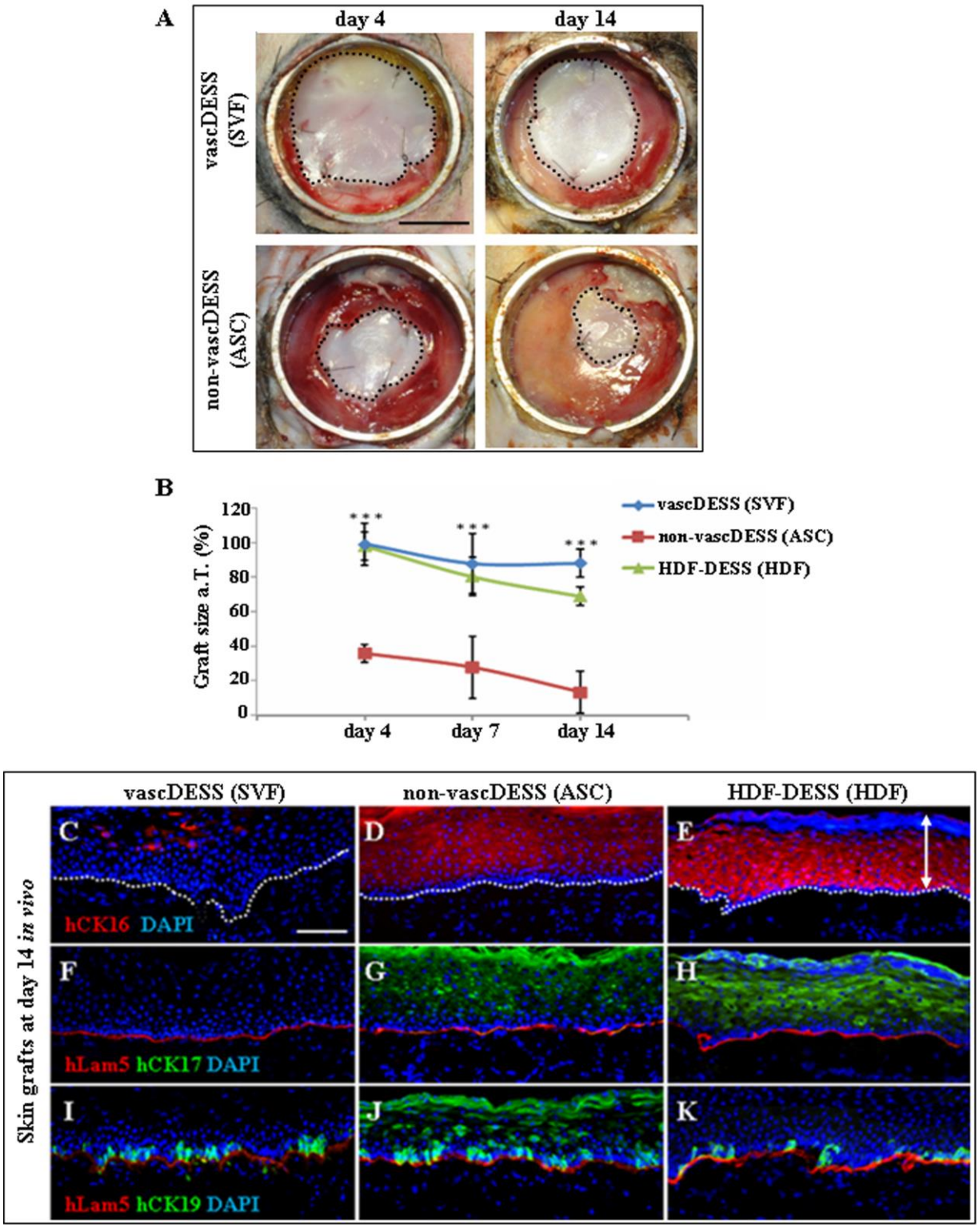

Figure 6. The SVF-based capillary plexus reduces shrinkage and accelerates the establishment of tissue homeostasis in vascDESS. (A) VascDESS (SVF) and non-vascDESS (ASC) at day 4 and 14 a.T. Black dotted lines indicate the area of each skin transplant used for planimetry analysis in (B). (B) Comparison of the areas covered by vascDESS with the two control groups, non-vascDESS and HDF-DESS respectively (in %), at day 4, 7 and 14 *in vivo* ($P<0.001$ vasc- versus non-vascDESS). (C-E) Immunofluorescence staining of CK16 indicates a typical wound healing situation in (D, E), whereas in (C) tissue homeostasis is significantly more advanced. (F-H) Co-expression of laminin 5 and CK17 confirms the data and conclusion of (C-E). (I-K) Laminin 5 and CK19

staining of the vascDESS and both control groups 14 days a.T. demonstartes that in non-vascDESS tissue homeostasis is delayed. For (B) data are representative of three donors for SVF and ASC (n=6 per condition), and four donors for HDF (n=4 per condition). DAPI stains the nuclei in blue. White dotted lines indicate the dermo-epidermal junction (C-K), white arrow the thickness of the epidermis (E). Abbreviations: CK: cytokeratin; HDF: human dermal fibroblasts; Lam5: laminin 5. Scale bars=1cm (A) and 100µm (C-K).

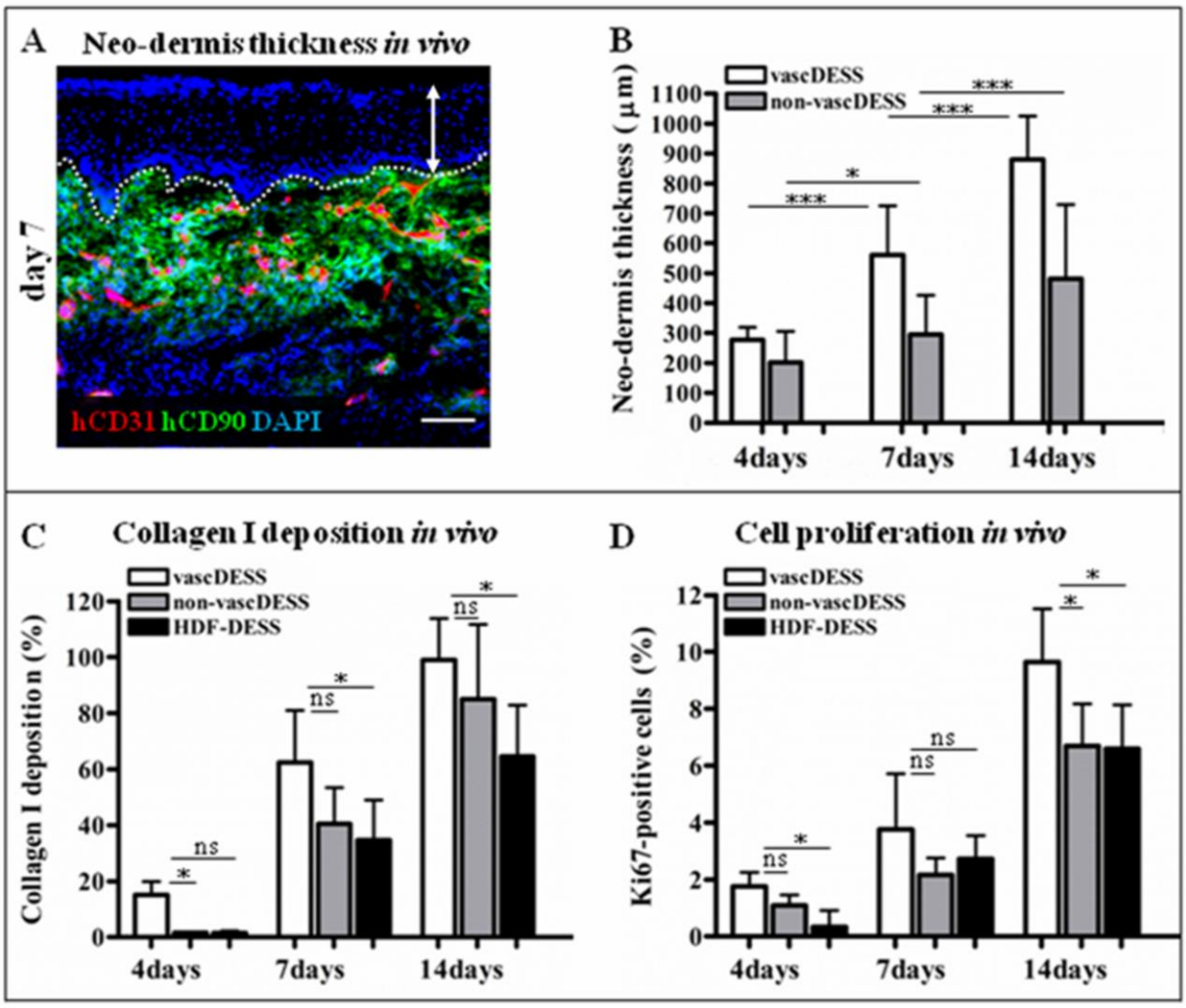

Figure 7. SVF-derived capillaries accelerate dermal regeneration in vascDESS. (A) The dimension (thickness) of a representative, highly vascularized neo-dermis of human origin in vascDESS is visualized by the human specific CD90-antibody co-stained by human CD31 at day 7 a.T. (B) The thickness of the neo-dermis increases in vascDESS *in vivo*. (C) Evaluation of dermal collagen type I deposition (in %) in vascDESS and the two control groups (non-vascDESS and HDF-DESS) *in vivo*. (D) Percentage of dermal and epidermal Ki67+ proliferating cells in vascDESS and both control groups *in vivo*. For (B), (C), and (D) data are representative of three donors for SVF and ASC (n=6 per condition), and four donors for HDF (n=4 per condition). The thickness of the epidermis is indicated by white arrow (A). DAPI stains the nuclei in blue. Scale bar=100µm.

Supplementary material

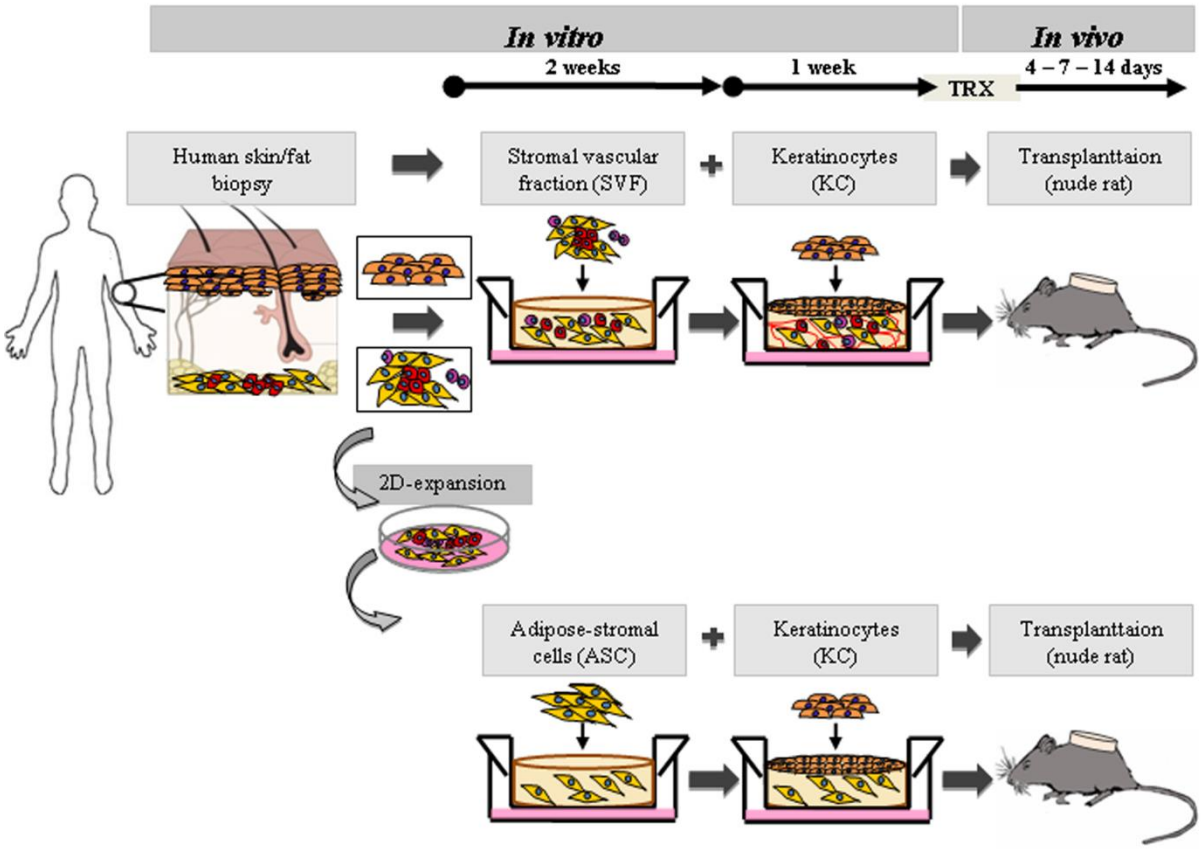

Supplementary Figure 1. Experimental study design. The vascDESS were prepared by embedding the freshly isolated SVF within 3D fibrin/collagen hydrogels allowing assembly into capillary networks within the dermal compartment (two weeks *in vitro* culture). Subsequently epidermal keratinocytes were seeded on the gels to form an epidermis (one week *in vitro* culture). Thereafter the grafts were transplanted onto immuno-incompetent rats. Non-vascDESS containing donor-matched adipose-derived stromal cells (ASC), as well as cell-free scaffolds were used as controls. At day 4, 7, and 14 after surgery, skin grafts were retrieved for macroscopic and histological analysis.

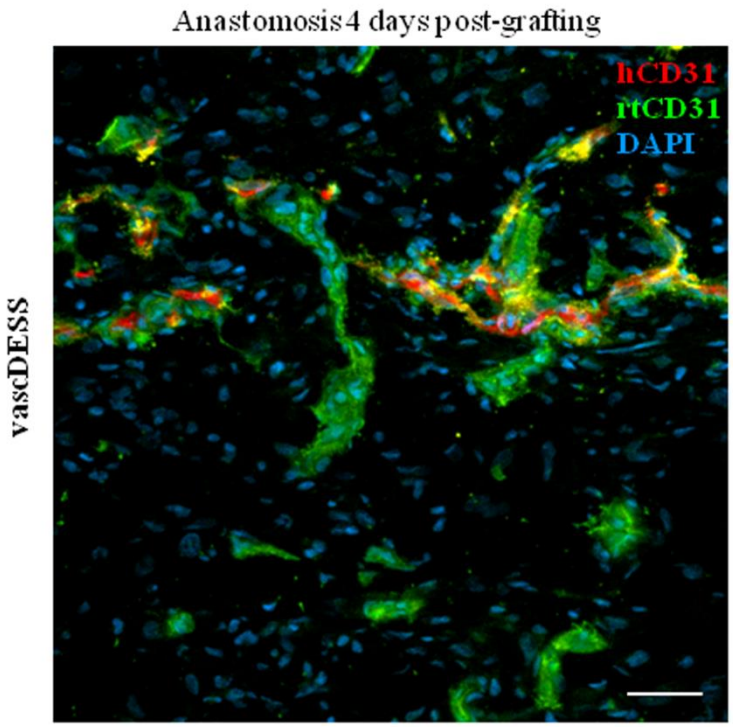

Supplementary Figure 2. Confocal image of anastomoses between human and rat capillaries. Merged image showing the extensive connection between human and rat CD31-positive capillaries at day four post-grafting. Scale bar=50µm.

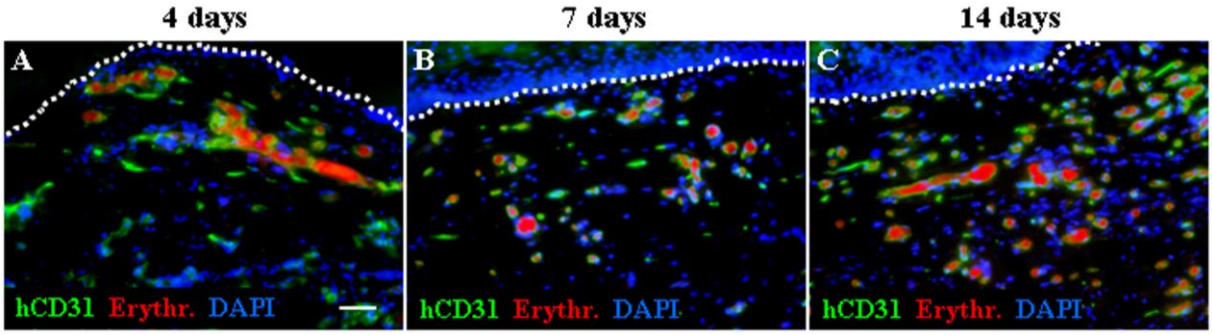

Supplementary Figure 3. Confocal image of total vs. perfused vessels at different time points. Immunostaining of total human CD31-positive capillaries after 4 (A), 7 (B), and 14 days (C) following transplantation. Some of these capillaries contain red erythrocytes (shown by autofluorescence) in their lumina, demonstrating the functional blood flow. White dotted lines indicate the dermo-epidermal junction. DAPI stains the nuclei in blue. Scale bar=50µm.

Supplementary Table 1. Quantification of human capillaries in vascDESS *in vivo*. All data are representative of three donors for SVF and ASC (n=6 per condition). The ratio of perfused vessels to total vessels is expressed as %. P-values compare day 7 versus day 4, and day 14 versus day 7 (Student's t test).

Number of human capillaries/mm^2	day 4	day 7	day 14
Total hCD31$^+$ capillaries	13±4	25±10 (p=0.0098)	45±12 (p=0.0026)
Perfused (containing erythrocytes)	4±3	20±11 (p=0.0012)	40±12 (p=0.0038)
% of perfused capillaries	29±15%	82±20%	89±10%

Supplementary Table 2. Quantification of total (hCD31+) and mature human (hCD31+αSMA+) capillaries in vascDESS in vivo. All data are representative of three donors for SVF (n=6 per condition). The ratio of mature to total human capillaries is expressed as %. P-values compare day 7 versus day 4, and day 14 versus day 7 (Student's t test).

Number of human capillaries/mm^2	day 4	day 7	day 14
Total: hCD31$^+$ capillaries	12±4	30±9 (p=0.0009)	51±22 (p=0.0004)
Mature: hCD31$^+$αSMA$^+$ capillaries	6±4	24±8 (p=0.0288)	49±23 (p=0.0003)
% of mature capillaries	50±21%	80±6%	96±5%

4.2 Optimizing in vitro culture conditions leads to a significantly shorter production time of human dermo-epidermal skin substitutes

Agnieszka S. Klar[1#], Luca Pontiggia[1#], Sophie Böttcher-Haberzeth[1, 2], Thomas Biedermann[1], Martin Meuli[2], and Ernst Reichmann[1*]

[#] Authors contributed equally to this paper

[1]Tissue Biology Research Unit, University Children's Hospital Zurich, Switzerland

[2]Department of Surgery, University Children's Hospital Zurich, Switzerland

[*]Corresponding author: Prof. Dr. Ernst Reichmann, Tissue Biology Research Unit, August Forel Str. 7, CH-8008 Zurich, Switzerland, Email: Ernst.Reichmann@kispi.uzh.ch

Published in:

Pediatr Surg Int, 2013, 29(3):249-56

Abstract

Introduction: Autologous dermo-epidermal skin substitutes (DESS) generated *in vitro* represent a promising therapeutic means to treat full-thickness skin defects in clinical practice. A serious drawback with regard to acute patients is the relatively long production time of three to four weeks. With this experimental study we aimed to decrease the production time of DESS without compromising their quality.

Methods: Two *in vitro* steps of DESS construction were varied: the pre-cultivation time of fibroblasts in hydrogels (1, 3, and 6 days), and the culture time of keratinocytes (3, 6, and 12 days) before transplantation of DESS on nude rats. Additionally, the impact of the air-liquid interface culture during three days before transplantation was investigated. Three weeks after transplantation, the macroscopic appearance was evaluated and histological sections were produced to analyze structure and thickness of epidermis and dermis, the stratification of the epidermis, and the presence of a basal lamina.

Results: Optimal DESS formation was obtained with a fibroblast pre-cultivation time of 6 days. The minimal culture time of keratinocytes on hydrogels was also 6 days. The air-liquid interface culture did not improve graft quality.

Conclusion: By optimizing our *in vitro* culture conditions, it was possible to very substantially reduce the production time for DESS from 21 to 12 days. However, pre-cultivation of fibroblasts in the dermal equivalent and proliferation of keratinocytes before transplantation remain crucial for an equilibrated maturation of the epidermis and cannot be completely skipped.

Keywords: Tissue-engineering - Dermo-epidermal skin substitutes - Skin reconstruction - Air-liquid interface - Collagen hydrogels

Introduction

Cultured skin substitutes have been used in both experimental and clinical settings for over 40 years [1]. In the global picture, culture time was always between 3-4 weeks, independent of what type of skin substitute was produced (cultured epithelial autografts (CEA) alone [2-5], CEA+allografts [6]), or cultured skin substitutes (CSS) [7-8].

For obvious reasons, culture time does not play a dominant role when a cultured skin substitute is transplanted onto a patient undergoing elective plastic or reconstructive surgery since the patient can be called in for the operation when the graft is ready. In contrast, culture time does play a crucial, potentially even vital, role when cultured skin substitutes are to be applied on acute and massive burn patients. Therefore, a significant reduction of culture time would represent a substantial progress provided the more rapid production is not associated with quality loss. Here, we present a culture modality to minimize culture time of tissue-engineered human cell-derived dermo-epidermal skin substitutes (DESS) suitable for clinical application.

Material and Methods

Primary cell cultures

Human skin samples from scalp, eyelid, neck or foreskins were obtained from patients aged between 4 months and 56 years (Tab. 1). Approval was obtained from the Ethics Committee of the Canton Zurich and informed consent was given by parents or patients. Keratinocytes and fibroblasts were isolated, cultured, and stored in liquid nitrogen until needed as previously described [9].

Organotypic cultures and transplantation of cultured dermo-epidermal composites: standard procedure

Organotypic cultures and transplantation experiments were performed as previously published [9] with some modifications: hydrogels were prepared by mixing 0.6 ml chilled neutralization buffer containing 0.15 M NaOH [10], 0.3 ml DMEM/10%FCS containing 40'000 fibroblasts and 2.1 ml of rat tail collagen type I (3.2-3.4 mg/ml, BD Biosciences, Allschwil Switzerland)

into 4.2 cm^2-cell culture inserts (BD Falcon, Basel, Switzerland; [11]). After jellification (10 min at room temperature and 2 hours at 37°C) the thickness of the dermal equivalents was reduced from 7 to 1 mm by compression [12] and grown in DMEM/10%FCS for 1 to 6 days.

Subsequently, keratinocytes were seeded onto each dermal equivalent at a density of $125x10^3$ cells per cm^2 within polypropylene rings of 5 mm in diameter. After 6 hours the rings were removed and culture medium was added in the upper and lower chamber. The skin equivalents were cultured for two weeks; 3-4 days before transplantation on nude rats [9], the substitutes were raised to the air/liquid interface.

Variations of the standard protocol: experimental schedule

In the first experiment, the pre-incubation time of fibroblasts in the dermal template was modulated (Fig. 1A). We isolated fibroblasts from foreskin or neck skin biopsies of three different patients and cultured them to passage 1-2. The age of the patients varied between 4 months and 2 years (Tab. 1). One, 4, or 6 days before the pre-determined date of keratinocytes seeding (green squares) fibroblasts were included in collagen I hydrogels. At day 0 (black dots), foreskin-keratinocytes were applied onto the hydrogels and cultured for two weeks before transplantation (TRX).

In the second part of the experiment, the pre-incubation time of fibroblasts in the dermal template was maintained constant at 7 days (Fig. 1B). Thereafter, at day 0 (red dot) keratinocytes were seeded on the hydrogels and incubated for 3, 6, or 12 days before transplantation. Two sets of the 6- and 12-days series were produced. One of them was exposed to the air-liquid interface 3 days before transplantation (Fig.1C), while the other remained submerged (Fig. 1B). In all experiments, grafts were removed for analysis 3 weeks after transplantation.

Fluorescein diacetate (FdA) vital cell staining

In order to visualize cell viability and homogenous epidermal cell coverage of the hydrogels, FdA staining was performed as published [13]. Briefly, from an acetone 5 mM-stock solution, FdA (Sigma, Buchs, Switzerland) was added to the culture medium in the lower and upper chamber to a final concentration of 5 μM. After 2 min FdA was removed by washing twice in PBS before fresh culture medium was applied. The substitutes were analysed by fluorescence microscopy.

Histology and immunofluorescence microscopy

The epidermal substitutes were prepared to produce cryo- and paraffin sections. Histology and three-color immunofluorescence stainings were performed as previously described. For details refer to Biedermann *et al.* [9].

Antibodies

For the purpose of determining DESS quality, antibodies to the following markers were applied for immunofluorescence stainings:

Involucrin (clone SY5, 1:100; LabVision, P.H.Stehelin&CIE AG, Basel, Switzerland) is a marker for the cornification process and is associated with the formation of desmosomes and intermediate filaments in the granular layer [14]. It is expressed (in homeostatic conditions) in the granular and cornified layer. K1 (clone LHK1, 1:200; Chemicon) as late differentiation marker [15] is indicative of the degree of tissue homeostasis in normal human skin, where it is expressed in all suprabasal layers, with exception of the stratum corneum. Occludin (polyclonal, 1:50; Zymed, Invitrogen, Basel, Switzerland) is indicative for the formation of tight junctions in the granular layer. It represents a further confirmation of acquiring terminal functionality of the epidermis. α6 integrin (clone 4F10, 1:100; Chemicon, Millipore AG, Zug, Switzerland) is a component of hemidesmosomes and assures the stable anchorage to the basal lamina [16]. It is indicative for the quality of the dermo-epidermal junction. K19 (clone RCK108, 1:100; Dako, Baar, Switzerland) and K15 (clone spm190, 1:50; Santa Cruz, Labforce AG, Nunningen, Switzerland) are markers for a mature basal layer and general homeostasis: In homeostatic engineered epidermal substitutes K19-positive cells are clustered in the stratum basale as a subpopulation of K15-positive keratinocytes [11]. As a secondary antibody we used FITC-conjugated polyclonal goat $F(ab')_2$ fragments directed to mouse immunoglobulins (Dako).

For double immunofluorescence, some of the primary antibodies were pre-labeled with Alexa 555-conjugated polyclonal goat $F(ab')_2$ fragments, according to the instructions of the manufacturer (Zenon Mouse IgG Labeling Kit, Molecular Probes, Life Technologies, Zug, Switzerland).

Statistical Analysis

The thickness of epidermis and stratum corneum as well as the graft size were measured in 3 different representative areas. All results are reported as mean ± standard deviation. Statistical analysis was performed with GraphPad Prism 4.0 (Graph Pad software, La Jolla, CA, USA). Comparison between two groups was performed using the unpaired Student's t-test. Results were considered significant with a $p < 0.05$.

Results

Fibroblasts precultivation time

Immediately before transplantation we verified the presence of an epidermis via FdA staining. Fig. 2A shows the staining of the second series of substitutes (Tab. 1). Similar results were obtained with series 1 and 3: keratinocytes proliferation was more pronounced on the hydrogels which were conditioned by fibroblasts for 6 days (6dF): the whole surface of the gels was homogeneously covered (left panel), starting from a circle of 0.96 mm in diameter in the centre of the dermal template (dotted circle). A shorter pre-incubation of the fibroblasts of 4 days (4dF) or 1 day (1dF) was less supportive for keratinocytes proliferation (middle and right panel).

Three weeks after transplantation (Fig. 2B), the 6dF-DESS looked macroscopically more developed and the presence of the hydrophobic stratum corneum was clearly visible (left panel). Correspondingly the measurement of the graft area showed that 87±16% of the original graft size was maintained (Fig. 2C). In contrast, in 4dF and 1dF-DESS the graft area was reduced to 35±17%, and 6±5%, respectively (Fig. 2C).

Histological analyses confirmed in 6dF-DESS the formation of a stratified epidermis, which consisted of a stratum basale (sb), 12–20 suprabasal layers comprising stratum spinosum (ss) and stratum granulosum (sg), and a well-differentiated anuclear stratum corneum (sc, Fig. 3A). In 4dF-DESS, the epidermal thickness was reduced (middle panel). In 1dF-DESS, no epithelium was found (right panel).

Stratification markers in engineered DESS

As a complement to the morphological analysis, we verified the presence of some protein expression markers which are indicative for the grade of homeostasis of an engineered epidermal substitute.

We found involucrin expression (Fig. 3B, red stain) in the stratum spinosum of the substitutes, indicating a still ongoing differentiation process in 6dF-DESS (Fig. 3B, left). The thinner epidermis in 4dF showed a similar expression pattern (Fig. 3B, center). No involucrin expression was found in the in 1dF (Fig. 3B, right).

Both 6dF and 4dF showed a strong expression of K1 (Fig. 3B, green stain, left and center) in all suprabasal layers, with exception of the cornified envelope. In 1dF, only few K1-expressing epithelial cells were visible (Fig. 3B, right).

Occludin (Fig. 3C, green) was expressed in the upper stratum granulosum of 6dF and 4dF (left and center), but absent in 1dF (right). Integrin α6 staining (Fig. 3C, red) demarcated the dermo-epidermal junction in 6dF and 4dF, but was not visible in 1dF.

Fig. 3D shows that in 6dF and 4dF, but not in 1dF, K19-positive cells (red), are present in the basal layer as a subpopulation of K15-positive keratinocytes (green).

Keratinocyte pre-cultivation time

The second step of DESS generation consisted in the seeding of keratinocytes on the pre-cultivated hydrogels. We now varied the incubation time of keratinocytes on the dermal substitutes (and so the degree of pre-stratification of the graft) before transplantation while the pre-cultivation time of the fibroblasts in the gels was maintained identical (Fig. 1B). Fig. 4A illustrates the macroscopic overview of the two series of DESS three weeks after transplantation. The DESS generated with a three day keratinocyte (3dK) pre-cultivation time (left panels) do not show a hydrophobic, dry cornified surface. In contrast, the skin analogues formed with a 6 day (6dK) keratinocyte precultivation time show a cornified surface (center). Importantly 12 day (12dK) pre-cultivativation of DESS did not improve the outcome: vessels were locally visible under the substitute (right panels, arrow) indicating a reduced epidermal thickness. Fig. 4B statistically illustrates the measured size of the substitutes, pictured in Fig. 4A.

H/E-staining of 3dK confirmed the presence of a thin epidermal coverage in some areas, while in other areas no epidermis was found (Fig. 4C, left). 6dK produced a stratum

corneum and numerous keratinocytes layers (middle panels). 12dK showed a similar result, yet the thickness of the epidermis was reduced (right).

Relevance of the air-liquid interface cultivation for transplantation

The second set of 6dK and 12dK was raised to the air-liquid interface 3 days before transplantation ($6dK^{air}$ and $12dK^{air}$ in Fig.1C).

The graft size obtained from 6dk and $6dK^{air}$ respectively was similar in the first experimental series (75±2% vs. 74±3%) and slightly different in the second (52±5% vs. 78±1%, p=0.0188) (Fig. 5A). The epidermal thickness was generally reduced in $6dK^{air}$ (192±18 vs. 165±38 µm, not significant) but the cornification was more pronounced (38±11 to 73±27 µm, p=0.0001) (microscopic view in Fig. 5B, and statistical analysis in Fig. 5C).

The graft sizes obtained from 12dk and $12dK^{air}$ were different: 52±7% vs. 96±3% (p=0.0001) in the first series and 64±7% vs. 88±4% (p=0.0013) in the second (Fig. 5D). The epidermal thickness was similar in 12dK and $12dK^{air}$ (88±3 vs. 77±11 µm, not significant, Fig. 5F compares 5D) but again, the cornification was more pronounced in $12dK^{air}$ (27±6 vs. 95±4 µm, p=0.0001) (microscopic view in Fig. 5E, and statistical analysis in Fig. 5F).

Stratification markers in air-exposed DESS

Immunofluorescence analysis of the expression pattern of stratification markers confirmed the high quality of both air-exposed and non-air exposed DESS. No difference in the expression pattern of K1/Involucrin (Fig. 6A), Occludin/integrin-a6 (Fig. 6B), and K15/K19 (Fig. 6C) is apparent.

Discussion

The principal goal of this study was to test whether the culture time for human cell-derived DESS can be significantly reduced when compared to standard procedures commonly used in our laboratory. The findings obtained clearly demonstrate that it is possible to markedly reduce the current culture time from 21 to 12 days. Hereby, the main gain was attributable to a significant shortening of the incubation time of keratinocytes on the dermal template before transplantation, i.e. from 14 to 6 days.

How can this significant reduction of incubation time be explained? We speculate that the specific cell biology dynamics of keratinocytes in culture (as opposed to keratinocytes residing in their natural habitat) play a role. For a more detailed understanding, we provide a description of our current culture system and the key phenomena observed during DESS formation: Once isolated and cultured, keratinocytes are seeded onto collagen hydrogels (=dermal templates). Then, keratinocytes start to proliferate and migrate horizontally to form a confluent layer on the top of the dermal template. Subsequently, the ongoing cell proliferation leads to formation of a multilayer that starts to stratify. Once the in vitro construct is raised to the air liquid interphase, cornification gradually develops.

The above described processes typically last 14 days. Thereafter, our constructs are transplanted and usually produce an anatomically and functionally near normal skin [9]. We also know that if DESS incubation time is significantly lengthened to e.g. 21 days, quality and transplantation results are still satisfactory. If, however, DESS incubation time is further prolonged to 28 days or more, then we increasingly observed degenerative features ultimately leading to massive cell death and complete loss of DESS viability.

In other words, the above mentioned evolution can roughly be described as an in vitro DESS life cycle comprising a “juvenile” (less than 14 d), a “mature” (14-21 d), and a “senile” phase (>21 d).

The findings presented here clearly indicate that “juvenile” and not only “mature” DESS already have the potential to induce near normal skin after transplantation, i.e. following an only 6-day-long incubation time. Apparently, the 3-4 layers present at 6 days are sufficient to generate a normal epidermis after transplantation, i.e. there is no need to use “mature” DESS for a successful transplantation.

To our knowledge, there is no information available regarding significantly shortened culture times for similar skin substitutes. The product most closely related to our DESS, the commercially available Apligraf®, uses allogeneic fibroblasts and keratinocytes. The allogeneic specification makes it possible to completely avoid any waiting time for the patient. Yet its production requires 20 days [17-18].

Other approaches drastically reduce or even skip in vitro cultivation: Starting from a small split-thickness skin biopsy, cell suspensions are applied onto the wound bed after 5 days of culturing or immediately after preparation (ReCell®) [19]. Yet, this strategy is definitely not appropriate to treat 3rd degree burns and, generally speaking, its place in clinical practice is still controversial.

The last consideration regards the fibroblast preincubation time. We could only realize a minor gain of 1 day with the reduction of the fibroblast pre-incubation time before seeding keratinocytes. As a matter of fact, the minimal duration of this phase is critical for correct DESS development. The presence of fibroblasts in the dermal template of DESS has been shown to be crucially important [20-22]. Fibroblasts remodel the collagen hydrogel, prepare the formation of a basal lamina and the anchorage of epithelial cells, secrete growth factors, and finally sustain epidermal regeneration [23]. To fulfil these tasks, fibroblasts need a defined minimal amount of time. It is generally assumed that raising the number of fibroblasts in the gel would accelerate the organization of the dermal template [24], but this acceleration may also be accompanied by abundant production of granulation tissue and wound contraction, both of which are unwanted effects [25]. Therefore, we believe that the fibroblast preincubation time cannot be significantly shortened.

In summary and conclusion, this appears to be the first article to describe a very substantial shortening of the production time for laboratory grown human skin substitutes from 21 to 12 days without an obvious loss of graft quality. Our study may have important clinical implications in that a marked reduction of waiting time until autologous skin substitutes are ready for transplantation can definitely improve the fate of burn patients.

Acknowledgments

This work was financially supported by the EU-FP6 project EuroSTEC (soft tissue engineering for congenital birth defects in children: contract: LSHB-CT-2006-037409), by the EU-FP7 project EuroSkinGraft (FP7/2007-2013: grant agreement n° 279024), by the EU-FP7 (MultiTERM, grant agreement nr 238551), and by the University of Zurich. We are particularly grateful to the Foundation Gaydoul and the sponsors of “DonaTissue” (Thérèse Meier, Robert Zingg) for their generous financial support and interest in our work.

Conflict of interest:

The authors have declared that no conflict of interest exists.

References

[1] Rheinwald JG and Green H. (1975). Serial cultivation of strains of human epidermal keratinocytes: the formation of keratinizing colonies from single cells. Cell 6:331-43.

[2] O'Connor NE, Mulliken JB, Banks-Schlegel S, Kehinde O and Green H. (1981). Grafting of burns with cultured epithelium prepared from autologous epidermal cells. Lancet 1:75-8.

[3] Gallico GG, 3rd, O'Connor NE, Compton CC, Kehinde O and Green H. (1984). Permanent coverage of large burn wounds with autologous cultured human epithelium. N Engl J Med 311:448-51.

[4] Munster AM. (1996). Cultured skin for massive burns. A prospective, controlled trial. Ann Surg 224:372-5; discussion 375-7.

[5] Krupp S, Benathan M, Meuli M, Deglise B, Holzer E, Wiesner L, Delacretaz F and Chiolero R. (1992). Current concepts in pediatric burn care: management of burn wounds with cultured epidermal autografts. Eur J Pediatr Surg 2:210-5.

[6] Cuono C, Langdon R and McGuire J. (1986). Use of cultured epidermal autografts and dermal allografts as skin replacement after burn injury. Lancet 1:1123-4.

[7] Boyce ST, Goretsky MJ, Greenhalgh DG, Kagan RJ, Rieman MT and Warden GD. (1995). Comparative assessment of cultured skin substitutes and native skin autograft for treatment of full-thickness burns. Ann Surg 222:743-52.

[8] Gobet R, Raghunath M, Altermatt S, Meuli-Simmen C, Benathan M, Dietl A and Meuli M. (1997). Efficacy of cultured epithelial autografts in pediatric burns and reconstructive surgery. Surgery 121:654-61.

[9] Biedermann T, Pontiggia L, Bottcher-Haberzeth S, Tharakan S, Braziulis E, Schiestl C, Meuli M and Reichmann E. (2010). Human Eccrine Sweat Gland Cells Can Reconstitute a Stratified Epidermis. J Invest Dermatol 130:1996-2009.

[10] Costea DE, Loro LL, Dimba EA, Vintermyr OK and Johannessen AC. (2003). Crucial effects of fibroblasts and keratinocyte growth factor on morphogenesis of reconstituted human oral epithelium. J Invest Dermatol 121:1479-86.

[11] Pontiggia L, Biedermann T, Meuli M, Widmer D, Bottcher-Haberzeth S, Schiestl C, Schneider J, Braziulis E, Montano I, Meuli-Simmen C and Reichmann E. (2009). Markers to evaluate the quality and self-renewing potential of engineered human skin substitutes in vitro and after transplantation. J Invest Dermatol 129:480-90.

[12] Braziulis E, Diezi M, Biedermann T, Pontiggia L, Schmucki M, Hartmann-Fritsch F, Luginbuhl J, Schiestl C, Meuli M and Reichmann E. (2012). Modified Plastic Compression of Collagen Hydrogels Provides an Ideal Matrix for Clinically Applicable Skin Substitutes. Tissue Eng Part C Methods.

[13] Armour AD, Powell HM and Boyce ST. (2008). Fluorescein diacetate for determination of cell viability in tissue-engineered skin. Tissue Eng Part C Methods 14:89-96.

[14] Candi E, Schmidt R and Melino G. (2005). The cornified envelope: a model of cell death in the skin. Nat Rev Mol Cell Biol 6:328-40.

[15] Stark HJ, Baur M, Breitkreutz D, Mirancea N and Fusenig NE. (1999). Organotypic keratinocyte cocultures in defined medium with regular epidermal morphogenesis and differentiation. J Invest Dermatol 112:681-91.

[16] Borradori L and Sonnenberg A. (1999). Structure and function of hemidesmosomes: more than simple adhesion complexes. J Invest Dermatol 112:411-8.

[17] Wilkins LM, Watson SR, Prosky SJ, Meunier SF and Parenteau NL. (1994). Development of a bilayered living skin construct for clinical applications. Biotechnol Bioeng 43:747-56.

[18] Parenteau NL, Nolte CM, Bilbo P, Rosenberg M, Wilkins LM, Johnson EW, Watson S, Mason VS and Bell E. (1991). Epidermis generated in vitro: practical considerations and applications. J Cell Biochem 45:245-51.

[19] Wood FM. (2003). Clinical Potential of Autologous Epithelial Suspension. Wounds 15:16-22.

[20] Marionnet C, Pierrard C, Vioux-Chagnoleau C, Sok J, Asselineau D and Bernerd F. (2006). Interactions between fibroblasts and keratinocytes in morphogenesis of dermal epidermal junction in a model of reconstructed skin. J Invest Dermatol 126:971-9.

[21] Nolte CJ, Oleson MA, Hansbrough JF, Morgan J, Greenleaf G and Wilkins L. (1994). Ultrastructural features of composite skin cultures grafted onto athymic mice. J Anat 185 (Pt 2):325-33.

[22] Okamoto E and Kitano Y. (1993). Expression of basement membrane components in skin equivalents--influence of dermal fibroblasts. J Dermatol Sci 5:81-8.

[23] Auger FA, Rouabhia M, Goulet F, Berthod F, Moulin V and Germain L. (1998). Tissue-engineered human skin substitutes developed from collagen-populated hydrated gels: clinical and fundamental applications. Med Biol Eng Comput 36:801-12.

[24]. Stark HJ, Willhauck MJ, Mirancea N, Boehnke K, Nord I, Breitkreutz D, Pavesio A, Boukamp P and Fusenig NE. (2004). Authentic fibroblast matrix in dermal equivalents normalises epidermal histogenesis and dermoepidermal junction in organotypic co-culture. Eur J Cell Biol 83:631-45.

[25] Lamme EN, Van Leeuwen RT, Brandsma K, Van Marle J and Middelkoop E. (2000). Higher numbers of autologous fibroblasts in an artificial dermal substitute improve tissue regeneration and modulate scar tissue formation. J Pathol 190:595-603.

Figures and Tables

Figure 1. Schematic schedule of the experiments.

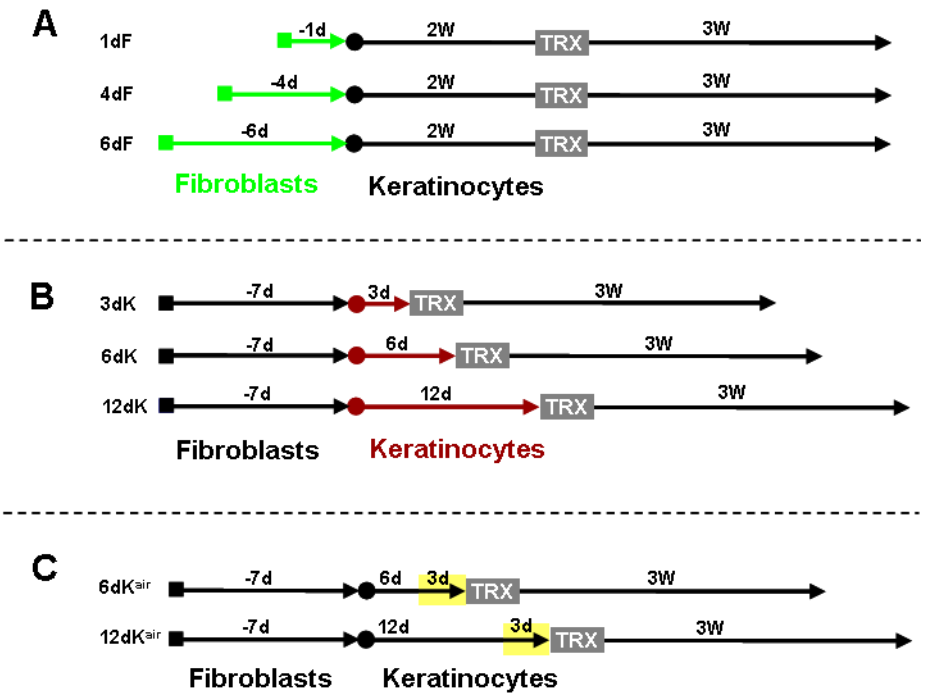

Figure 1. Schematic representation of the experimental design. We evaluated modifications of our standard protocol for the *in vitro*-DESS construction in 3 steps. (a) In the first part of the study, fibroblasts were included in collagen I hydrogels and cultivated (green line) for 1 (1dF), 4 (4dF), and 6 (6dF) days before being covered by a keratinocyte sheet (black dot). After 2 weeks, DESS were transplanted (TRX) on nude rats and grafts were removed for analysis 3 weeks post transplantation. (b) In the second part of the study, fibroblasts were included in collagen I hydrogels and cultivated for 7 days before being covered by a keratinocyte sheet (red dot). After further cultivation (red line) for 3 (3dK), 6 (6dK), and 12 (12dK) days DESS were transplanted (TRX) on nude rats and grafts were removed for analysis after 3 weeks. (c) A second set of 6dK and 12dK were treated in the same way as in b), but they were exposed to the air-liquid interface 3 days before transplantation ($6dK^{+air}$ and $12dK^{+air}$) while the original DESS remained submerged.

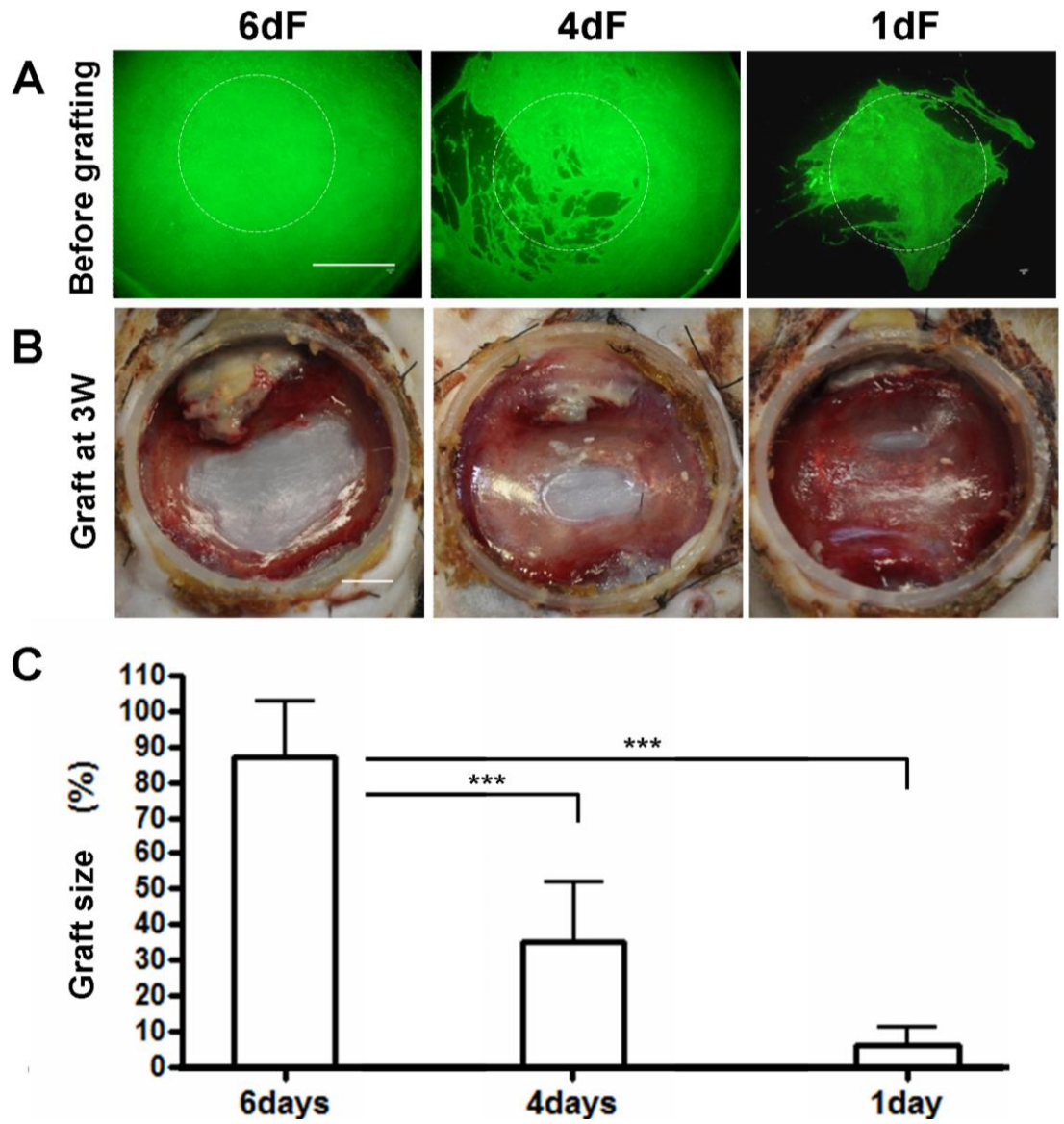

Figure 2. Modulation of the pre-incubation time of fibroblasts in DESS: Effect on graft take *in vivo*. (a) Fluorescein diacetate (FdA) staining of one set of DESS immediately before transplantation (upper panels): The white dotted circles denote the keratinocyte seeding area. (b) Macroscopic view of the grafts 3 weeks thereafter. Scale bars = 5mm. (c) Graft size three weeks after grafting in % of the originally transplanted DESS (mean±SD, n=3). ***= $p<0.0002$.

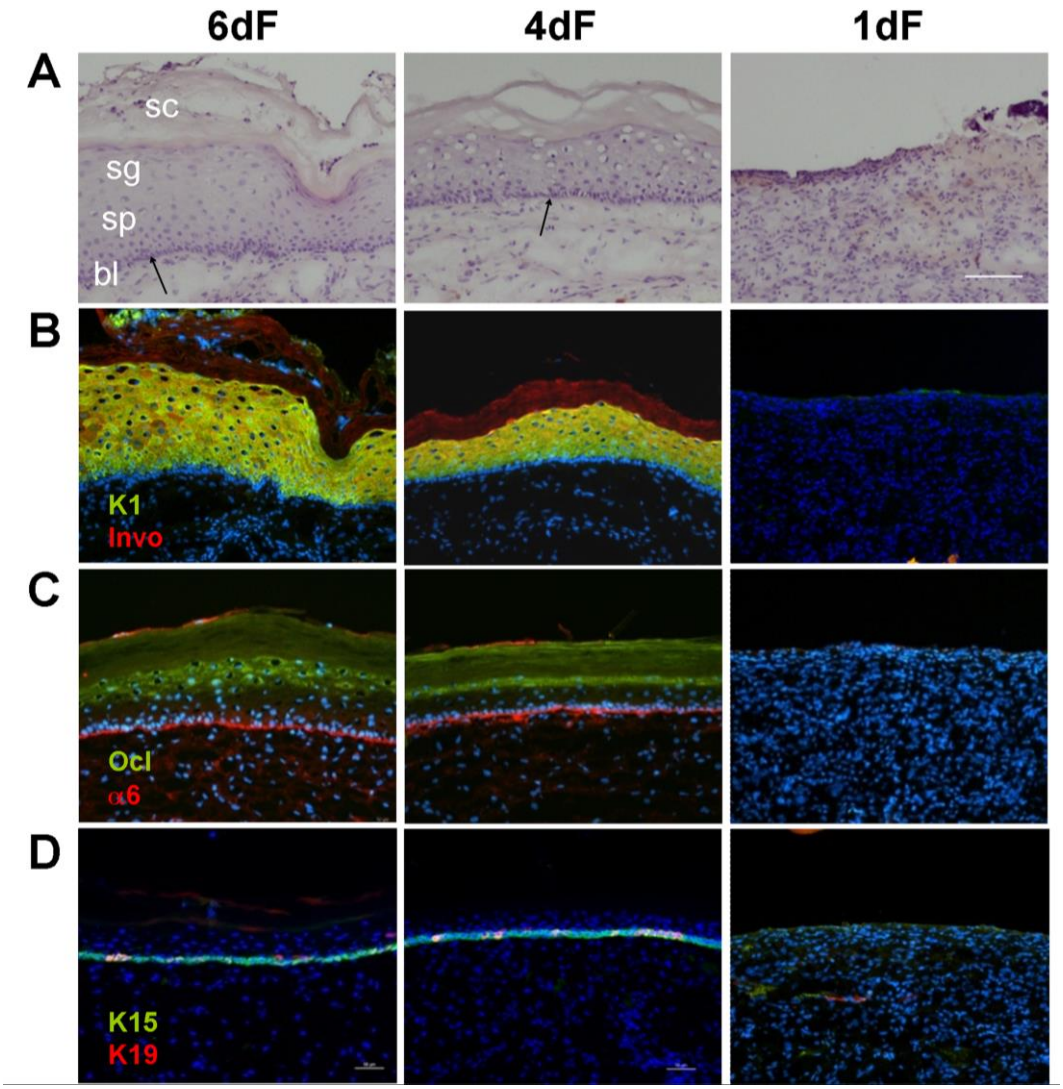

Figure 3. Expression of structural markers for advanced epidermal histogenesis. (a) Eosin/Hematoxylin-stained paraffin sections of 6dF, 4dF, and 1dF-DESS 3 weeks after transplantation. bl: basal layer (arrow), sp: stratum spinosum, sg: stratum granulosum, sc: stratum corneum. (b) Immunofluorescence double-staining of cryosections with antibodies against cytokeratin K1 (green) and involucrin (red), (c) occludin (green), and integrin α6 (red), or (d) K15 (green) and K19 (red). Scale bar for all panels = 100 μm.

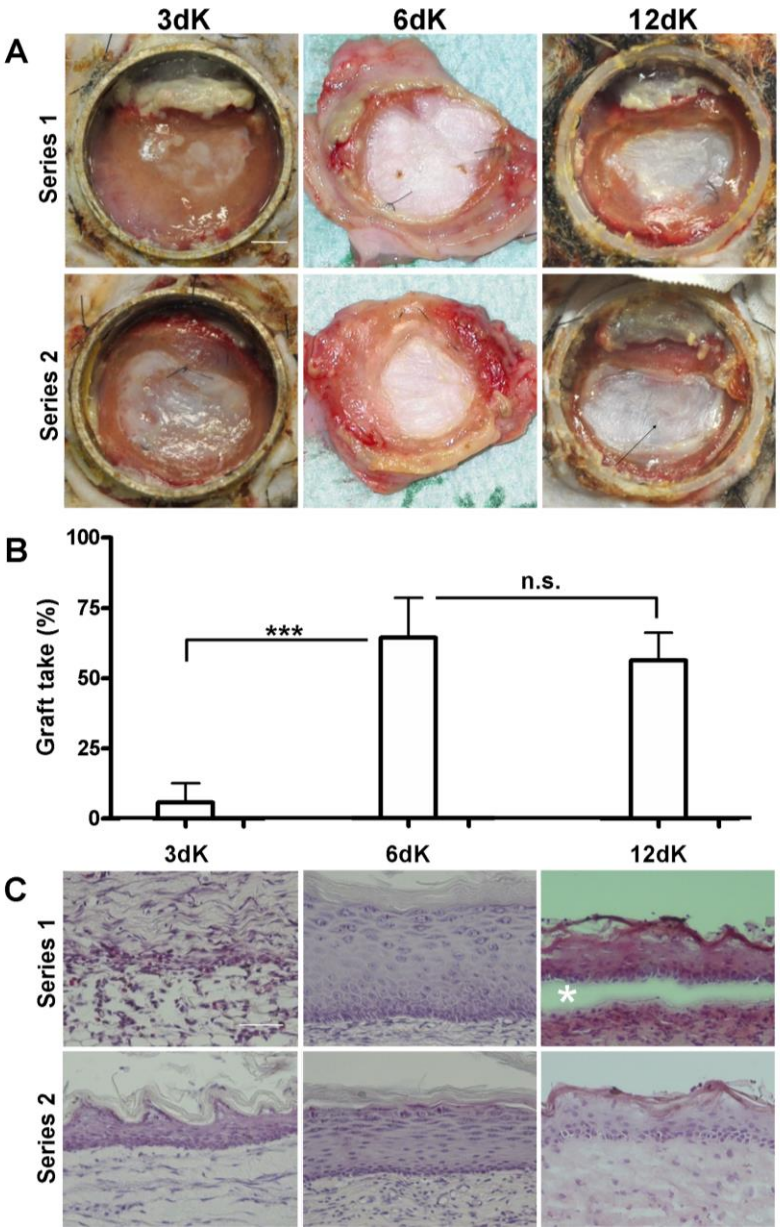

Figure 4. Variation of the incubation time of keratinocytes on the dermal substitutes before transplantation: Effect on graft take and stratification *in vivo*. (a) Macroscopic view of the grafts 3 weeks after transplantation. Both series of substitutes (refer to Tab. 1) are shown. Scale bar = 5mm. (b) Size of the transplanted DESS three weeks after grafting. Both series are included in the mean (mean±SD, n=6). ***= $p<0.0001$, n.s: not significant. (c) Eosin/Hematoxylin-stained paraffin sections of 3dK, 6dK, and 12dK-DESS 3 weeks after transplantation. The asterisk in 12dK of series 1 indicates a technical artefact. Scale bar = 50 µm.

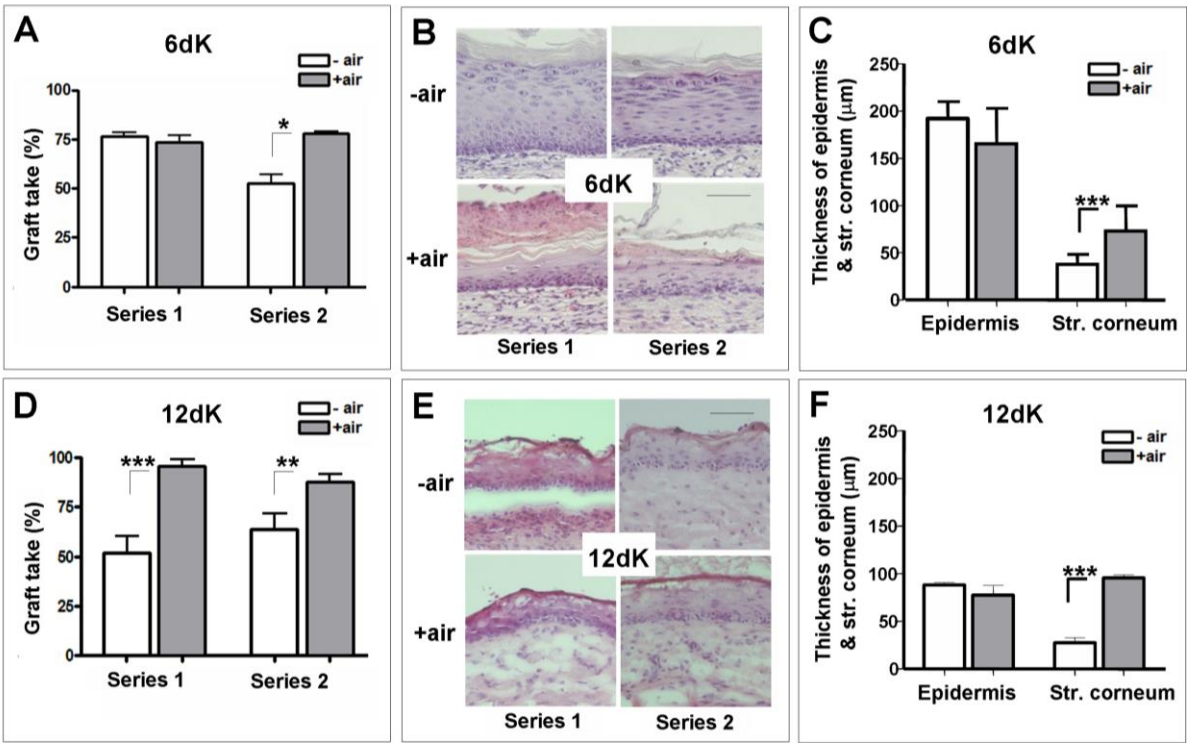

Figure 5. Effect of air-liquid interface cultivation of DESS on graft take and stratification *in vivo*. (a,d) Size of the 6dK and 12dK (white) and 6dK+air and 12dK+air (grey) grafts three weeks after transplantation (mean±SD, n=3). Both experimental series are shown. (b,e) Eosin/Hematoxylin-stained paraffin sections of air-exposed (+air) and non-air exposed (-air) 6dK and 12dK 3 weeks after transplantation. Scale bar = 50 µm. (c,f) Thickness of the obtained air-exposed and non air-exposed 6dK and 12dK in µm (entire epidermis and stratum corneum only, mean±SD, n=3). ***= $p<0.0001$, **= $p<0.0013$, *= $p<0.0188$.

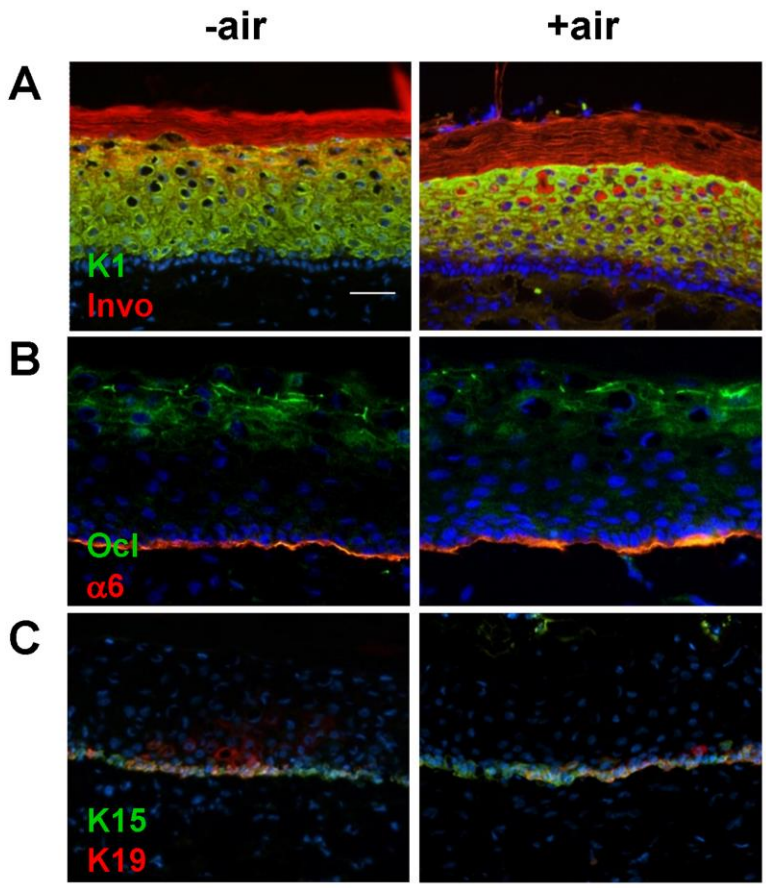

Figure 6. Stratification markers in air-exposed 6dK-DESS. (a) Immunofluorescence double-staining of cryosections with antibodies against K1 (green) and involucrin (red), (b) occludin (green) and integrin α6 (red), or (c) K15 (green) and K19 (red). Scale bar for all panels = 50 μm.

4.3 "Trooping the colour" - Restoring the original donor skin color by addition of melanocytes to bioengineered skin analogs

Sophie Böttcher-Haberzeth[1, 2], **Agnieszka S. Klar**[1], Thomas Biedermann[1], Clemens Schiestl[2], Claudia Meuli-Simmen[3], Ernst Reichmann[1], Martin Meuli[2*]

[1]Tissue Biology Research Unit, University Children's Hospital Zurich, Switzerland

[2]Department of Surgery, University Children's Hospital Zurich, Switzerland

[3]Clinic of Plastic- Reconstructive- and Hand Surgery, Kantonsspital, Aarau, Switzerland

[*]Corresponding author: Martin Meuli, Department of Surgery, University Children's Hospital Zurich, Steinwiesstrasse 75, 8032 Zurich, Switzerland, Email: martin.meuli@kispi.uzh.ch

Published in:

Pediatr Surg Int, 2013, 29(3):239-47

Abstract

Purpose: Autologous skin substitutes to cover large skin defects are used since several years. Melanocytes, although essential for solar protection and pigmentation of skin, are not yet systematically added to such substitutes. In this experimental study we reconstructed melanocyte-containing dermo-epidermal skin substitutes from donor skins of different skin pigmentation types and studied them in an animal model. Features pertinent to skin color were analyzed and compared in both skin substitutes and original donor skin.

Methods: Keratinocytes, melanocytes, and fibroblast were isolated, cultured, and expanded from skin biopsies of light and dark pigmented patients. For each donor, melanocytes and keratinocytes were seeded in different ratios (1:1, 1:5, 1:10) onto collagen gels previously populated with autologous fibroblasts. Skin substitutes were then transplanted onto full-thickness wounds of immuno-incompetent rats. After eight weeks, macroscopic and microscopic analyses were conducted with regard to skin color and architecture.

Results: Chromameter evaluation revealed that skin color of reconstructed light and dark pigmented skin was very similar to donor skin, independent of which melanocyte/keratinocyte ratio was added. Histological analyses of the skin analogs confirmed these findings.

C*onclusion:* These data suggest that adding autologous melanocytes to bioengineered dermo-epidermal skin analogs can sustainably restore the patients' native skin color.

Keywords: Melanocytes - Melanocyte/keratinocyte ratio - Tissue engineering – Skin analog - Skin color - Rat model

Introduction

One promising approach to cover large full-thickness skin defects is tissue engineering of skin [1]. Several laboratories worldwide, including our own research group, have been working on this ambitious project and have made substantial progress over the last years [2-5]. At our center, we first used simple autologous cultured epidermal autografts (CEA) for burn and reconstructive surgery [6, 7]. However, they did not fulfill the expectations in that they showed inconsistent CEA take as well as inconsistent functional and aesthetic results.

Consequently, we invested several years on the development of a near natural dermo-epidermal skin equivalent, based on the hypothesis that a skin substitute closely resembling native skin might ultimately produce more satisfactory clinical results [8-10]. Then, we managed to bioengineer capillaries *in vitro* in order to prevascularize skin substitutes [11]. Also, we looked at numerous options to strengthen the dermal compartment for better surgical handling and are now successfully working with a compressed hydrogel that serves as dermal template [12]. Finally, and with clinical application in mind, we developed a system to produce large scale (7.5 x 7.5 cm) skin analogs that were favorably tested in a large animal model (pig) [2, 3].

Most recently, we directed our work also at pigmentation that, for obvious reasons, is a crucial issue since it plays a fundamental functional role in terms of skin protection against ultraviolet (UV) radiation, and, additionally, it has a paramount cosmetic impact for the patient. If melanocytes, the cells responsible for skin pigmentation, are missing in skin analogs, the grafts appear unnaturally white like vitiligo-affected areas [13]. Therefore, we have designed a project with the principal goal to provide our autologous human skin analogs with appropriate pigmentation matching as closely as possible the native color present at the presumptive site of transplantation. To achieve this goal, we added human melanocytes in different ratios to the epidermal compartment of laboratory-engineered, human dermo-epidermal skin analogs, tested these in a rat model, and compared the obtained pigmentation features to those of the original donor skin.

Materials and Methods

Human skin samples

The study was conducted according to the "Declaration of Helsinki Principles" and after permission by the ethic commission of the Canton Zurich. Parents or patients gave informed consent to use skin samples. The human foreskins used were obtained from light and dark skin pigmentation types from patients 1 to 16 years of age. The skin samples were used for the isolation of human epidermal keratinocytes, melanocytes, and dermal fibroblasts. Tissues samples for histological examinations were embedded in OCT compound (Sakura Finetek, Switzerland) and kept at -30 °C, or prepared for paraffin sections.

Isolation and culturing of primary cells

Keratinocytes and fibroblasts were isolated and cultured as described in Pontiggia *et al.* [10], melanocytes as specified in Böttcher-Haberzeth *et al*. [8].

Preparation of tissue engineered skin analogs

The skin analogs were prepared as previously described [10]. Briefly, rat collagen type I was mixed with $1x10^5$ human dermal fibroblasts (passage 1) and placed in cell culture inserts with membranes of 3.0 μm pore-size (all BD Falcon, Germany). These dermal equivalents were grown in Dulbecco's modified Eagle's medium (DMEM, Invitrogen, Switzerland) for six days to allow for gel contraction. On each dermal equivalent $5x10^5$ keratinocytes and melanocytes (passage 1) of the corresponding donor skin were seeded in different ratios (melanocytes:keratinocytes 1:1, 1:5, or 1:10). The skin analogs were cultured for one week in a 1:1 mix of keratinocyte medium (SFM, Invitrogen, Switzerland) and melanocyte growth medium (Promocell, Germany), and subsequently transplanted (Table 1).

Table 1 Overview of the study design

	Melanocytes:Keratinocytes 1:1	Melanocytes:Keratinocytes 1:5	Melanocytes:Keratinocytes 1:10
Light skin analogs	1	4	4
Dark skin analogs	1	4	4

N Number of skin analogs prepared for transplantation

Transplantation of tissue engineered skin analogs

The surgical protocol was approved by the local Committee for Experimental Animal Research (permission number 76/2011). Immuno-incompetent female nu/nu rats, eight to ten weeks old (Harlan Laboratories, Netherlands), were prepared and anesthetized as previously described [14, 15]. Skin analogs were transplanted onto full-thickness skin defects created surgically on the backs of the rats. To prevent wound closure from surrounding rat skin and to protect the skin analogs, surgical steel rings (26 mm in diameter) were sutured to the skin defects, using non-absorbable polyester sutures (Ethibond®, Ethicon, USA). The skin analogs were covered with a silicone foil (Silon-SES, BMS, USA), a polyurethane sponge (Ligasano, Ligamed, Austria), and a tape as wound dressing. Dressing changes and photographic documentations were performed once per week. After eight weeks the transplanted skin analogs were excised in toto and processed for cryo- and paraffin sections, and electron microscopy.

Chromameter measurements

The International Commission on Illumination (Commission internationale de l'Eclairage, CIE) principles of 1976 describes a uniform, three-dimensional color space (L*a*b*) because color vision is trichromatic. The L value correlates to perceived lightness. It can range from absolute black (0) to absolute white (+100). As it is the most sensitive of the trichromatic values to skin analog color change, only the L value (mean ± SD) of the reflectance spectroscopy used to measure the visible spectrum of light reflected from the patients' foreskins and skin analogs was recorded in this study. The spectroscopy was conducted by employing a Chromameter CR-200 (Minolta, Osaka, Japan).

Histological analysis

Paraffin sections (5 µm) were stained with hematoxylin and eosin (Sigma, Switzerland) to assess the histological morphology and with the Fontana Masson technique to visualize melanin [16] in the transplanted skin analogs.

Immunohistochemical staining

Immunofluorescence staining was performed as described in Böttcher-Haberzeth *et al.* [15], and Böttcher-Haberzeth *et al.* [8]. To detect melanosomes, an anti-melanosome antibody was used (HMB-45, 1:50, Dako, Switzerland). To visualize the basement membrane, a staining against laminin-5 was performed (clone P3H9-2, 1:100, Santa Cruz, Germany). Pictures of immunofluorescence stainings were taken with a DXM1200F digital camera connected to a Nikon Eclipse TE2000-U inverted microscope. The device is equipped with Hoechst 33342-, FITC-, and TRITC-filter sets (Nikon AG, Switzerland; Software: Nikon ACT-1 vers. 2.70). Images were processed with Photoshop 7.0 (Adobe Systems Inc, Germany).

Electron microscopy

For transmission electron microscopy analyses, tissue blocs (approximately $1mm^3$) were prefixed in 0.1 M cacodylate buffer (Merck, Germany), pH 7.3 containing 2.5% glutaraldehyde for two hours, washed in cacodylate buffer, postfixed with an aqueous solution of 1% OsO4 and 1.5% K4Fe(CN)6 for one hour, dehydrated, and finally embedded in EPON 812 (Catalys AG, Switzerland). Ultrathin sections (approximately 50-70 nm) were collected on copper grids, contrasted with 4% uranyl acetate and 3% lead citrate, and examined with a CM 100 transmission electron microscope (Philips, The Netherlands). All reagents were from Sigma unless mentioned otherwise.

Statistical analysis

Melanocytes in the basal layer of the donor skin and of the skin analogs were evaluated by counting HMB-45 positive cells and cell nuclei (Hoechst staining) four times in each of five representative sections from each skin sample. The results were calculated (Microsoft Excel) to display the mean ± SD graphically.

Results

Macroscopic appearance and color measurement of transplants

Eight weeks after transplantation, the reconstructed human skin analogs from light and dark pigmented donor skin showed a strong resemblance to the latter regarding color and structure, independent of which melanocyte/keratinocyte ratio was used (Fig. 1). Pigmentation was very homogenous and even throughout the entire transplant of all specimens. The chromameter evaluation (L value) of the reconstructed light skin showed a mean deviation from the native light skin of 4.33% (SD 1.91%) for the constructs with a 1:1 melanocyte/keratinocyte ratio, of 3.68% (SD 0.63%) for the constructs with a 1:5 melanocyte/keratinocyte ratio, and of 1.91% (SD 3.27%) for the constructs with a 1:10 melanocyte/keratinocyte ratio. The chromameter evaluation of the reconstructed dark skin showed a mean deviation from the native dark skin of 2.04% (SD 0.96%) for the constructs with a 1:1 melanocyte/keratinocytes ratio, of 3.26% (SD 7.94%) for the constructs with a 1:5 melanocyte/keratinocyte ratio, and of 0.71% (SD 5.55%) for the constructs with a 1:10 melanocyte/keratinocyte ratio.

Epidermal structure

The epidermis of the constructs was comparable to the histology of the donor skin with regard to epidermal stratification, cellular differentiation, and absence of parakeratotic cells (Fig. 2). Results were very similar in both light and dark skin. A noticeable difference between the two was the heavily pigmented basal layer of the dark skin. An obvious difference between the analogs and the donor skin was the absence of rete ridges in the engineered skin.

Melanocytes and melanogenesis

HMB-45 staining visualized the melanocytes in the epidermis of the constructs (arrowheads Fig. 3). They resided in a physiologic position in the basal layer with contact to the basal membrane and projected dendrites into the upper layers of the epidermis (arrows Fig. 3). Fontana Masson staining demonstrated the typical melanin distribution within epidermal cells (supranuclear melanin cap) (Fig. 4). There were distinct differences between the light- and dark-pigmented constructs: There was more melanin in dark constructs and, in contrast to light constructs, melanin was found in all epidermal layers. Generally, the engineered

constructs showed similar melanin quantities and distribution to the donor skin, independent of which melanocyte/keratinocyte seeding ratio was used.

By transmission electron microscopy, the melanosomes inside melanocytes and their dendrites as well as melanin inside keratinocytes was analyzed more in detail (Fig. 5): In the light skin analogs, melanocytes produced less melanin and lighter melanin granules in the melanosomes, whereas melanocytes in the dark skin analogs produced more melanin and darker melanin granules in the melanosomes. The keratinocytes of the light skin constructs contained less pigment than the ones of the dark skin constructs. In both analogs, melanin was arranged in a supranucelar position (supranuclear cap).

Melanocyte density

The melanocyte/keratinocyte ratio in the basal layer of all analogs was very similar to that in the corresponding donor skin. Results in both, the light- and dark-pigmented skin analogs, were independent of which melanocyte/keratinocyte ratio had been added initially (Fig. 6).

Discussion

This is an experimental study looking at the question whether the original, i.e. “constitutive”, skin color of a patient can be reproduced when melanocytes are added to tissue engineered full-thickness skin analogs. In particular, we looked at results of reconstructed light- and dark-pigmented skin types when all cell types used (keratinocytes, melanocytes, and fibroblasts) were taken from the same donor skin and melanocytes were added in different ratios. Generally speaking, this study demonstrates that providing bioengineered skin analogs with melanocytes does in fact result in a skin color that is not only subjectively (photographic documentation) but also objectively (chromameter evaluation) almost identical to the color of the native donor skin. A number of aspects call for a detailed comment.

The fact that normal skin color is restored in our skin substitutes indicates that all sophisticated and often multi-step maneuvers from removal of the skin biopsy to cell isolation and culture, to assembling the substitutes, to transplantation, to middle-term maturation of the human transplanted skin in a rat model, do not seem to alter the involved cells (keratinocytes, melanocytes, and fibroblasts) in any measurable way. These cells apparently maintain their

inherent programs enabling them to communicate and interact with each other and work as a functional epidermal melanin unit (EMU) [17, 18].

Interestingly, the above mentioned color production is independent of the original number of melanocytes added to the constructs. Even a significant deviation from the physiological 1:5 ratio of melanocytes to keratinocytes in the basal layer towards a higher (1:1) and a lower ratio (1:10) of melanocytes to keratinocytes, does not result in any measurable color difference. It is known that a minimum density of melanocytes is required to restore pigmentation completely [13]. In our analogs, this minimum number of melanocytes necessary to enable pigmentation of the skin was used.

On a histological level, the macroscopic findings were precisely reflected. Particularly relevant is the fact that melanogenesis and the distribution of melanin transferred to keratinocytes very closely resembled the well-documented pattern known from physiological EMUs [19-21]. Also, the typical differences between light- and dark-pigmented skin types [21, 22], such as poorly pigmented supranuclear melanosomes and melanosome-free upper epidermis in light skin as well as heavily pigmented melanosomes throughout the cytoplasm of keratinocytes and melanosome presence throughout the entire epidermis in dark skin were largely replicated in our skin analogs.

Taken together, there is compelling evidence that adding melanocytes to bioengineered skin substitutes results in an almost physiological restoration of those cellular and molecular processes usually involved in the complex dynamics of skin pigmentation.

The importance of using all three cell types (keratinocytes, melanocytes, and fibroblasts) from the same donor skin must also be highlighted. It is known that keratinocytes, melanocytes, and fibroblasts are highly interactive and communicate with each other via cell/cell contacts and secreted factors to regulate skin phenotype and functionality [21]. In this context, it is crucial to underline the importance of using these three key player cells from the same donor skin sample (as shown here) in order to reproduce the original skin color in bioengineered skin analogs. Interestingly, combining keratinocytes and melanocytes from one skin pigment type with fibroblasts from another skin pigment type results in disparate skin colors of engineered skin substitutes [22]. Clearly, for clinical applications, the requirement for fully autologous skin substitutes is indispensable for obvious reasons.

With regard to skin physiology, the novel possibility to provide tissue engineered skin analogs with a near natural color represents a significant progress not only in general terms of cosmesis, but especially in terms of cancer prevention and the potential to correct stigmatizing pigmentation defects [23, 24].

This study, however, does not address all important issues regarding this topic. First, we did not generate any data demonstrating that tissue engineered EMUs possess the ability to appropriately react to UV radiation. Definitely, the well-documented up- and down-regulation processes (e.g. PAR-2 receptor expression, melanin production) must be studied in this context [25-28]. Secondly, this study does not provide long-term data. Although the results shown here are amazingly physiological and although there are no obvious reasons why this functional capability should significantly change over time, formal long-term studies must address the question whether hypo- or hyper-pigmentation may occur over time [13, 29]. Finally, the evergreen-issue of whether manipulating melanocytes is associated with an increased risk of eventual melanoma-formation, must be mentioned. Even though our study period is definitely not sufficiently long to answer these questions and even though we have not looked in detail at markers used for melanoma diagnostic work-up (e.g. S100, Melan A, Ki67), we have not found any irritating histological features indicative of melanocyte dysplasia, such as epidermal cluster-formation or dermal compartment invasion.

In conclusion, this is, to the best of our knowledge, the first study demonstrating that adding autologous melanocytes to tissue engineered full-thickness skin analogs allows the so reconstructed skin to produce a near normal skin color almost identical to the native color present in the donor skin. It appears crucial that all three cell types originate from the same donor skin. These findings have significant clinical implications in that transplanting a skin analog containing functional EMUs is much more physiological, protects against harmful UV radiation, and improves cosmetic outcome.

Acknowledgments

This work was financially supported by the EU-FP6 project EuroSTEC (soft tissue engineering for congenital birth defects in children: contract: LSHB-CT-2006-037409), by the EU-FP7 project EuroSkinGraft (FP7/2007-2013: grant agreement n° 279024), by the EU-FP7 (MultiTERM, grant agreement nr 238551), and by the University of Zurich. We are particularly grateful to the Foundation Gaydoul and the sponsors of “DonaTissue” (Thérèse Meier and Robert Zingg) for their generous financial support and interest in our work.

Conflict of interest

The authors declare that they have no conflict of interest.

References

[1] Böttcher-Haberzeth S, Biedermann T, Reichmann E (2010) Tissue engineering of skin. Burns 36(4):450-460

[2] Braziulis E, Biedermann T, Hartmann-Fritsch F, Schiestl C, Pontiggia L, Böttcher-Haberzeth S, Reichmann E, Meuli M (2011) Skingineering I: Engineering Porcine Dermo-Epidermal Skin Analogues for Autologous Transplantation in a Large Animal Model. Pediatr Surg Int 27(3):241-247

[3] Schiestl C, Biedermann T, Braziulis E, Hartmann-Fritsch F, Böttcher-Haberzeth S, Arras M, Cesarovic N, Nicolls F, Linti C, Reichmann E, Meuli M (2011) Skingineering II: Transplantation of Large Scale Laboratory-Grown Skin Analogs in a New Pig Model. Pediatr Surg Int 27(3):249-254

[4] MacNeil S (2007) Progress and opportunities for tissue-engineered skin. Nature 445(7130):874-880

[5] Boyce ST (2001) Design principles for composition and performance of cultured skin substitutes. Burns 27(5):523-533

[6] Gobet R, Raghunath M, Altermatt S, Meuli-Simmen C, Benathan M, Dietl A, Meuli M (1997) Efficacy of cultured epithelial autografts in pediatric burns and reconstructive surgery. Surgery 121(6):654-661

[7] Meuli M, Raghunath M (1997) Burns (Part 2). Tops and flops using cultured epithelial autografts in children. Pediatr Surg Int 12(7):471-477

[8] Böttcher-Haberzeth S, Biedermann T, Pontiggia L, Braziulis E, Schiestl C, Hendriks B, Eichhoff OM, Widmer DS, Meuli-Simmen C, Meuli M, Reichmann E (2012) Human eccrine sweat gland cells turn into melanin-uptaking keratinocytes in stratifying dermo-epidermal skin substitutes. J Invest Dermatol in press

[9] Biedermann T, Pontiggia L, Böttcher-Haberzeth S, Tharakan S, Braziulis E, Schiestl C, Meuli M, Reichmann E (2010) Human eccrine sweat gland cells can reconstitute a stratified epidermis. J Invest Dermatol 130(8):1996-2009

[10] Pontiggia L, Biedermann T, Meuli M, Widmer D, Böttcher-Haberzeth S, Schiestl C, Schneider J, Braziulis E, Montaño I, Meuli-Simmen C, Reichmann E (2009) Markers to evaluate the quality and self-renewing potential of engineered human skin substitutes in vitro and after transplantation. J Invest Dermatol 129(2):480-490

[11] Montaño I, Schiestl C, Schneider J, Pontiggia L, Luginbühl JF, Böttcher-Haberzeth S, Biedermann T, Braziulis E, Meuli M, Reichmann E (2010) Formation of human capillaries in vitro: The engineering of pre-vascularized matrices. Tissue Eng Part A 16(1):269-282

[12] Braziulis E, Diezi M, Biedermann T, Pontiggia L, Schmucki M, Hartmann-Fritsch F, Luginbühl J, Schiestl C, Meuli M, Reichmann E (2012) Modified plastic compression of collagen hydrogels provides an ideal matrix for clinically applicable skin substitutes. Tissue Eng Part C Methods 18(6):464-474

[13] Swope VB, Supp AP, Boyce ST (2002) Regulation of cutaneous pigmentation by titration of human melanocytes in cultured skin substitutes grafted to athymic mice. Wound repair and regeneration 10(6);378-386

[14] Schneider J, Biedermann T, Widmer D, Montano I, Meuli M, Reichmann E, Schiestl C (2009) Matriderm versus Integra: a comparative experimental study. Burns 35(1):51-57

[15] Böttcher-Haberzeth S, Biedermann T, Schiestl C, Hartmann-Fritsch F, Schneider J, Reichmann E, Meuli M (2012) Matriderm® 1mm versus Integra® Single Layer 1.3mm for one-step closure of full thickness skin defects: A comparative experimental study in rats. Pediatr Surg Int 28(2):171-177

[16] Weiner L, Han R, Scicchitano BM, Li J, Hasegawa K, Grossi M, Lee D, Brissette JL (2007) Dedicated epithelial recipient cells determine pigmentation patterns. Cell 130(5):932-942

[17] Jimbow K, Quevedo WC Jr, Fitzpatrick TB, Szabo G (1976) Some aspects of melanin biology: 1950-1975. J Invest Dermatol 67(1):72-89

[18] Fitzpatrick TB, Breathnach AS (1963) The epidermal melanin unit system. Dermatol Wochenschr 147:481-489

[19] Yamaguchi Y, Hearing VJ (2009) Physiological factors that regulate skin pigmentation. Biofactors 35(2):193-199

[20] Nordlund JJ (2007) The melanocytes and the epidermal melanin unit: an expanded concept. Dermatol Clin 25 271-281

[21] Yamaguchi Y, Brenner M, Hearing VJ (2007) The regulation of skin pigmentation. J Biol Chem 282(38):27557-27561

[22] Yoshida Y, Hachiya A, Sriwiriyanont P et al (2007) Functional analysis of keratinocytes in skin color using a human skin substitute model composed of cells derived from different skin pigmentation types. FASEB J 21(11):2829-2839

[23] Masnari O, Landolt MA, Roessler J, Weingaertner SK, Neuhaus K, Meuli M, Schiestl C (2012) Self- and parent-perceived stigmatisation in children and adolescents with congenital or acquired facial differences. J Plast Reconstr Aesthet Surg Jul 6 [Epub ahead of print]

[24] Landolt MA, Buehlmann C, Maag T, Schiestl C (2009). Brief report: quality of life is impaired in pediatric burn survivors with posttraumatic stress disorder. J Pediatr Psychol, 34(1):14-21

[25] Hearing VJ (2011) Determination of melanin synthetic pathways. J Invest Dermatol 131(E1):E8-E11

[26] Miyamura Y, Coelho SG, Wolber R, Miller SA, Wakamatsu K, Zmudzka BZ, Ito S, Smuda C, Passeron T, Choi W, Batzer J, Yamaguchi Y, Beer JZ, Hearing VJ (2007) Regulation of human skin pigmentation and responses to ultraviolet radiation. Pigment Cell Res 20(1):2-13

[27] Boissy RE (2003) Melanosome transfer to and translocation in the keratinocyte. Exp Dermatol 12 Suppl 2:5-12

[28] Seiberg M (2001) Keratinocyte-melanocyte interactions during melanosome transfer. Pigment Cell Res 14(4):236-242

[29] Boyce ST, Kagan RJ, Yakuboff KP, Meyer NA, Rieman MT, Greenhalgh DG, Warden GD (2002) Cultured skin substitutes reduce donor skin harvesting for closure of excised, full-thickness burns. Ann Surg 235(2):269-279

Figures and Tables

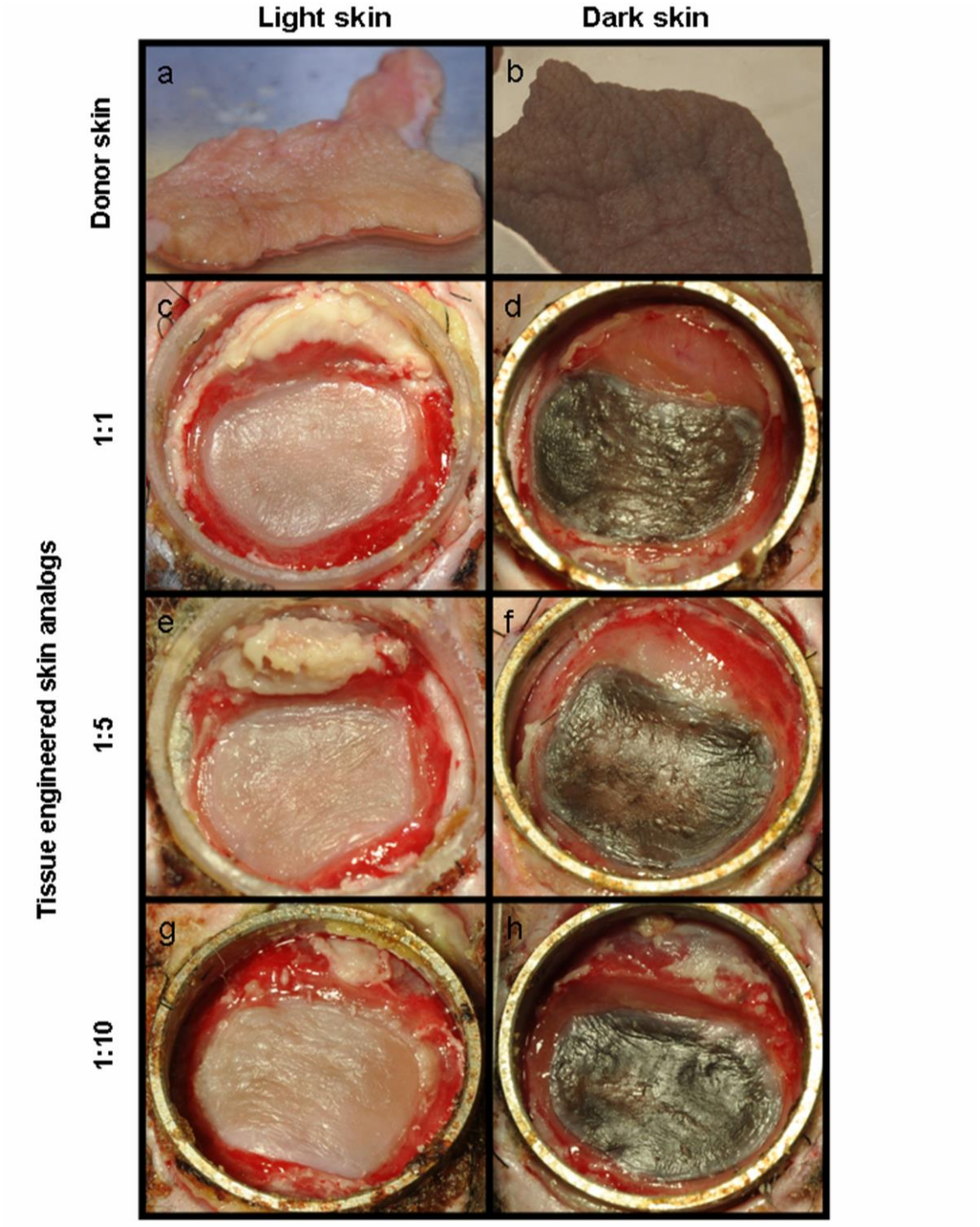

Figure 1. Macroscopic view of light and dark donor skin and its corresponding tissue engineered skin analogs eight weeks after transplantation. a Light and b dark donor skin before tissue preparation for cell isolation; c, e, g Tissue engineered skin analogs of light skin with a melanocyte/keratinocyte ratio of 1:1, 1:5, and 1:10; d, f, h Tissue engineered skin analogs of dark skin with a melanocyte/keratinocyte ratio of 1:1, 1:5, and 1:10. All analogs show a similar color to its donor skin, independent of which melanocyte/keratinocyte ratio was used initially.

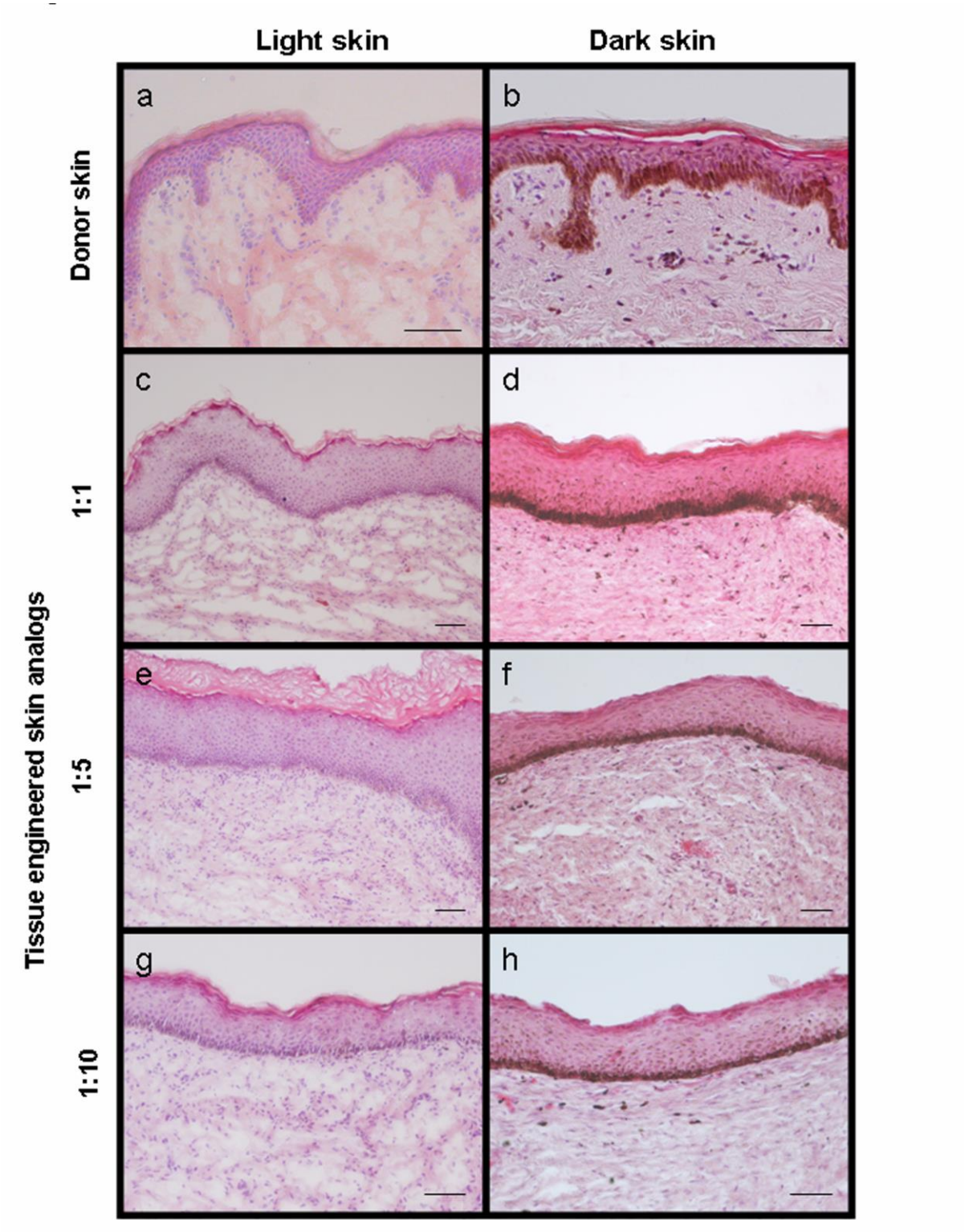

Figure 2. Histological evaluation of light and dark donor skin and of excised corresponding tissue engineered skin analogs eight weeks after transplantation (haematoxylin and eosin staining). a Light and b dark donor skin; c, e, g Tissue engineered skin analogs of light skin with a melanocyte/keratinocyte ratio of 1:1, 1:5, and 1:10; d, f, h Tissue engineered skin analogs of dark skin with a melanocyte/keratinocyte ratio of 1:1, 1:5, and 1:10. All analogs show a well developed, stratified epidermis very comparable to the corresponding donor skin structure. In the dark skin analogs the heavily pigmented basal layer can easily be detected. Scale bars 50 µm

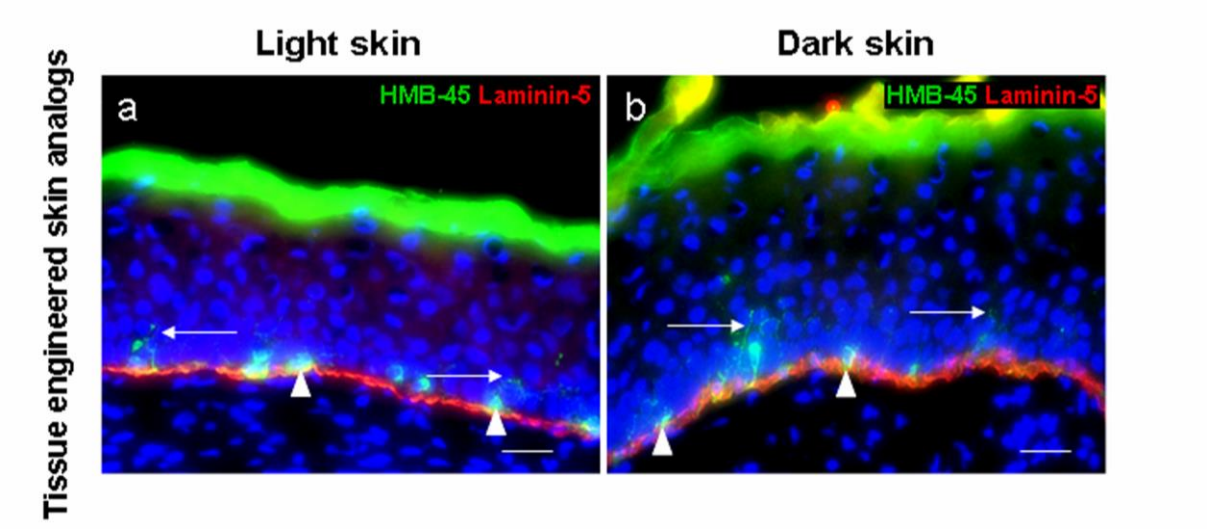

Figure 3. Melanocyte position in light and dark tissue engineered skin analogs eight weeks after transplantation. a Representative image of a light tissue engineered skin analog; b Representative image of a dark tissue engineered skin analog. Melanocytes are stained with HMB-45 (green), the basement membrane with Laminin-5 (red), cell nuclei are stained with Hoechst (blue). Melanocytes are distributed throughout the basal layer (arrowheads) on the basement membrane. Dendrites can be seen projecting to the upper layers of the epidermis (white arrows). Scale bars 50 µm

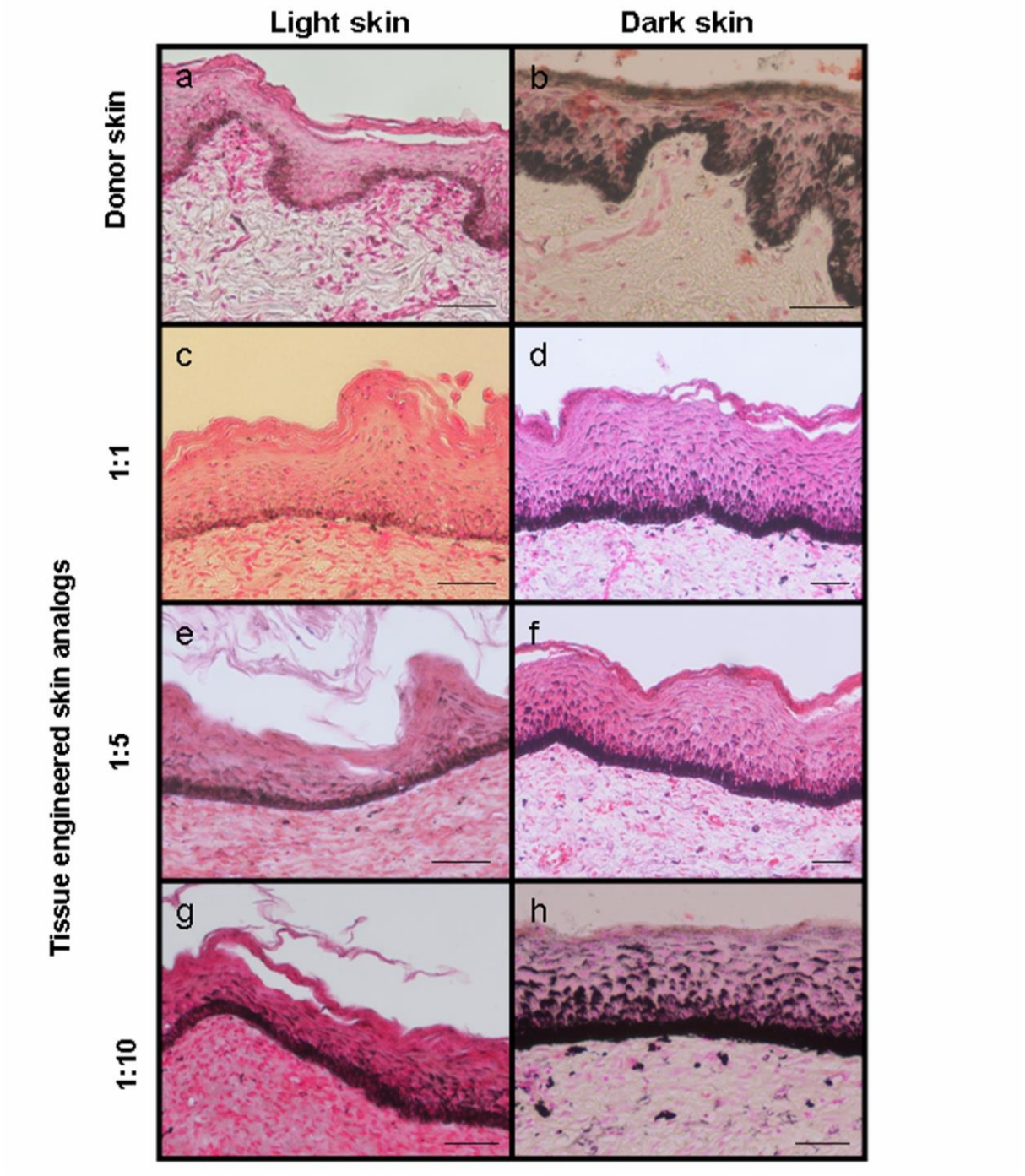

Figure 4. Fontana Masson staining of light and dark donor skin and of the excised corresponding tissue engineered skin analogs eight weeks after transplantation. a Light and b dark donor skin; c, e, g Tissue engineered skin analogs of light skin with a melanocyte/keratinocyte ratio of 1:1, 1:5, and 1:10; d, f, h Tissue engineered skin analogs of dark skin with a melanocyte/keratinocyte ratio of 1:1, 1:5, and 1:10. Melanin granules stain black. Melanin quantity and distribution in skin analogs is very comparable to the corresponding donor skin, however, much more pronounced in dark skin analogs. Melanin is physiologically arranged as supranuclear caps in all transplants. Scale bars 50 µm

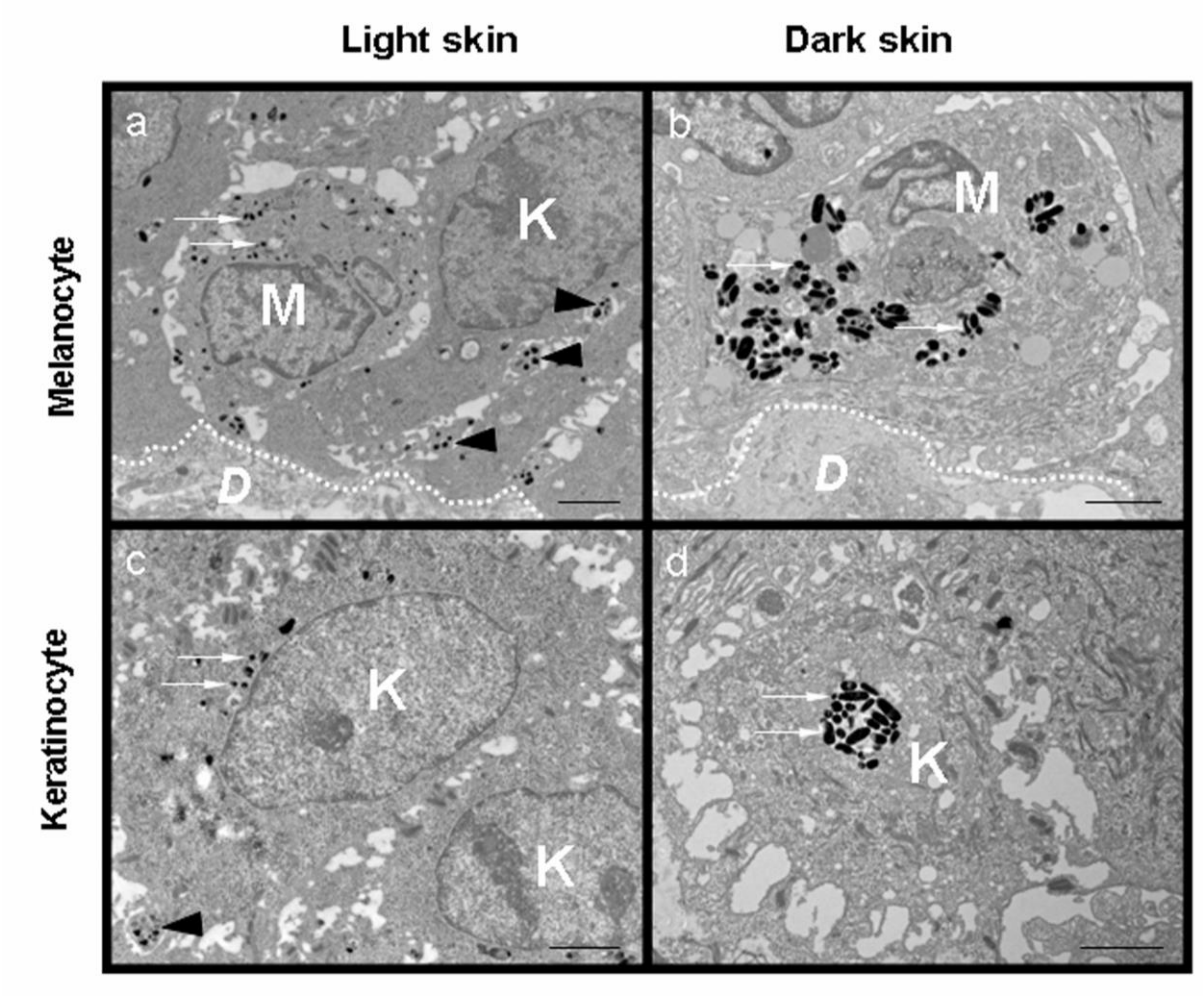

Figure 5. Ultrastructural evaluation of light and dark tissue engineered skin analogs eight weeks after transplantation. a Melanocyte in light tissue engineered skin analog; b Melanocyte in dark tissue engineered skin analog; c Keratinocyte in light tissue engineered skin analog; d Keratinocyte in dark tissue engineered skin analog. Melanocytes (M) are located in the basal layer of the epidermis on the basement membrane (dotted line). The adjacent dermis (D) can be identified by its collagen fibers. Melanin (white arrows) is clearly more pronounced in melanocytes (M) and keratinocytes (K) of the dark skin analog. Dendrites (black arrowheads) can be detected between cells. Scale bars 2 µm

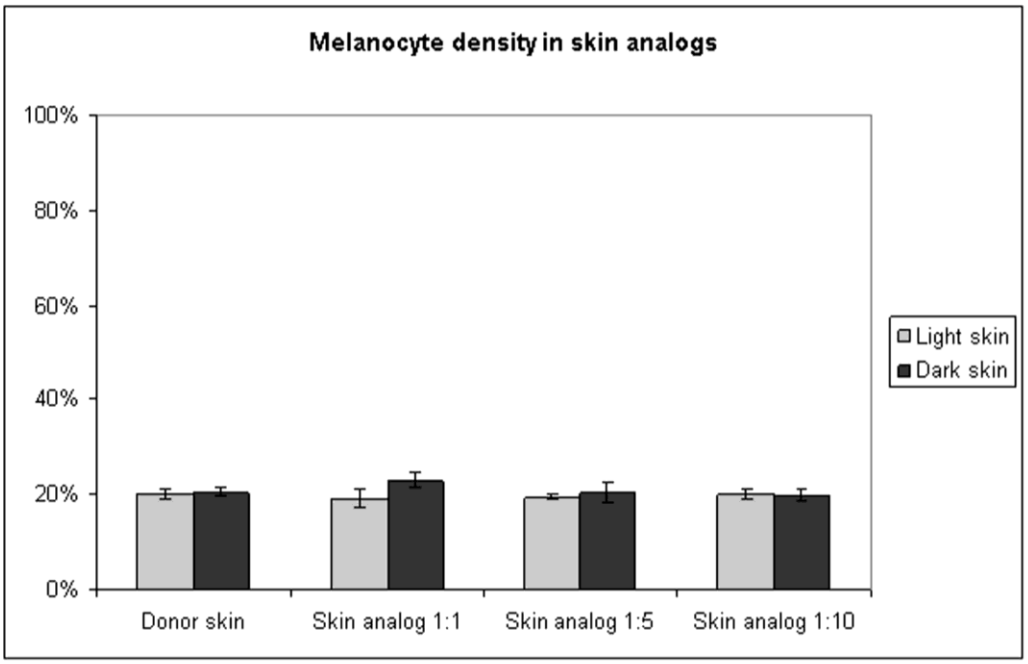

Figure 6. Percentage of melanocytes in the basal layer of light and dark donor skin and of the corresponding tissue engineered skin analogs with melanocyte/keratinocyte ratios of 1:1, 1:5, and 1:10.

4.4 Analysis of blood and lymph vascularization patterns in tissue-engineered human dermo-epidermal skin analogs of different pigmentation

Agnieszka S. Klar[1#], Sophie Böttcher-Haberzeth[1, 2#], Thomas Biedermann[1], Clemens Schiestl[2], Ernst Reichmann[1], and Martin Meuli[2*]

# Authors contributed equally to this paper

[1] University Children's Hospital Zurich, Tissue Biology Research Unit, Zurich, Switzerland

[2] University Children's Hospital Zurich, Department of Surgery, Zurich, Switzerland

[*]Corresponding author: Martin Meuli, Department of Surgery, University Children's Hospital Zurich, Steinwiesstrasse 75, 8032 Zurich, Switzerland, Email: martin.meuli@kispi.uzh.ch

Published in:

Pediatr Surg Int, 2014, 30(2):223-31

Abstract

Purpose: Bioengineered dermo-epidermal skin analogs containing melanocytes represent a promising approach to cover large skin defects including restoration of the patient's own skin color. So far, little is known about the development of blood and lymphatic vessels in pigmented skin analogs after transplantation. In this experimental study we analyzed the advancement and differences of host blood and lymphatic vessel ingrowth into light- and dark-pigmented human tissue-engineered skin analogs in a rat model.

Methods: Keratinocytes, melanocytes, and fibroblasts from light- and dark-pigmented skin biopsies were isolated, cultured, and expanded. For each donor, melanocytes and keratinocytes were seeded in ratios of 1:1, 1:5, and 1:10 onto fibroblast-containing collagen gels. The skin analogs were subsequently transplanted onto full-thickness wounds of immuno-incompetent rats and quantitatively analyzed for vascular and lymphatic vessel density after 8 and 15 weeks.

Results: The skin analogs revealed a significant difference in vascularization patterns between light- and dark-pigmented constructs after 8 weeks, with a higher amount of blood vessels in light compared to dark skin. In contrast, no obvious difference could be detected within the light- and dark-pigmented group when varying melanocyte/keratinocyte ratios were used. However, after 15 weeks, the afore-mentioned difference in blood vessel density between light and dark constructs could no longer be detected. Regarding lymphatic vessels, light and dark analogs showed similar vessel density after 8 and 15 weeks, whilst there were generally less lymphatic than blood vessels.

Conclusion: These data suggest that, at least during early skin maturation, keratinocytes, melanocytes, and fibroblasts from different skin color types used to construct pigmented dermo-epidermal skin analogs have distinct influences on the host tissue after transplantation. We speculate that different VEGF expression patterns might be involved in this disparate revascularization pattern observed.

Keywords: Melanocytes - Melanocyte/keratinocyte ratio - Tissue-engineering - Light-/dark-pigmented skin analog - Skin vascularization - Blood vessels - Lymphatic vessels - Rat model

Introduction

The therapy of large full-thickness skin wounds, as e.g. in massive burns, is often difficult due to their complex systemic impact, but also due to lack of sufficient autologous donor skin. Theoretically, tissue-engineered full thickness skin analogs offer an important alternative to conventional autologous skin grafts. For several years, our laboratory has made substantial efforts to develop and characterize a tissue-engineered dermo-epidermal skin equivalent [1-5]. Most recently, we reconstituted pigmented dermo-epidermal skin analogs from different pigmentation types and achieved very satisfactory in vivo results restoring the patients' native skin color [5]. This strategy holds promise for treatment of full-thickness skin defects as well as skin pigmentation disorders [6] in that the transplanted skin not only covers the defect, but also protects against ultraviolet radiation and provides the original skin color.

It has been shown, that the skin of light- and dark-pigmented individuals exhibits numerous intrinsic physiological differences. Montagna *et al.* reported that the epidermis of black skin has more and larger singly distributed melanosomes in keratinocytes, and contains more cell layers in the stratum corneum than that of white skin [7]. The dermis of black skin demonstrates more collagen fibrils, glycoproteins, and larger, more numerous fibroblasts, as well as more apocrine and ecrine sweat glands than white skin [8]. Moreover, black skin shows a higher density of superficial (subepidermal) blood vessels as well as more numerous, larger lymphatic vessels, as well as more nerve fibers than white skin [8]. Black subjects' skin is also less susceptible to cutaneous irritation induced by either chemicals or UV light and displays less erythema, less blood vessel reactivity, and cutaneous blood flow than white skin [9-12].

However, little is known about the development of blood and lymphatic vessels in tissue-engineered pigmented skin analogs of different pigmentation types after transplantation and, in particular, there is no data regarding the aforementioned physiologic differences between black and white skin.

In this experimental study, we investigated the differences of host blood and lymphatic vessel ingrowth into human tissue-engineered skin analogs derived from light- and dark-pigmented donor skin at 8 and 15 weeks after transplantation in a rat model.

Materials and Methods

Human skin samples

The investigation has been conducted according to Declaration of Helsinki principles and after acceptance of the Ethic Commission of the Canton Zurich. Children's parents gave informed consent to use skin samples. The human foreskin samples were obtained from light and dark skin pigmentation types from patients 1 to 16 years of age. Human epidermal keratinocytes, melanocytes, and dermal fibroblasts were isolated from the skin samples. Tissue samples for histological examinations were embedded in paraffin, or in OCT compound (Sakura Finetek, Switzerland) and kept at -20 °C.

Isolation and culturing of primary cells

Keratinocytes and fibroblasts were isolated and cultured as described by Pontiggia *et al.* [4] and Biedermann *et al.* [13], melanocytes as specified in Böttcher-Haberzeth *et al.* [5].

Preparation of tissue-engineered skin analogs

Transwell cell culture plates in 6-well format containing inserts with 3.0 µm pore-size membranes (BD Falcon, Switzerland) were used to prepare skin analogs [3]. To reconstruct the dermal compartment, rat collagen type I was mixed with 0.2 ml neutralization buffer containing 0.15M NaOH and with 1x105 human dermal fibroblasts (passage 1-3). After 10 min polymerization at room temperature and 45 min in an incubator at 37 °C, the dermal equivalents were grown for seven days in Dulbecco's modified Eagle's (DMEM) medium enriched with 10% FCS and Hepes (DMEM, Invitrogen, Switzerland). Subsequently, 5x105 keratinocytes and melanocytes (passage 1-3) of the corresponding donor skin were seeded in different ratios (melanocyte/keratinocytes 1:1, 1:5, or 1:10) onto dermal equivalents. The skin analogs were cultured for one week in a 1:5 mix of melanocyte growth medium (Promocell, Germany) and keratinocyte medium (SFM, Invitrogen, Switzerland), and subsequently transplanted.

Transplantation of cultured dermo-epidermal skin analogs

All animal studies have been approved by the local Committee for Experimental Animal Research (permission number: 76/2011). Immuno-deficient female nu/nu rats, 8 to 10 weeks old (Harlan Laboratories, Netherlands) were anesthetized as previously described [14-15]. Full-thickness skin wounds were created on the backs of the rats. Subsequently, custom made steel rings (diameter 2.6 cm) were sutured into the skin wounds using non-absorbable polyester sutures (Ethibond®, Ethicon, USA) and the skin analogs were sutured into those rings. Steel rings protected the skin analogs and prevented the closure of the wound by the surrounding rat skin. The transplants were then covered with a silicone foil (Silon-SES, BMS, USA), a polyurethane sponge (Ligasano, Ligamed, Austria), a cohesive conforming bandage (Sincohaft, Theo Frey AG, Switzerland), and tape as wound dressing. Dressing changes and photographic documentations were performed once per week. After 8 (N = 20) or 15 (N = 9) weeks the transplanted skin analogs were excised in toto and processed for paraffin- and cryo-sections.

Histological analysis

Paraffin sections (5 µm) were stained with hematoxylin and eosin (Sigma, Switzerland) to assess the histological morphology.

Immunohistochemical staining

Immunofluorescence staining was performed as described in Böttcher-Haberzeth *et al.* [15-16]. Double immunofluorescence stainings were performed to visualize rat blood and/or lymphatic vessels (CD31 [clone TDL-3A12, 1:50, BD Pharmingen, Switzerland], LYVE1 [polyclonal, 1:200, Novus Biologicals, UK]), and human fibroblasts (CD90 [clone 5E10, 1:50, Dianova, Germany]). The human control skin samples were double-stained for human CD31 [clone JC70A, 1:50, Dako, Switzerland], LYVE1 [clone ab10278, 1:200, Abcam, UK]), and human fibroblasts (CD90 [clone AS02, 1:50, Dianova, Germany]).

Pictures of immunofluorescence stainings were taken with a DXM1200F digital camera connected to a Nikon Eclipse TE2000-U inverted microscope. The device is equipped with Hoechst 33342-, FITC-, and TRITC-filter sets (Nikon AG, Switzerland; Software: Nikon

ACT-1 vers. 2.70). Images were processed with Photoshop 7.0 (Adobe Systems Inc, Germany).

Rat blood and lymphatic vessel quantification

Vessel profiles in skin analogs were counted on 6-8 μm thick cryo-sections double-stained for rat CD31/LYVE1 and human CD90. Five random fields at ×10 magnification were counted in three different sections of each skin analog after 8 or 15 weeks (n = 3-6). Vessel density was expressed as the average number of blood/lymphatic vessels from all fields counted in each skin analog. By double-staining for CD31 and LYVE1, it was possible to distinguish and separately quantify LYVE1-CD31+ blood vessels and LYVE1+CD31+ lymph vessels. All results are reported as mean ± standard deviation (SD). Statistical analysis was performed with GraphPad Prism 4.0 (Graph Pad software, La Jolla, CA, USA). Comparison between two groups was performed using the unpaired Student's t test. Results were considered significant with a $P < 0.05$.

Results

Analysis of normal human and rat skin

Native human and rat skin show specific differences, as demonstrated by a hematoxylin and eosin staining (Fig. 1a, b). In comparison to human foreskin (Fig. 1a), rat back skin (Fig. 1b) is composed of less epidermal layers. It also contains hair follicles and sebaceous glands throughout the dermis. To show the presence of human fibroblasts in the dermal compartment of human skin, we used a human specific anti-CD90 antibody, which does not stain rat fibroblasts (green, Fig. 1c, d). Human and rat blood vessels, specifically labeled with the anti-human or -rat CD31 antibody (red, Fig 1 c, d), were very abundant in the dermis of both species.

To distinguish lymphatic vessels from blood vessels in the skin, we used an antibody to stain LYVE1, a lymphatic endothelium-specific marker (green, Fig. 1e-f). Both human and rat blood vessels were LYVE1-negative, however, lymphatic vessels also showed a faint CD31-staining.

Macroscopic appearance and epidermal structure of human light- and dark-pigmented skin analogs

Eight weeks after transplantation the reconstructed human skin analogs from light- and dark-pigmented donor skin showed a strong resemblance to the donor skin regarding color and structure, independent of which melanocyte/keratinocyte ratio (1:1, 1:5, 1:10) was used (data not shown). Pigmentation was homogenous throughout the entire transplant of all specimens.

Also, 15 weeks after transplantation, light- and dark-pigmented skin analogs prepared with a melanocyte/keratinocyte ratio of 1:5 showed macroscopically a light and dark aspect with homogenous pigmentation (Fig. 2a, b). Microscopically, both skin analogs showed a stratified and cornified epidermis on a cellularized neodermis (Fig. 2a, b). However, a noticeable difference between the two analogs was the strongly pigmented basal layer of the dark skin analog (Fig. 2b). Moreover, skin appendages and rete ridges were absent in all engineered skin samples.

Blood vessel patterns of transplanted human tissue-engineered skin analogs

Eight weeks post-transplantation, light- and dark-pigmented skin analogs prepared with different ratios of melanocytes/keratinocytes (1:1, 1:5, 1:10) were excised and analyzed. The human dermal compartment was delineated by an anti-human CD90-staining (green, Fig. 3). The ingrowth of host blood vessels into the human transplants was analyzed using a staining against rat-CD31 (red, Fig. 3) and thereafter quantified (Fig. 4).

After eight weeks, light- and dark-pigmented skin analogs were entirely vascularized showing blood vessels throughout the human CD90-stained dermal compartment with a dense superficial vascular network underneath the epidermis (Fig. 3). The quantification revealed that the light-pigmented group contained a significantly higher number of blood vessels than the dark-pigmented group (Fig. 4a). However, the overall blood vessel density within the light-pigmented group did not show any obvious differences when varying melanocyte/keratinocyte ratios were used: 50 ± 14 vessels/mm^2 (1:1 ratio); 45 ± 8 vessels/mm^2 (1:5 ratio); 51 ± 8 vessels/mm^2 (1:10 ratio). A similar observation was made within the dark-pigmented group: 31 ± 6 vessels/mm^2 (1:1 ratio); 34 ± 8 vessels/mm^2 (1:5 ratio); 34 ± 11 vessels/mm^2 (1:10 ratio) (Fig. 4a).

After 15 weeks, significantly fewer blood vessels were detected in both light- and dark-pigmented skin analogs (melanocyte/keratinocyte ratio 1:5). The light-pigmented

analogs contained 23 ± 10 vessels/mm^2 and the dark-pigmented analogs 25 ± 6 vessels/mm^2 (Fig. 5a, b; Fig. 6a).

Lymphatic vessel patterns of transplanted human tissue-engineered skin analogs

Eight weeks after transplantation, the human skin analogs were analyzed for the presence of lymphatic, LYVE1-positive, vessels in the human CD90-stained neodermis and quantified (Fig. 4b). The lymphatic vessels were randomly distributed throughout the human dermal compartment, but were rare in close proximity to the dermo-epidermal junction. They displayed an irregular shape and were slightly larger in diameter than blood capillaries. Moreover, ingrowth was established five weeks post-transplantation as compared to blood vessel networks, which were already completely established after three weeks in vivo (data not shown).

After eight weeks, we did not detect any statistically significant difference in the lymphatic vessel densities between varying melanocyte/keratinocyte ratios of light- ((6 ± 3 vessels/mm^2 (1:1 ratio); 7 ± 3 vessels/mm^2 (1:5 ratio); 9 ± 3 vessels/mm^2 (1:10 ratio)), and dark-pigmented group ((9 ± 3 vessels/mm^2 (1:1 ratio); 9 ± 5 vessels/mm^2 (1:5 ratio); 8 ± 4 vessels/mm^2 (1:10 ratio). Of note, they occurred at a much lower density as compared to blood vessels (Fig. 4b).

The number of lymphatic vessels did not change after 15 weeks post-transplantation and was comparable to the amount at 8 weeks in both light- (7 ± 3 vessels/mm^2) and dark-pigmented skin analogs (9 ± 4 vessels/mm^2) (both 1:5 ratio) (Fig. 5c, d; Fig. 6b).

Discussion

To the best of our knowledge, this is the first study investigating the blood and lymphatic vessel patterns in differentially pigmented human tissue-engineered skin analogs at 8 and 15 weeks after transplantation. In particular, we analyzed quantitative differences in revascularization patterns between light- and dark-pigmented skin analogs. Overall our study demonstrates distinctly disparate blood vessel densities in the early wound healing stages at 8 weeks post-transplantation between the light- and the dark-pigmented groups. Interestingly, this clear differences can no longer be observed at a later stage, namely at 15 weeks post-transplantation. Of note, these differences can not be seen regarding lymph vessel ingrowth. Some aspects deserve to be addressed in more detail.

The fact that we observe a disparate vascularization pattern between light- and dark-pigmented constructs eight weeks after transplantation, with a significantly higher amount of blood vessels in the light- compared to the dark-pigmented skin analog group, is clearly surprising. Little is known about differences concerning blood and/or lymphatic vessel densities in light and dark-pigmented human skin. What has already been described is that the facial skin of dark-pigmented individuals contains a higher density of superficial blood vessels than the facial skin of light-pigmented persons [8]. Of note, dark skin is less susceptible to different chemical irritants, most probably due to decreased blood vessel reactivity, and therefore less cutaneous blood flow [9-12]. Our results from 8 weeks after transplantation do not demonstrate a vascularization pattern reflecting this distinct physiological morphology but rather show the opposite. We hypothesize, that this time point might be too early for skin analogs to show distinct differences as seen in a physiological, i.e. homeostatic situation. Another explanation could be that the differences between dark and light facial skin reported by Montagna *et al.* [8], might simply not be present in light and dark foreskins as used in our study, because these cells exhibit diverse angiogenic characteristics. Indeed, when analyzing native light and dark foreskin samples, we were not able to detect any apparent differences regarding blood vessels or VEGFA expression patterns (data not shown). Nonetheless, the fact that we observe significant differences in the early, i.e. probably not yet homeostatic, vascular pattern between light- and dark-pigmented skin analogs, suggests that intrinsic signals stemming from keratinocytes, melanocytes, or fibroblasts must be responsible for this transient phenomenon.

Interestingly, 15 weeks post-transplantation no more differences could be detected in the number of vessels present light and dark grafts. We propose the following interpretation for this change from 8 to 15 weeks. Shortly after transplantation, skin tissue demands to be quickly revascularized to ensure cell survival and adequate integration of the transplant into the host tissue [17-18]. Later, as the graft matures and reaches the remodeling stage, the initially needed, but now redundant vascular networks are reduced [19-20].

Of note, although we do notice the described, temporary difference in the vascularization dynamics, all transplants exhibit an apparently competent capillary network within the dermal compartment, ensuring survival and, presumably, also supporting maturation of the dermo-epidermal skin analogs.

Regarding lymphatic vessels, we observe an equal density at 8 and 15 weeks after transplantation. However, their ingrowth occurs later and the number of lymphatic vessels is clearly less compared to blood vessels. Interestingly, an abundant rat blood capillary network

can be identified in the dermal compartment as early as three weeks post transplantation, whereas a beginning lymphatic vessel ingrowth in our skin analogs was seen only five weeks after transplantation (data not shown). It is reasonable to argue that the establishment of a rapid vascular supply within the transplanted skin has the highest priority with regard to immediate graft take and long-term survival, and therefore occurs earlier than lymphatic vessel ingrowth. Of note, Nogami *et al.* [21] followed the recovery of lymphatic vessels in rat skin incision wounds up to 12 weeks and found that lymphatic vessels were not present in the wound area, but only in the surrounding intact tissue. In contrast, we observed that lymphatic vessels regenerated ubiquitously and abundantly in the dermis of our skin analogs already five weeks after transplantation. Furthermore, previous reports showed that lymphatic regeneration across scar tissues is severely impaired and that fibrosis in a wound can be directly responsible for lymphedema formation due to reduced lymphatic endothelial cell proliferation and abnormal lymphatic microarchitecture [22-23]. In light of the above, our findings are particularly important with regard to our planned clinical application of laboratory engineered skin substitutes. It appears tenable that a competent lymphatic vessel supply will also develop when our skin substitutes are autologously transplanted onto human patients.

In summary and conclusion, this appears to be the first article demonstrating that differently pigmented human tissue-engineered dermo-epidermal skin analogs show a near physiological ingrowth of both blood and lymphatic in a rat model. Further, our results suggest that different cells, especially keratinocytes, melanocytes, and fibroblasts of light- and dark-pigmented skin analogs seem to orchestrate temporarily disparate vascularization patterns. It appears likely that favorable blood and lymphatic vessels ingrowth dynamics take place when autologous tissue-engineered skin analogs are transplanted onto human patients.

Acknowledgments

This work was financially supported by the EU-FP6 project EuroSTEC (soft tissue engineering for congenital birth defects in children: contract: LSHB-CT-2006-037409), by the EU-FP7 project EuroSkinGraft (FP7/2007-2013: grant agreement nr 279024), by the EU-FP7 (MultiTERM, grant agreement nr 238551), and the Clinical Research Priority Programs (CRPP) of the Faculty of Medicine of the University of Zurich. We are particularly grateful to the Gaydoul Foundation and the sponsors of “DonaTissue” (Thérèse Meier and Robert Zingg) for their generous financial support and interest in our work.

Conflict of interest

The authors declare that they have no conflict of interest.

References

[1] Braziulis E, M Diezi, T Biedermann, L Pontiggia, M Schmucki, F Hartmann-Fritsch, J Luginbuhl, C Schiestl, M Meuli and E Reichmann (2012) Modified plastic compression of collagen hydrogels provides an ideal matrix for clinically applicable skin substitutes. Tissue Eng Part C Methods 18:464-74

[2] Biedermann T, S Bottcher-Haberzeth, AS Klar, L Pontiggia, C Schiestl, C Meuli-Simmen, E Reichmann and M Meuli (2013) Rebuild, restore, reinnervate: do human tissue engineered dermo-epidermal skin analogs attract host nerve fibers for innervation? Pediatr Surg Int 29:71-8

[3] Pontiggia L, A Klar, S Bottcher-Haberzeth, T Biedermann, M Meuli and E Reichmann (2013) Optimizing in vitro culture conditions leads to a significantly shorter production time of human dermo-epidermal skin substitutes. Pediatr Surg Int 29:249-56

[4] Pontiggia L, T Biedermann, M Meuli, D Widmer, S Bottcher-Haberzeth, C Schiestl, J Schneider, E Braziulis, I Montano, C Meuli-Simmen and E Reichmann (2009) Markers to evaluate the quality and self-renewing potential of engineered human skin substitutes in vitro and after transplantation. J Invest Dermatol 129:480-90

[5] Bottcher-Haberzeth S, AS Klar, T Biedermann, C Schiestl, C Meuli-Simmen, E Reichmann and M Meuli (2013) "Trooping the color": restoring the original donor skin color by addition of melanocytes to bioengineered skin analogs. Pediatr Surg Int 29:239-47

[6] Plensdorf S and J Martinez (2009) Common pigmentation disorders. Am Fam Physician 79:109-16

[7] Weigand DA, C Haygood and JR Gaylor (1974) Cell layers and density of Negro and Caucasian stratum corneum. J Invest Dermatol 62:563-8

[8] Montagna W and K Carlisle (1991) The architecture of black and white facial skin. J Am Acad Dermatol 24:929-37

[9] Marshall EC (1989) Racial differences in the presentation of chronic open-angle glaucoma. J Am Optom Assoc 60:760-7

[10] Wedig JH and HI Maibach (1981) Percutaneous penetration of dipyrithione in man: effect of skin color (race). J Am Acad Dermatol 5:433-8

[11] Berardesca E and HI Maibach (1988) Sodium Lauryl Sulfate Induced Cutaneous Irritation - Comparison of White and Hispanic Subjects. Contact Dermatitis 19:136-140

[12] Berardesca E and HI Maibach (1988) Racial-Differences in Sodium Lauryl Sulfate Induced Cutaneous Irritation - Black and White. Contact Dermatitis 18:65-70

[13] Biedermann T, L Pontiggia, S Bottcher-Haberzeth, S Tharakan, E Braziulis, C Schiestl, M Meuli and E Reichmann (2010) Human Eccrine Sweat Gland Cells Can Reconstitute a Stratified Epidermis. Journal of Investigative Dermatology 130:1996-2009

[14] Schneider J, T Biedermann, D Widmer, I Montano, M Meuli, E Reichmann and C Schiestl (2009) Matriderm versus Integra: a comparative experimental study. Burns 35:51-7

[15] Bottcher-Haberzeth S, T Biedermann, C Schiestl, F Hartmann-Fritsch, J Schneider, E Reichmann and M Meuli (2012) Matriderm(R) 1 mm versus Integra(R) Single Layer 1.3 mm for one-step closure of full thickness skin defects: a comparative experimental study in rats. Pediatr Surg Int 28:171-7

[16] Bottcher-Haberzeth S, T Biedermann, L Pontiggia, E Braziulis, C Schiestl, B Hendriks, OM Eichhoff, DS Widmer, C Meuli-Simmen, M Meuli and E Reichmann (2013) Human eccrine sweat gland cells turn into melanin-uptaking keratinocytes in dermo-epidermal skin substitutes. J Invest Dermatol 133:316-24

[17] Bhora FY, BJ Dunkin, S Batzri, HM Aly, BL Bass, AN Sidawy and JW Harmon (1995) Effect of growth factors on cell proliferation and epithelialization in human skin. J Surg Res 59:236-44

[18] Martin P (1997) Wound healing--aiming for perfect skin regeneration. Science 276:75-81

[19] Gurtner GC, S Werner, Y Barrandon and MT Longaker (2008) Wound repair and regeneration. Nature 453:314-321

[20] Blanpain C and E Fuchs (2009) Epidermal homeostasis: a balancing act of stem cells in the skin. Nat Rev Mol Cell Biol 10:207-17

[21] Nogami M, T Hoshi, T Arai, Y Toukairin, M Takama and I Takahashi (2009) Morphology of lymphatic regeneration in rat incision wound healing in comparison with vascular regeneration. Leg Med (Tokyo) 11:213-8

[22] Warren AG and SA Slavin (2007) Scar lymphedema: fact or fiction? Ann Plast Surg 59:41-5

[23] Avraham T, NW Clavin, SV Daluvoy, J Fernandez, MA Soares, AP Cordeiro and BJ Mehrara (2009) Fibrosis Is a Key Inhibitor of Lymphatic Regeneration. Plastic and Reconstructive Surgery 124:438-450

Figures and Tables

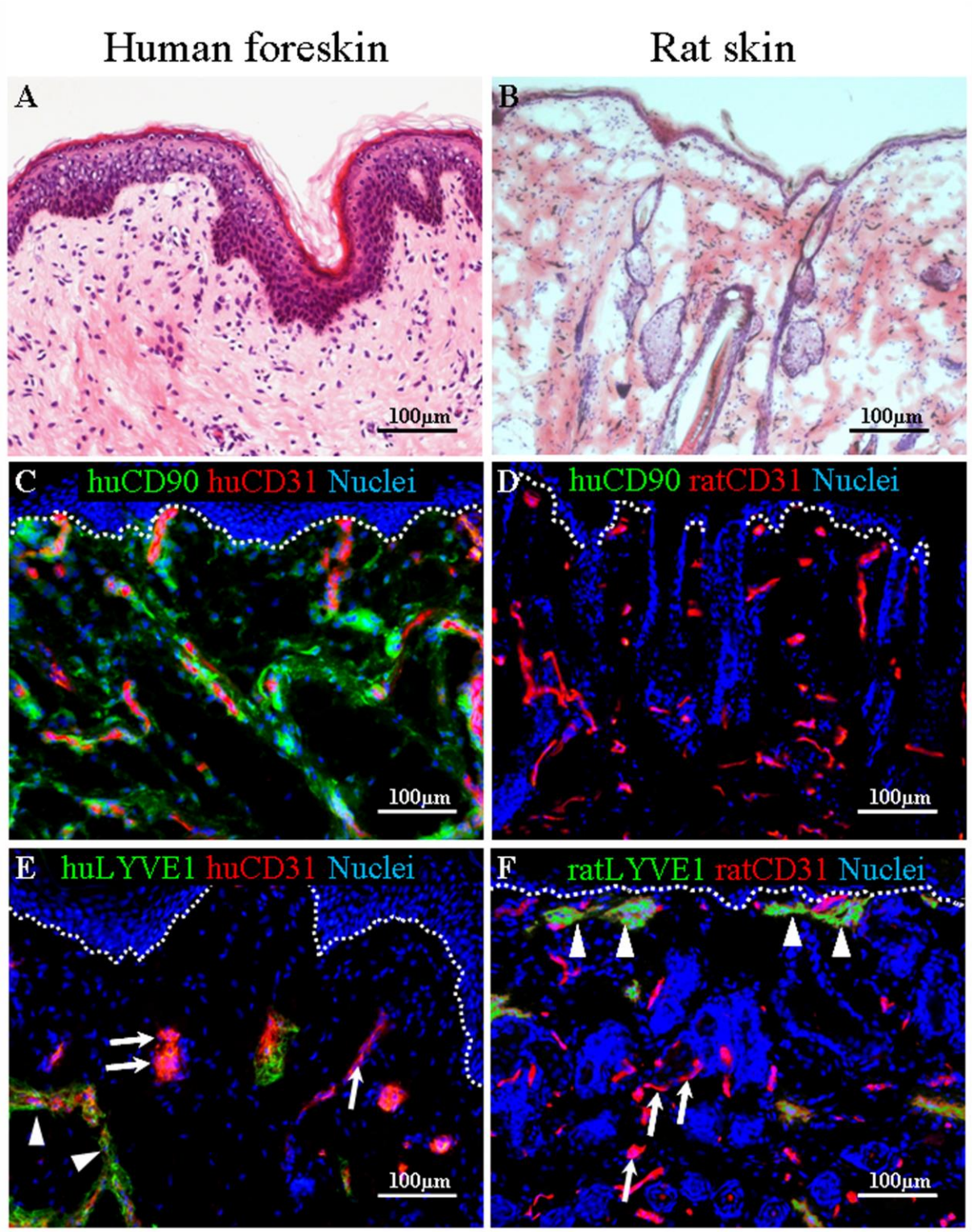

Figure 1. Evaluation of normal human foreskin and rat back skin and the expression of blood- and lymphatic-specific markers. a, b Hematoxylin and eosin staining showing a comparison of normal human versus rat skin; rat skin reveals less layers in the epidermis and abundant hair follicles in the dermis. c, d Immunofluorescence double staining of human and rat skin with antibodies against human CD90 (staining of human dermal

compartment, green) and against human and rat CD31 (staining of blood vessels, red). e, f Immunofluorescence double staining of human and rat skin with antibodies against human and rat LYVE1 (lymphatic vessels, green) and against human and rat CD31 (blood vessels, red), distinguishing human and rat lymphatic vessels (white arrowheads) from blood vessels (white arrows). LYVE1-positive lymphatic vessels are faintly positive for CD31 too; however, blood vessels are LYVE1 negative. Thus, LYVE1 was used as a lymphatic-specific marker for all further experiments. Cell nuclei are stained with Hoechst (blue). Scale bars 100 μm.

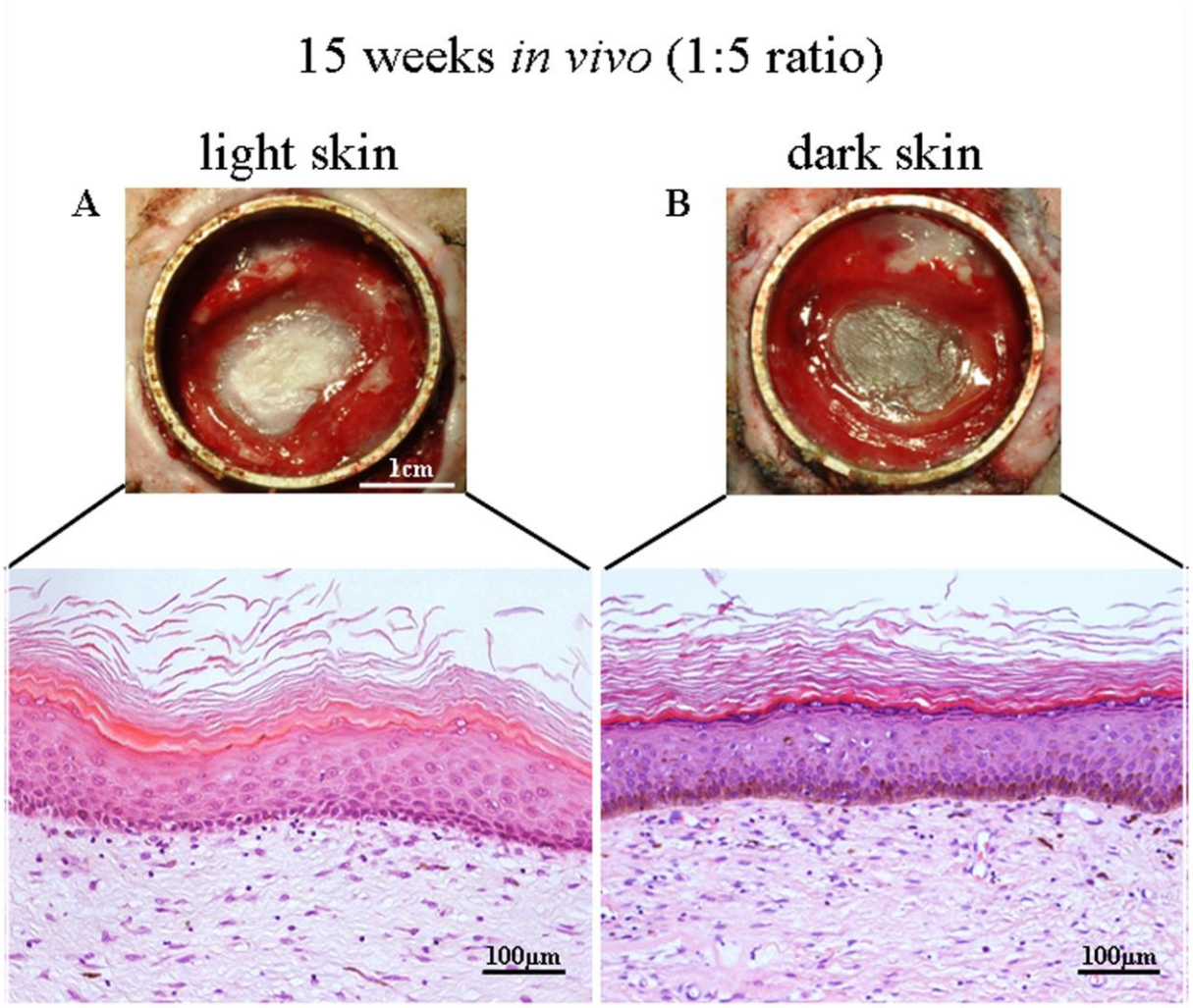

Figure 2. Tissue-engineered human skin analogs constructed with keratinocytes and melanocytes (1:5 ratio) derived from light or dark donor skin 15 weeks after transplantation. Macroscopic aspect and hematoxylin and eosin staining of light- (a) and dark-pigmented (b) skin analogs. The constructs both demonstrate a macroscopic and microscopic appearance that, except for the absence of rete ridges and skin appendages, closely resemble normal human light- and dark-pigmented skin. Scale bars 100 µm

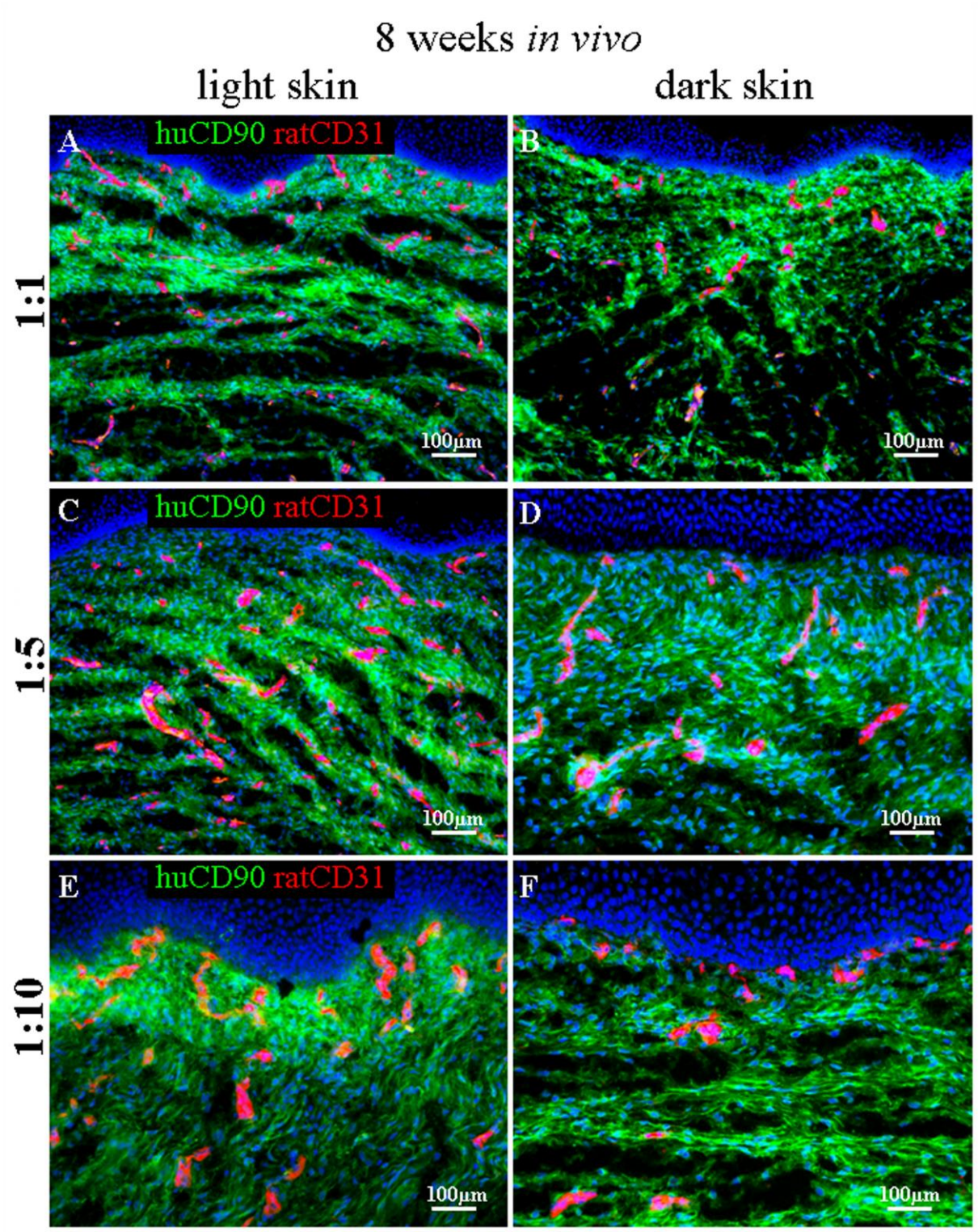

Figure 3. Host vascularization of light- and dark-pigmented skin analogs (melanocyte/keratinocyte ratio 1:1, 1:5, 1:10) 8 weeks after transplantation. a, c, e Rat blood vessels of light skin are stained with an antibody against rat CD31 (red). b, d, f Rat blood vessels of dark skin are stained with an antibody against rat CD31 (red). Human dermal compartment is delineated by an anti-human CD90 staining (green), and cell nuclei with Hoechst (blue). Light- and dark-pigmented skin analogs show ubiquitous and abundant blood vessels throughout the human CD90-stained neodermis. Scale bars 100 µm

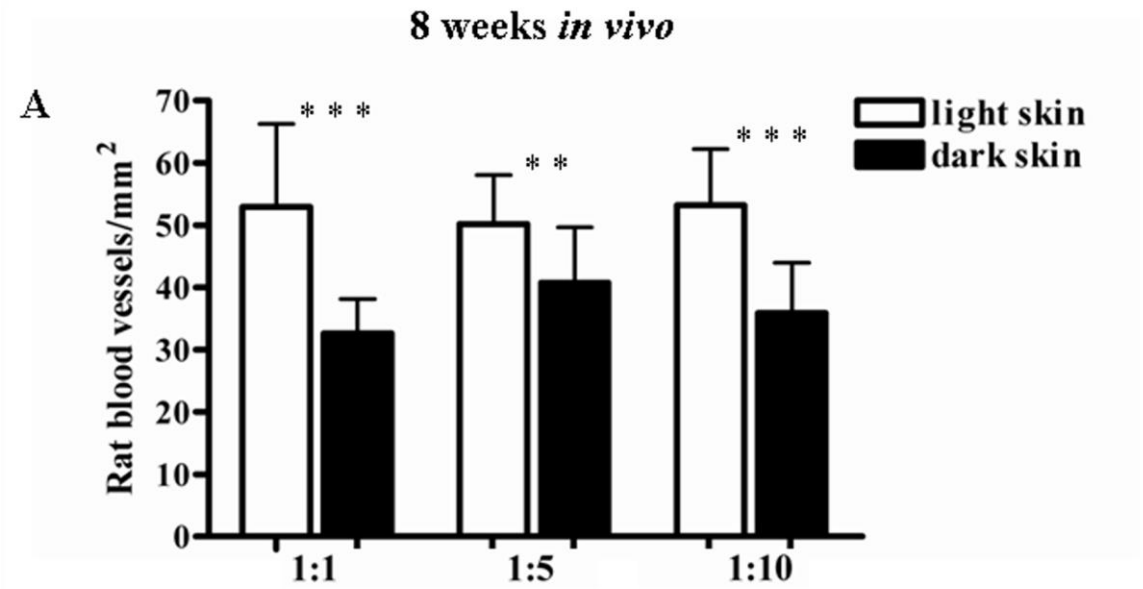

Number of rat blood vessels/mm²	light skin	dark skin	p-value
1:1 (Mean ± SD)	53 ± 13 (N = 3)	33 ± 5 (N = 3)	p < 0.0001
1:5 (Mean ± SD)	50 ± 8 (N = 4)	41 ± 9 (N = 4)	p = 0.003
1:10 (Mean ± SD)	53 ± 9 (N = 3)	36 ± 8 (N = 3)	p < 0.0001

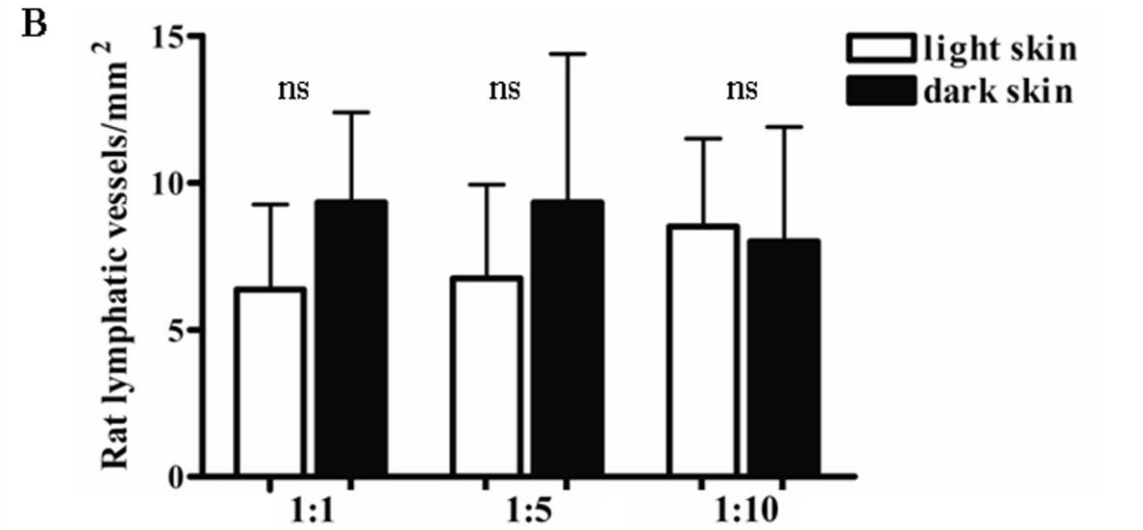

Number of rat lymphatic vessels/mm²	light skin	dark skin	p-value
1:1 (Mean ± SD)	6 ± 3 (N = 3)	9 ± 3 (N = 3)	ns (p= 0.1683)
1:5 (Mean ± SD)	7 ± 3 (N = 4)	9 ± 5 (N = 4)	ns (p= 0.1292)
1:10 (Mean ± SD)	9 ± 3 (N = 3)	8 ± 4 (N = 3)	ns (p= 0.8345)

Figure 4. The density of rat blood and lymphatic vessels in light- and dark-pigmented skin analogs (melanocyte/keratinocyte ratio 1:1, 1:5, 1:10) 8 weeks after transplantation. a Blood vessel (CD31) density of

light- (white bars) and dark-pigmented analogs (black bars). Note a significantly higher number of blood vessels in the light- than the dark-pigmented group. b Lymphatic vessel (LYVE1) density of light- (white bars) and dark-pigmented analogs (black bars). Of note, lymphatic vessel ingrowth occurred at a much lower density as compared to blood vessels, regardless of the pigmentation pattern. Table shows values as the mean (± SD) number of rat blood (a)/lymphatic (b) vessels quantified per mm2. N = 3 or 4 for each group

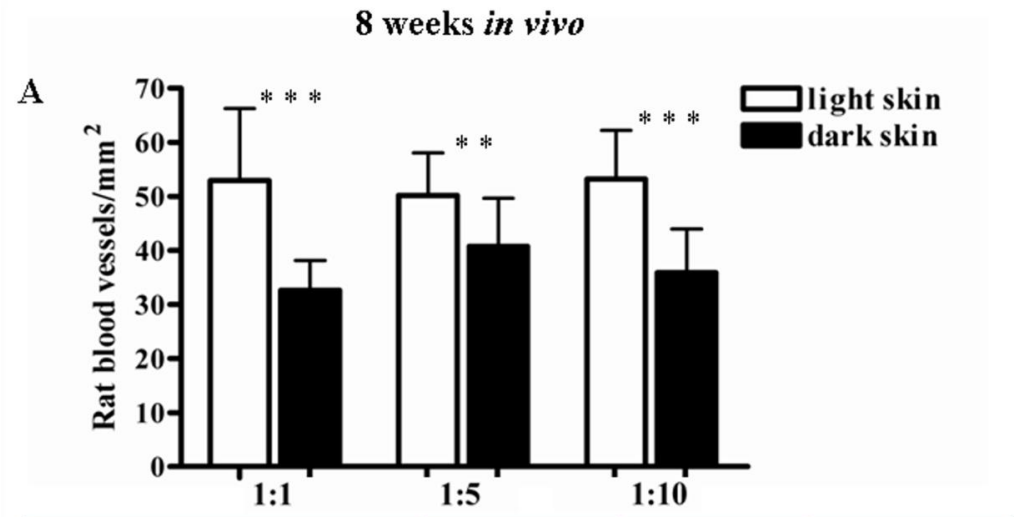

Number of rat blood vessels/mm²	light skin	dark skin	p-value
1:1 (Mean ± SD)	53 ± 13 (N = 3)	33 ± 5 (N = 3)	p < 0.0001
1:5 (Mean ± SD)	50 ± 8 (N = 4)	41 ± 9 (N = 4)	p = 0.003
1:10 (Mean ± SD)	53 ± 9 (N = 3)	36 ± 8 (N = 3)	p < 0.0001

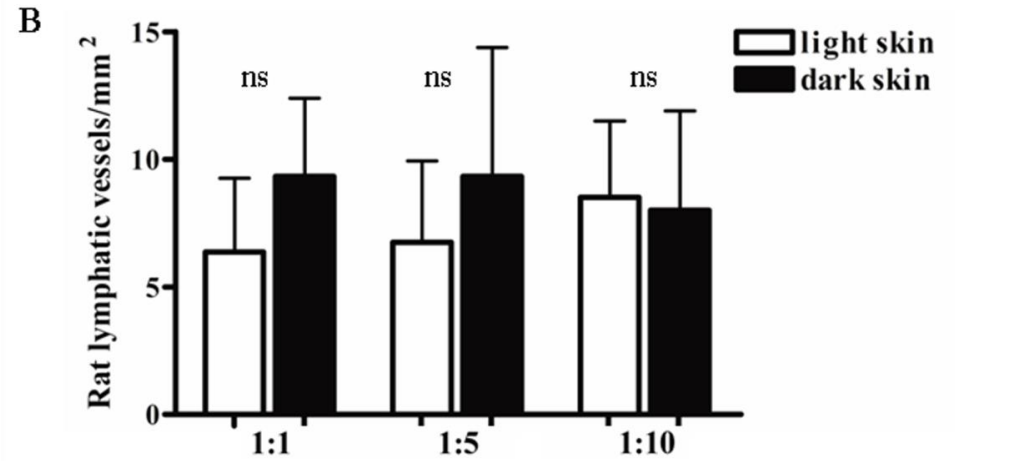

Number of rat lymphatic vessels/mm²	light skin	dark skin	p-value
1:1 (Mean ± SD)	6 ± 3 (N = 3)	9 ± 3 (N = 3)	ns (p= 0.1683)
1:5 (Mean ± SD)	7 ± 3 (N = 4)	9 ± 5 (N = 4)	ns (p= 0.1292)
1:10 (Mean ± SD)	9 ± 3 (N = 3)	8 ± 4 (N = 3)	ns (p= 0.8345)

Figure 4. The density of rat blood and lymphatic vessels in light- and dark-pigmented skin analogs (melanocyte/keratinocyte ratio 1:1, 1:5, 1:10) 8 weeks after transplantation. a Blood vessel (CD31) density of light- (white bars) and dark-pigmented analogs (black bars). Note a significantly higher number of blood vessels in the light- than the dark-pigmented group. b Lymphatic vessel (LYVE1) density of light- (white bars) and dark-pigmented analogs (black bars). Of note, lymphatic vessel ingrowth occurred at a much lower density as compared to blood vessels, regardless of the pigmentation pattern. Table shows values as the mean (± SD) number of rat blood (a)/lymphatic (b) vessels quantified per mm^2. N = 3 or 4 for each group

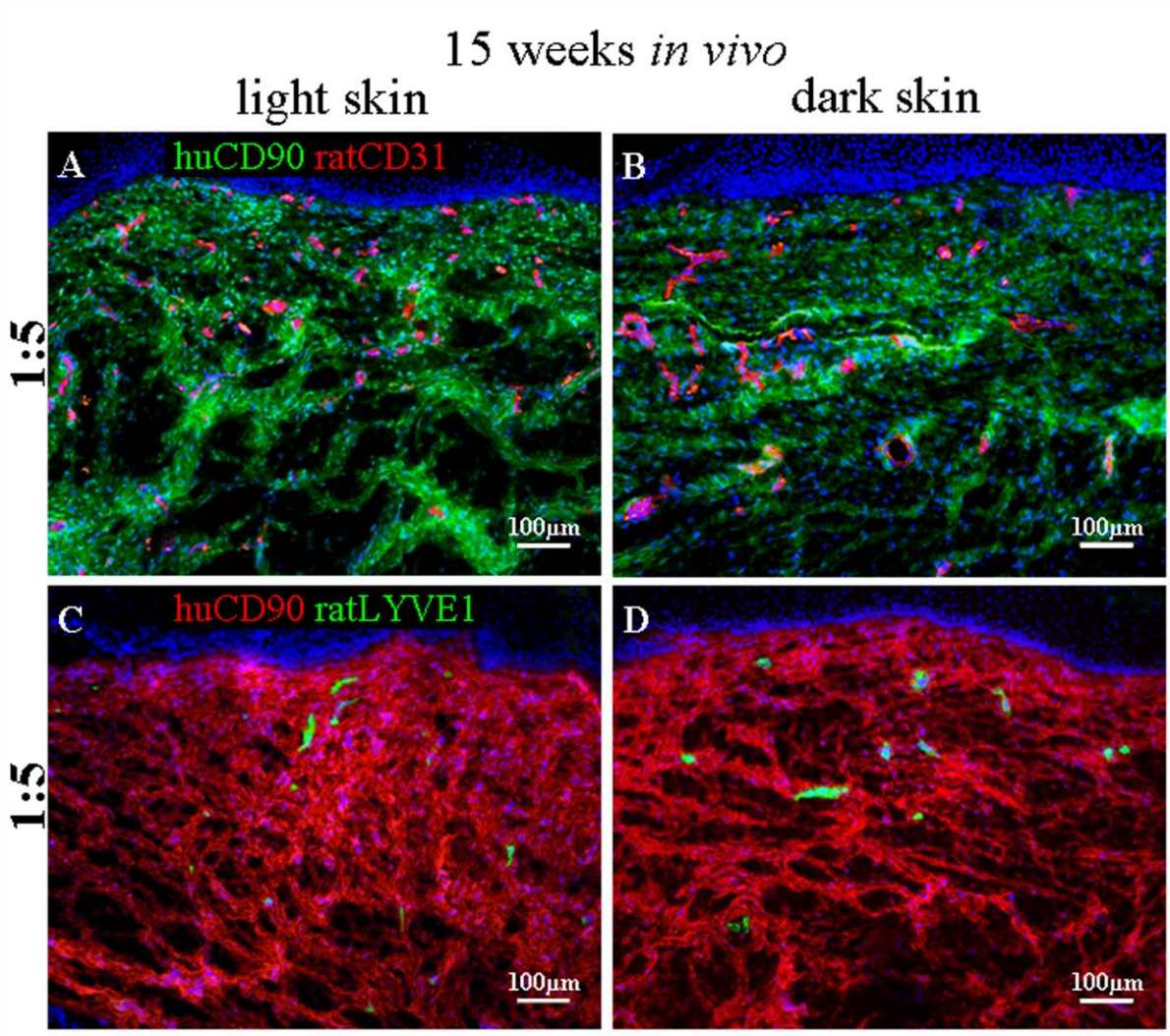

Figure 5. Host blood and lymphatic vessels in light and dark skin analogs (melanocyte/keratinocyte ratio 1:5) 15 weeks after transplantation. Rat blood vessels of light- (a) and dark-pigmented (b) skin analogs are stained with an antibody against rat CD31 (red). Differentially pigmented skin analogs show similar blood vessel patterns throughout the human CD90-stained neodermis (green). Lymphatic vessels of light (c) and dark (d) skin analogs stained with LYVE1 (green) appear at much lower density in human CD90-dermal compartment (red) as compared to blood vessels. Cell nuclei are stained with Hoechst (blue). Scale bars 100 µm

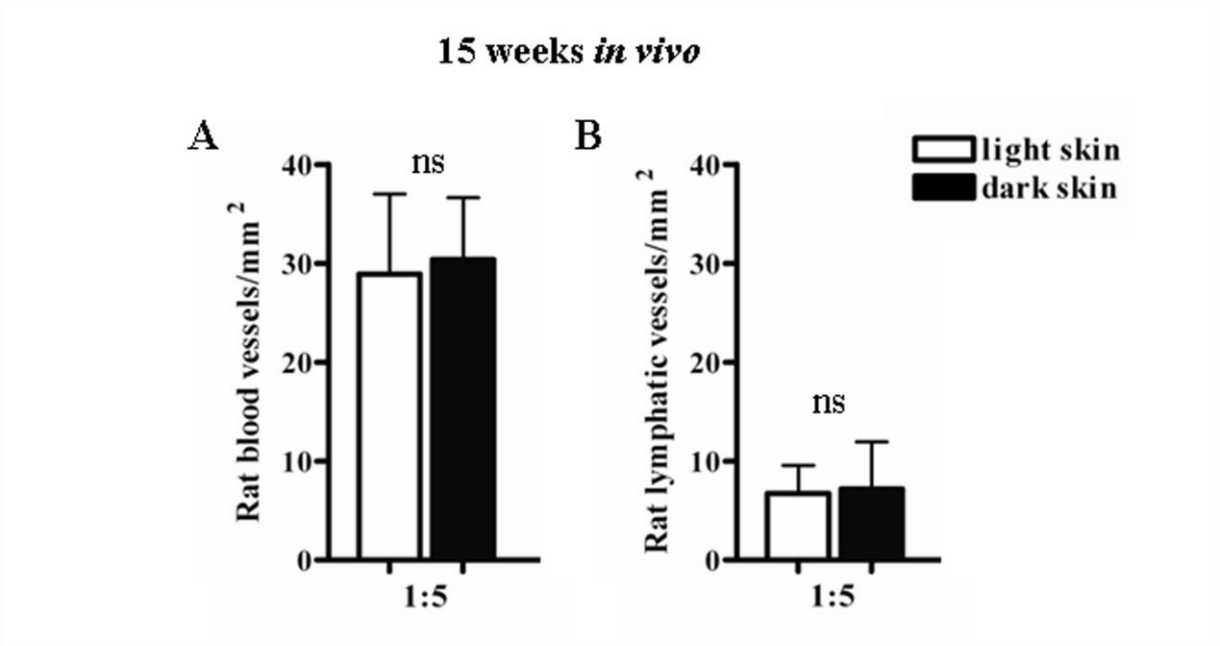

Number of rat blood vessels/mm²	light skin	dark skin	p-value
1:5 (Mean ± SD)	29 ± 8 (N = 6)	30 ± 6 (N = 3)	ns (p= 0.6428)

Number of rat lymphatic vessels/mm²	light skin	dark skin	p-value
1:5 (Mean ± SD)	7 ± 3 (N = 6)	8 ± 4 (N = 3)	ns (p = 0.7116)

Figure 6. The density of rat blood and lymphatic vessels in light- and dark-pigmented skin analogs (1:5 ratio) 15 weeks after transplantation. a Patterns of blood vessel (CD31) in light (white bars) and dark analogs (black bars) do not reveal any statistically significant difference. b Lymphatic vessel (LYVE1) patterns of light (white bars) and dark analogs (black bars) are comparable and appear at lower density than those of blood vessels. Table show values as the mean (± SD) number of rat blood (a)/lymphatic (b) vessels quantified per mm^2. N = 3 or 4 for each group

4.5 Tissue-engineered dermo-epidermal skin analogs exhibit de novo formation of a near natural neurovascular link 10 weeks after transplantation

Agnieszka S. Klar[1#], Thomas Biedermann[1#], Sophie Böttcher-Haberzeth[1,2], Clemens Schiestl[2], Ernst Reichmann[1], and Martin Meuli[2*]

[#] Authors contributed equally to this paper

[1]Tissue Biology Research Unit, University Children's Hospital Zurich, Switzerland

[2]Department of Surgery, University Children's Hospital Zurich, Switzerland

[*]Corresponding author: Martin Meuli, Department of Surgery, University Children's Hospital Zurich, Steinwiesstrasse 75, 8032 Zurich, Switzerland, Email: martin.meuli@kispi.uzh.ch

Published in:

Pediatr Surg Int, 2014, 30(2):165-72

Abstract

Purpose: Human autologous tissue-engineered skin grafts are a promising way to cover skin defects. Clearly, it is mandatory to study essential biological dynamics after transplantation, including reinnervation. Previously, we have already shown that human tissue-engineered skin analogs are reinnervated by host nerve fibers as early as 8 weeks after transplantation. In this study, we tested the hypothesis that there is a *de novo* formation of a "classical" neurovascular link in tissue-engineered and then transplanted skin substitutes.

Methods: Keratinocytes, melanocytes, and fibroblasts were isolated from human skin biopsies. After expansion in culture, keratinocytes and melanocytes were seeded on dermal fibroblast-containing collagen type I hydrogels. These human tissue-engineered dermo-epidermal skin analogs were transplanted onto full-thickness skin wounds on the back of immuno-incompetent rats. Grafts were analyzed after 3 and 10 weeks. Histological sections were examined with regard to the ingrowth pattern of myelinated and unmyelinated nerve fibers into the skin analogs using markers such as PGP9.5, NF-200, and NF-160. Blood vessels were identified with CD31, lymphatic vessels with Lyve1. In particular, we focused on alignment patterns between nerve fibers and either blood and/or lymphatic vessels with regard to neurovascular link formation.

Results: Three weeks after transplantation, blood vessels, but no nerve fibers or lymphatic vessels could be observed. 10 weeks after transplantation, we could detect an ingrowth of myelinated and unmyelinated nerve fibers into the skin analogs. Nerve fibers were found in close proximity to CD31-positive blood vessels, but not alongside Lyve1-positive lymphatic vessels.

Conclusion: These data suggest that host-derived innervation of tissue-engineered dermo-epidermal skin analogs is initiated by and guided alongside blood vessels present early post-transplantation. This observation is consistent with the concept of a cross talk between neurovascular structures, known as the neurovascular link.

Keywords: Human skin analog – Tissue engineering – Blood vessels - Nerve fibers - Innervation – Neurovascular link – Lymphatic vessels

Introduction

Loss of full-thickness skin is unequivocally accompanied by loss of skin sensibility. Although there is a large spectrum of surgical methods to cover skin defects (transplantation of full-thickness skin, split-thickness skin, biosynthetic skin substitutes, cultured epithelial cells, and combinations thereof), initially there is no sensibility present as nerve fibers migrate only slowly from the wound bed into the transplant [1-6]. Little is known about the chain of events leading to reinnervation, especially since skin appendages such as hair follicles and sweat glands known to provide guidance cues for nerve fibers are also missing [7, 8].

It is well documented that blood vessels commonly reside alongside peripheral nerves [9]. Interestingly, nerves and vessels influence one another with regard to patterning, branching, development, and regeneration after injury [10-12]. For example, smooth muscle cells surrounding blood vessels secret artemin, a glial cell-derived neurotrophic factor (GDNF), which binds the Ret/GFRα3 receptor of neurons and so guides the nerve fiber to the target organ [13]. In addition, it appears that vascular endothelial cell derived VEGF-A can control axon cone growth of neurons and guide nerve sprouting along arterial networks via VEGF-receptor 2 signaling [14, 15].

We have recently shown that tissue engineered and then transplanted dermo-epidermal skin analogs are distinctly vascularized by host blood capillaries after three weeks [16]. However, the ingrowth of nerve fibers into the transplant was observed only eight weeks after transplantation.

We now investigated if the nerve fibers are attracted by and grow alongside the blood vessel network into the transplanted skin analogs and if there is also a topographical relationship between nerve fibers and the lymphatic vessels.

Materials and Methods

Human skin samples

This experimental study was performed in accordance with the Declaration of Helsinki Principles and after permission by the Ethic Committee of the Canton Zurich. Informed consent was given by parents and/or patients. Human foreskins or skin samples from scalp or

abdomen were obtained from patients aged between 1 and 18 years. The skin biopsies were used for isolation of human epidermal keratinocytes, melanocytes, and dermal fibroblasts.

Isolation and culturing of primary cells

Keratinocytes and fibroblasts were isolated and cultured as described by Biedermann *et al.* [17]. Melanocytes were isolated and kept in culture as specified in Böttcher-Haberzeth *et al.* [18].

Preparation of dermo-epidermal skin analogs

Skin analogs were prepared in six well cell culture inserts with 3.0 µm pore size membranes in a transwell system (BD Falcon, Switzerland) [19]. To generate the dermal compartment, the membranes were covered with collagen type I hydrogels containing human dermal fibroblasts. Rat tail collagen type I (0.7 ml) (BD Biosciences, Switzerland) was mixed with 0.2 ml chilled neutralization buffer containing 0.15 M NaOH and $1x10^5$ fibroblasts (passage 1). After polymerization (10 min at room temperature and 20 min at 37 ºC), the dermal equivalents were cultured in DMEM containing 10 % FCS for five days. Subsequently, keratinocytes and melanocytes (ratio 5:1, passage 1-3) were seeded onto each dermal equivalent at a density of $4x10^5$ cells. The skin analogs were cultured in SFM (Invitrogen, Switzerland) for one week before transplantation. The medium was changed every second day.

Transplantation of cultured dermo-epidermal skin analogs

The surgical procedure was approved by the local committee for Experimental Animal Research (permission numbers 65/2009, 76/2011). Immuno-incompetent female nu/nu rats, 8–10 weeks old (Harlan Laboratories, Netherlands) were anesthetized prior to operation as previously described [20, 21]. To protect the skin analogs and to prevent wound closure from surrounding rat skin, surgical steel rings (diameter 2.6 cm) were sutured into full-thickness skin defects made on the backs of the rats, using non-absorbable polyester sutures (Ethibond®, Ethicon, USA). The transplants were then covered with a silicone foil (Silon-SES, BMS, USA), a polyurethane sponge (Ligasano, Ligamed, Austria), and a tape as wound dressing. Dressing changes and photographic documentations were performed on a weekly basis.

Analysis of the transplants

After 3 or 10 weeks, animals were killed using CO_2. Transplants and rat control skin were excised and embedded in OCT compound (Sakura Finetek/Digitana AG, Switzerland). Cryosections were stained with haematoxylin and eosin (Sigma, USA), and mounted within Eukitt (Fluka, Switzerland) for histological analysis. Double immunofluorescence stainings were performed to visualize myelinated and/or unmyelinated rat nerve fibers [ubiquitin carboxyl-terminal hydrolase L1 (PGP9.5, clone 13C4/J3C4, 1:50, Abcam, Germany)], 200 kDa neurofilament (NF200, clone NF01, 1:50, Abcam, Germany), 160 kDa neurofilament (NF160, clone NN18, 1:50, Sigma-Aldrich, Germany), rat vascular endothelial cells [CD31 (clone TDL-3A12, 1:50, BD Pharmingen, Switzerland)], rat lymphatic endothelial cells [Lyve1 (polyclonal, 1:200, Novus Biologicals, UK)], vascular basement membrane protein [Laminin1+2 (clone ab7463, 1:500, Abcam, Germany)], and human fibroblasts [CD90 (clone AS02, 1:50, Dianova, Germany)]. Cryosections were fixed and permeabilized in acetone/methanol for 5 min at -20 ºC, air dried, and washed 3x in phosphate-buffered saline (PBS, Invitrogen, Switzerland). Thereafter, sections were blocked in PBS containing 2 % BSA (Sigma, Switzerland) for 30 min. Incubation with the diluted first antibody was performed in blocking buffer for 1 h at room temperature. Afterwards, slides were washed three times for 5 min in PBS and blocked for additional 15 min. To visualize the primary antibody, FITC-conjugated polyclonal goat $F(ab´)_2$ fragments directed to mouse immunoglobulins (Dako, Switzerland) were added to the sections. Slides were washed three times for 5 min in PBS and blocked for additional 15 min. For double immunofluorescence, NF and CD31 primary antibodies were prelabeled with Alexa 555-conjugated polyclonal goat $F(ab´)_2$ fragments according to the manufacturer's instructions (Zenon Mouse IgG Labeling Kit, Molecular Probes/Invitrogen, Switzerland) and added to the sections. Finally, the slides were incubated for 5 min in PBS containing 1 µg/ml Hoechst 33342 (Sigma, Switzerland), washed twice for 5 min in PBS, and mounted with Dako mounting solution (Dako, Switzerland).

Pictures of immunofluorescence stainings were taken with a DXM1200F digital camera connected to a Nikon Eclipse TE2000-U inverted microscope. The device is equipped with Hoechst 33342, FITC, and TRITC filter sets (Nikon AG, Switzerland; Software: Nikon ACT-1 vers. 2.70). Images were processed with Photoshop 10.0 (Adobe Systems Inc., Germany).

Results

Expression of blood- and lymphatic endothelial markers in normal rat skin

Native rat skin from the back was tested for blood- and lymphatic endothelial marker expression (Fig. 1). Skin samples were double-stained for endothelial cells (CD31, red, Fig. 1a, b) and basement membrane markers (Laminin1+2, green, Fig. 1a). In contrast to the CD31 and Laminin1+2 positive blood vessels (white arrows, Fig. 1a), the lymphatic vessels were faintly CD31 positive and showed no staining for Laminin1+2 (white arrowheads, Fig. 1a).

To further confirm the identity of blood and lymphatic vessels, anti-CD31 staining was combined with LYVE1, which is a marker for lymphatic endothelial cells. As depicted in Fig. 1b, the blood vessels were CD31-positive but LYVE1-negative (white arrowheads), whereas the lymphatic vessels showed a faint CD31-staining and strong LYVE1-expression (white arrows).

Innervation and vascularization pattern of normal rat skin

Native rat skin from the back was co-stained for nerve fiber marker expression using antibodies against NF200 (green), and blood (CD31, red, Fig. 1c) or lymphatic vessels (LYVE1, red; Fig. 1d). We observed that nerve fibers are located in close proximity to blood vessels (white arrows, Fig. 1c), whereas no co-localization of nerve fibers with lymphatic vessels was noted (Fig. 1d).

Innervation and vascularization pattern of transplanted human tissue engineered skin analogs

After excision of the human tissue engineered skin analogs ten weeks after transplantation, anti rat-CD31 staining showed an abundant capillary network throughout the dermal compartment delineated with a CD90-staining of human fibroblasts (Fig. 2a). In contrast to blood vessels, the LYVE1-positive lymphatic vessels appeared in lower numbers, were irregular in shape, and larger in diameter as compared to blood vessels (Fig. 2b). Host myelinated and unmyelinated rat nerve fibers (green) were detected in the human dermal compartment (CD90, red) by staining for NF200 and PGP9.5 (Fig. 2c, d).

As a control, the presence of established rat blood and lymphatic vessel networks was investigated three weeks after transplantation. Blood vessels (CD31, Fig. 2e) occurred

abundantly in the human dermal compartment (CD90, green), whereas no lymphatic vessels were detected in the human dermis (Fig. 2f). The earliest ingrowth of lymphatic capillaries into the skin analogs appeared five weeks after transplantation (data not shown).

Pattern of nerve fibers and blood vessels in human tissue engineered skin analogs

Ten weeks post-transplantation, host blood vessels were visualized in the human dermal compartment by anti-CD31 (red) staining. Myelinated nerve fibers were visualized by staining for NF200 (Fig. 3a, b) and NF160 (Fig. 3c, d), while unmyelinated nerve fibers were identified by anti-PGP9.5 staining (Fig. 3e, f). In almost all sections, rat nerve fibers were aligned along blood vessels (white arrows).

Pattern of nerve fibers and lymphatic vessels in human tissue engineered skin analogs

Ten weeks after transplantation, sections with lymphatic vessels staining positive for LYVE1 were co-stained with nerve fiber markers such as NF200 (Fig. 4a, b), NF160 (Fig. 4c, d), and PGP9.5 (Fig. 4e, f). We observed lymphatic vessels in vicinity to nerve fibers, but we did not detect any alignment of the structures.

Discussion

This is an experimental study investigating the question whether host-derived innervation of previously transplanted human tissue engineered skin analogs is guided alongside host blood or lymphatic vessels. In general, our findings demonstrate a clear cut topographical relationship between blood vessels and nerve fibers, but not between lymphatic vessels and nerve fibers. Thus, our hypothesis that a *de novo* formation of a typical neurovascular link occurs in tissue engineered skin grafts after transplantation, proves true.

The dynamics of host blood vessels, lymphatic vessels, and nerve fibers populating transplanted human tissue engineered skin analogs are fundamentally different. We have shown previously that an established vascular network can be detected as early as three weeks post-transplantation while innervation of the dermal compartment is present only eight weeks post-transplantation [16]. Certainly, early vascularization of a transplanted skin analog by capillaries and larger blood vessels is crucial to ensure sustained graft take and long-term

survival and has therefore the highest physiological "priority" regarding the establishment of host structures within the transplanted tissue. In contrast, lymphatic vessels and nerve fibers are not indispensable for graft survival during the early stage after transplantation. Therefore, we decided to investigate the skin analogs 10 weeks after transplantation in order to detect eventual topographical relationships between blood or lymphatic vessels and nerves fibers.

It has been described previously that vascular and nervous networks develop in close proximity during development, reflecting their mutual dependency [22]. To enable an alignment, the structures need to communicate with each other through signals, a molecular exchange called "neurovascular crosstalk" [23]. Herby, several guidance molecules, such as artemin, VEGF, or endothelin-3, are secreted from blood vessels and attract nerve fibers along a certain ligand-gradient to establish innervation [12, 14, 15]. On the other hand, guidance signals are also secreted from the peripheral nervous system. For instance, VEGF leads to an attraction and branching of blood vessels as well as to arterial differentiation in the skin [24].
Based on the above mentioned evidence, we developed our hypothesis that initially non-vascularized and non-innervated laboratory grown skin substitutes develop a kind of physiological perfusion and innervation system over time, a newly formed neurovascular link. Although we did not perform the extremely demanding molecular pathway studies that the aforementioned ground breaking papers described [12, 14, 15, 22-24], we could convincingly demonstrate that 10 weeks after transplantation a *de novo* formed neurovascular link was present in the dermal compartment of the perfectly well engrafted skin substitutes. In all specimens examined, there was a typical alignment between blood vessels and nerve fibers as seen in normal neurovascular links. On the other hand, such a relationship could not be seen between lymphatic vessels and blood vessels or nerve fibers.

Clearly, the presence of neurovascular links also means that neurovascular crosstalk must have occurred [23]. In our setting, the initiators of this neurovascular communication have certainly been blood vessels as they are present in these transplants much earlier than nerve fibers. Also it is a tenable assumption that the vascular network within the grafted area received an intrinsic innervation during the neurovascular link development enabling blood vessels to react to synaptically passed signals that cause vasoconstriction and vasodilatation [25, 26]. It might be interesting to look at this issue in a follow-up study.

Although, our dermo-epidermal skin analogs do not contain only adnexal structures such as hair follicles or sweat glands, a few considerations regarding the potential impact of skin appendages in the context of innervation are worth being made. It has been proposed that integrating such appendages into tissue engineered skin substitutes could enforce the ingrowth

of nerves, as glands and hair follicles are very well vascularized and innervated [8, 27-29]. It has also been described that the incorporation of Schwann cells or the use of modified scaffolds could promote the innervation of skin analogs [30, 31]. Possibly, the integration of human hair follicles and sweat glands could, beside being a revolutionary step towards engineering normal skin, also improve the velocity and quality of reinnervation of our tissue engineered dermo-epidermal skin analogs.

Finally, we analyzed the dynamics of lymphatic vessel ingrowth into the transplants. After 10 weeks, we could detect lymphatic vessels and nerve fibers in the dermal compartment. Although lymphatic vessels were found in vicinity of nerve fibers, they did not show an alignment pattern as seen in the neurovascular link.

In conclusion, our data suggest that a *de novo* formation of a close to natural neurovascular link occurs over a time span of 10 weeks after transplantation of tissue engineered skin analogs that are initially devoid of any vascular and neural elements.

The fact that there is ingrowth of both, normal neurovascular structures as well as lymphatic vessels into engineered skin grafts has favorable clinical implications in view of the envisioned application of such grafts in human patients.

Conflict of interest

The authors declare that they have no conflict of interest.

Acknowledgment

This work was financially supported by the EU-FP7 project EuroSkinGraft (FP7/2007-2013: grant agreement no 279024), by the EU-FP7 (MultiTERM, grant agreement n° 238551) and the Clinical Research Priority Programs (KFSP: From basic research to the clinic: Novel tissue engineered skin grafts for Zurich) of the Faculty of Medicine of the University of Zurich. We are particularly grateful to the Fondation Gaydoul and the sponsors of "DonaTissue" (Thérèse Meier and Robert Zingg) for their generous financial support and interest in our work.

References

[1] Hermanson A, Dalsgaard CJ (1987) Sensory reinnervation and sensibility in skin transplants. Med Biol 65(1):49–52

[2] Altun V, Hakvoort TE, van Zuijlen PP, van der Kwast TH, Prens EP (2001) Nerve outgrowth and neuropeptide expression during the remodeling of human burn wound scars. A 7-month follow-up study of 22 patients. Burns 27(7):717–722

[3] Ward RS, Tucket RP, English KB, Johansson O, Saffle JR (2003) Substance P axons and sensory threshold increase in burn-graft human skin. J Surg Res 118:154–160

[4] Nedelec B, Hou Q, Sohbi I, Choiniüre M, Beauregard G, Dykes RW (2005) Sensory perception and neuroanatomical structures in normal and grafted skin of burn survivors. Burns 31:817–830

[5] Anderson JR, Zorbas JS, Phillips JK, Harrison JL, Dawson LF, Bolt SE, Rea SM, Klatte JE, Paus R, Zhu B, Giles NL, Drummond PD, Wood FM, Fear MW (2010) Systemic decreases in cutaneous innervation after burn injury. J Invest Dermatol 130:1948–1951

[6] Anderson JR, Fear MW, Phillips JK, Dawson LF, Wallace H, Wood FM, Rea SM (2011) A preliminary investigation of the reinnervation and return of sensory function in burn patients treated with INTEGRA®. Burns 37(7):1101–1108

[7] Botchkarev VA, Eichmuller S, Johansson O, Paus R (1997) Hair cycle-dependent plasticity of skin and hair follicle innervation in normal murine skin. J Comp Neurol 386(3): 379–395

[8] Gagnon V, Larouche D, Parenteau-Bareil R, Gingras M, Germain L, Berthod F (2011) Hair follicles guide nerve migration in vitro and in vivo in tissue-engineered skin. J Invest Dermatol 131(6):1375-1378

[9] Carmeliet P, Tessier-Lavigne M (2005) Common mechanisms of nerve and blood vessel wiring. Nature 436(7048):193–200

[10] Carmeliet P (2003) Blood vessels and nerves: common signals, pathways and diseases. Nat Rev Genet 4(9):710–720

[11] Glebova NO, Ginty DD (2005) Growth and survival signals controlling sympathetic nervous system development. Annu Rev Neurosci 28:191–222

[12] Marko SB, Damon DH (2008) VEGF promotes vascular sympathetic innervation. Am J Physiol Heart Circ Physiol 294(6):H2646–H2652

[13] Honma Y, Araki T, Gianino S, Bruce A, Heuckeroth R, Johnson E (2002) Artemin is a vascular-derived neurotropic factor for developing sympathetic neurons. Neuron 35(2):267– 282

[14] Long JB, Jay SM, Segal SS, Madri JA (2009) VEGF-A and Semaphorin3A: modulators of vascular sympathetic innervation. Dev Biol 334(1):119–132

[15] Chauvet S, Burk K, Mann F (2013) Navigation rules for vessels and neurons: cooperative signaling between VEGF and neural guidance cues. Cell Mol Life Sci 70(10):1685-1703

[16] Biedermann T, Böttcher-Haberzeth S, Klar AS, Pontiggia L, Schiestl C, Meuli-Simmen C, Reichmann E, Meuli M (2013) Rebuild, restore, reinnervate: do human tissue engineered dermo-epidermal skin analogs attract host nerve fibers for innervation? Pediatr Surg Int 29(1):71-78

[17] Biedermann T, Pontiggia L, Böttcher-Haberzeth S, Tharakan S, Braziulis E, Schiestl C, Meuli M, Reichmann E (2010) Human eccrine sweat gland cells can reconstitute a stratified epidermis. J Invest Dermatol 130(8):1996–2009

[18] Böttcher-Haberzeth S, Biedermann T, Pontiggia L, Braziulis E, Schiestl C, Hendriks B, Eichhoff OM, Widmer DS, Meuli-Simmen C, Meuli M, Reichmann E (2013) Human eccrine sweat gland cells turn into melanin-uptaking keratinocytes in stratifying dermo-epidermal skin substitutes. J Invest Dermatol 133(2):316-324

[19] Kiowski G, Biedermann T, Widmer DS, Civenni G, Burger C, Dummer R, Sommer L, Reichmann E (2012) Engineering melanoma progression in a humanized environment in vivo. J Invest Dermatol 132(1):144–153

[20] Schneider J, Biedermann T, Widmer D, Montaño I, Meuli M, Reichmann E, Schiestl C (2009) Matriderm versus Integra: a comparative experimental study. Burns 35(1):51–57

[21] Böttcher-Haberzeth S, Biedermann T, Schiestl C, Hartmann-Fritsch F, Schneider J, Reichmann E, Meuli M (2012) Matriderm® 1 mm versus Integra® Single Layer 1.3 mm for one-step closure of full thickness skin defects: a comparative experimental study in rats. Pediatr Surg Int 28(2):171–177

[22] Martin P, Lewis J (1989) Origins of the neurovascular bundle: interactions between developing nerves and blood vessels in embryonic chick skin. Int J Dev Biol 33(3):379–387

[23] Quaegebeur A, Lange C, Carmeliet P (2011) The neurovascular link in health and disease: molecular mechanisms and therapeutic implications. Neuron 71(3):406-424

[24] Mukouyama YS, Shin D, Britsch S, Taniguchi M, Anderson DJ (2002) Sensory nerves determine the pattern of arterial differentiation and blood vessel branching in the skin. Cell 109(6):693– 705

[25] Ruiz de Almodovar C, Lambrechts D, Mazzone M, Carmeliet P (2009) Role and therapeutic potential of VEGF in the nervous system. Physiol Rev 89(2):607-648

[26] Eichmann A, Thomas JL (2013) Molecular parallels between neural and vascular development. Cold Spring Harb Perspect Med 3(1):a006551

[27] Botchkarev VA, Eichmuller S, Johansson O, Paus R (1997) Hair cycle-dependent plasticity of skin and hair follicle innervation in normal murine skin. J Comp Neurol 386(3): 379–395

[28] Hendrix S, Picker B, Liezmann C, Peters EM (2008) Skin and hair follicle innervation in experimental models: a guide for the exact and reproducible evaluation of neuronal plasticity. Exp Dermatol 17(3):214–227

[29] Blais M, Parenteau-Bareil R, Cadau S, Berthod F (2013) Concise review: tissue-engineered skin and nerve regeneration in burn treatment. Stem Cells Transl Med 2(7):545-551

[30] Caissie R, Gingras M, Champigny MF, Berthod F (2006) In vivo enhancement of sensory perception recovery in a tissue-engineered skin enriched with laminin. Biomaterials 27(15):2988-2993

[31] Blais M, Grenier M, Berthod F (2009) Improvement of nerve regeneration in tissue-engineered skin enriched with Schwann cells. J Invest Dermatol 129(12):2895-2900

Figures and Tables

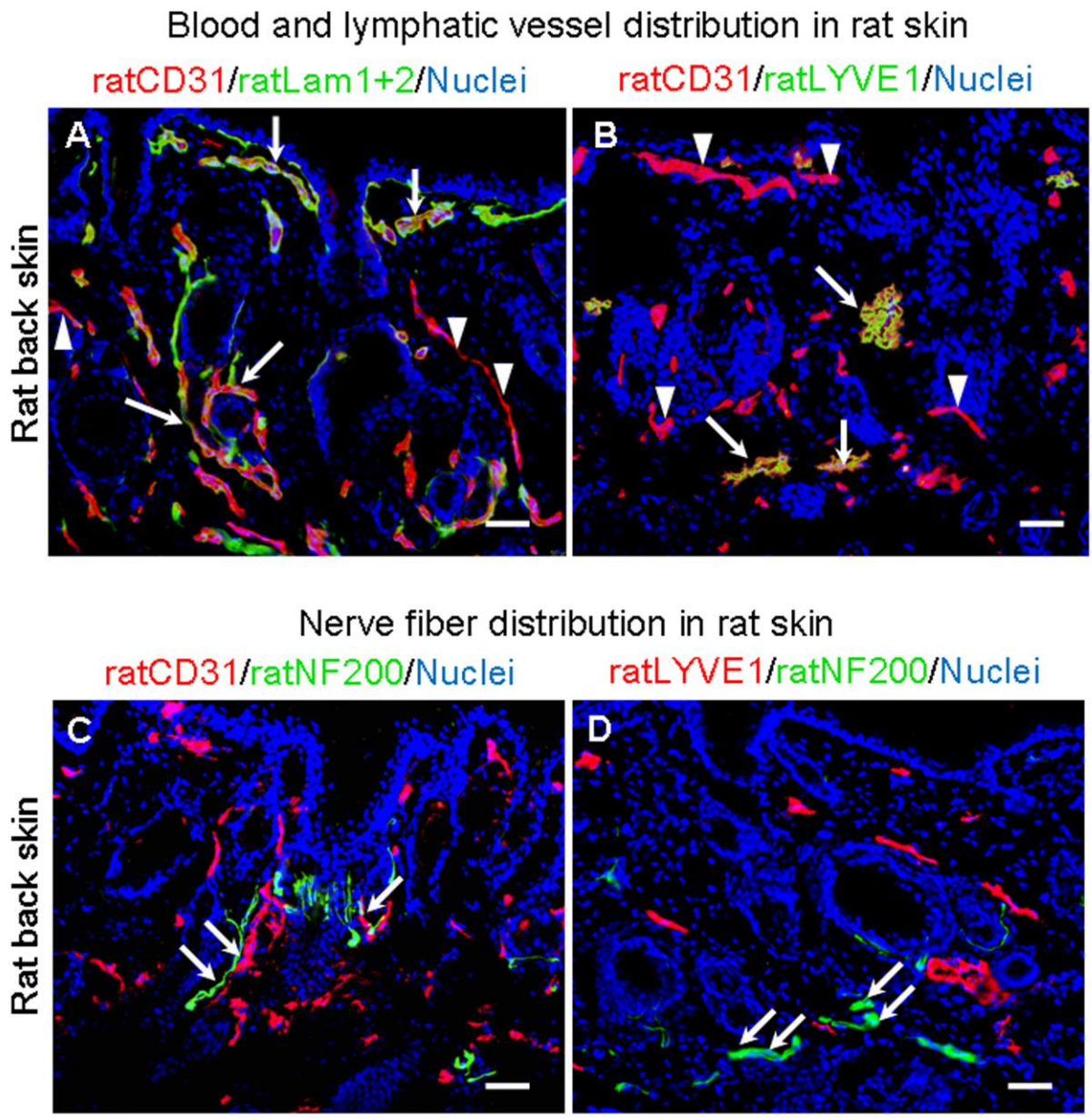

Figure 1. Evaluation of blood, lymphatic vessel, and nerve fiber distribution in normal rat back skin. **a** Staining of normal rat skin for CD31 (*red*) and basement membrane staining for Lam1+2 (*green*). Blood vessels show a double staining with CD31 and Laminin1+2 (*white arrows*); structures staining for CD31 only show lymphatic vessels (*white arrowheads*). **b** Staining of normal rat skin with LYVE1 (*green*) and CD31 (*red*). Lymphatic vessels display a double staining with LYVE1 and CD31 (*white arrows*); structures staining for CD31 only show blood vessels (white arrowheads).**c** Staining of blood vessels with CD31 (*red*) and of nerve fibers with NF200 (*green*). An alignment between blood vessels and nerve fibers can be detected (*white arrows*). **d** Staining of lymphatic vessels with LYVE1 (*red*) and of nerve fibers with NF200 (*green*). No co-localization between lymphatic vessels and nerve fibers can be noted (*white arrows*). Cell nuclei are stained with Hoechst (*blue*). Scale bar for all panels 50 µm.

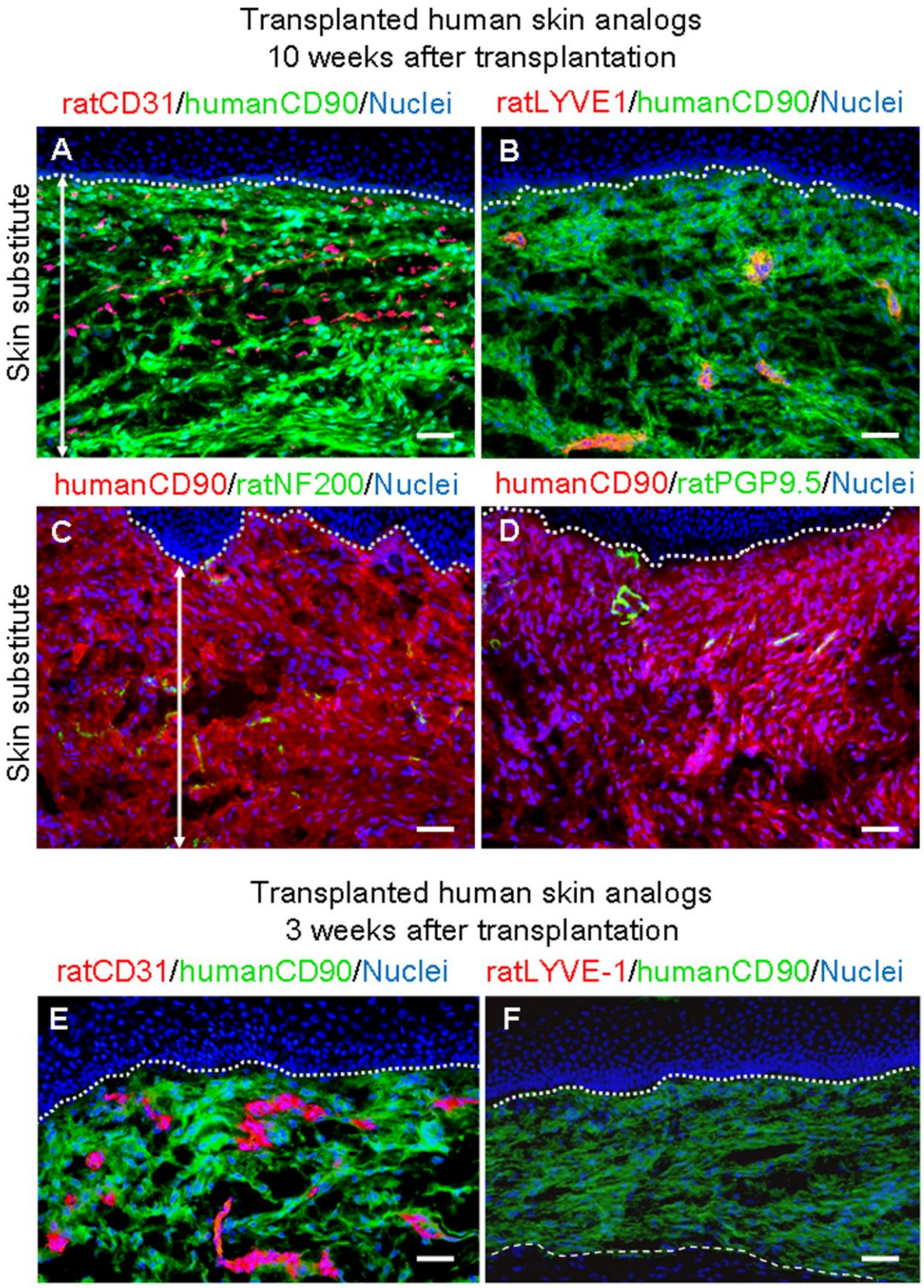

Figure 2. Evaluation of host blood and lymphatic vessel distribution as well as host innervation in human tissue engineered skin analogs 10 weks after transplantation. **a** Staining of rat blood vessels with CD31 (*red*) and of human fibroblasts with CD90 (*green*). **b** Staining of rat lymphatic vessels with LYVE1 (*red*) and of human

fibroblasts with CD90 (*green*). **c, d** Staining of rat nerve fibers with NF200 and PGP9.5 (*green*), human dermal fibroblasts are stained with CD90 (*red*). **e** Staining of rat blood vessels with CD31 (*red*) and of human fibroblasts with CD90 (*green*) 3 weeks after transplantation. **f** Staining of rat lymphatic vessels with LYVE1 (*red*) and of human fibroblasts with CD90 (*green*) 3 weeks after transplantation. Cell nuclei are stained with Hoechst (*blue*). The human dermal compartment is marked by a *two-sided arrow*, the basement membrane is delineated by a *dotted line*, the lower border of the human compartment by a *dashed line*. Scale bar for all panels 50 μm.

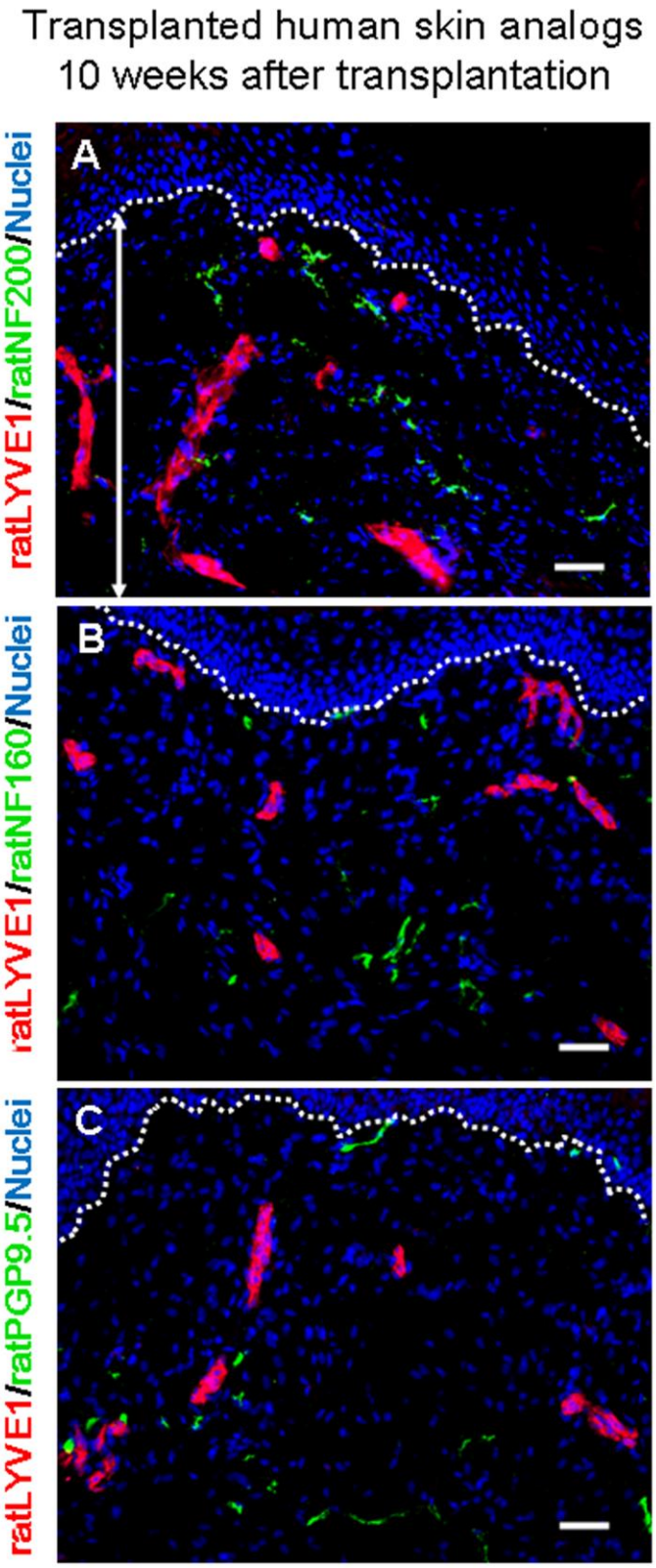

Figure 3. Evaluation of host innervation relating to host vascularization in human tissue engineered skin analogs 10 weeks after transplantation. a-f Staining of rat blood vessels with CD31 (red) and of rat nerve fibers with NF200, NF160, and PGP9.5 (green). Cell nuclei are stained with Hoechst (blue). The dermal compartment is marked by a two-sided arrow; the basement membrane is delineated by a dotted line. An alignment between host nerve fibers and blood vessels can be seen in several areas (arrows). Scale bar for all panels 50 μm.

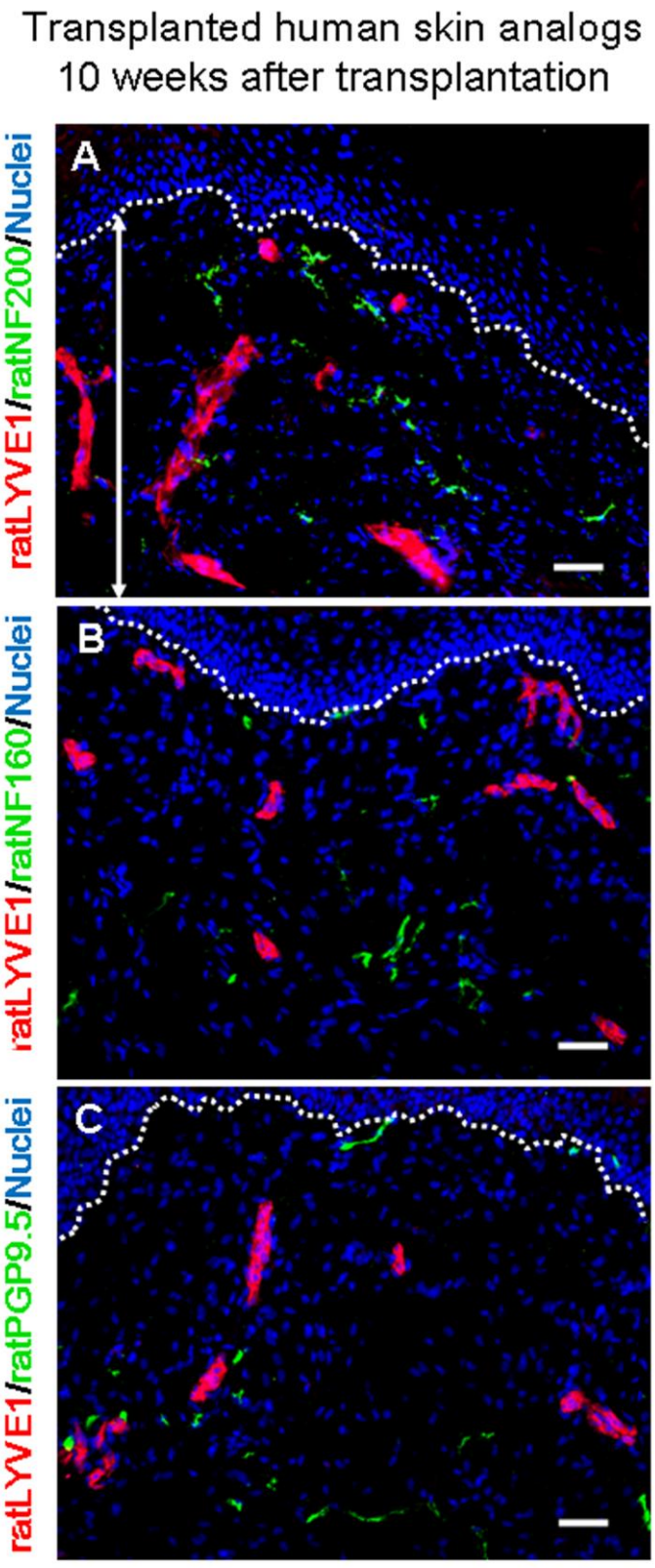

Figure 4. Evaluation of host innervation relating to host lymphatic vessels in human tissue engineered skin analogs 10 weeks after transplantation. a-f Staining of rat lymphatic vessels with LYVE1 (red) and of rat nerve fibers with NF200, NF160, and PGP9.5 (green). Cell nuclei are stained with Hoechst (blue). The dermal compartment is marked by a two-sided arrow; the basement membrane is delineated by a dotted line. A vicinity of lymphatic vessels and nerve fibers can be seen, but no alignment. Scale bar for all panels 50 μm.

5. CONCLUSIONS

Tissue-engineered dermo-epidermal skin grafts prevascularized with adipose-derived cells (chapter 4.1)

The absence of perfusable vascular networks still remains one of the central hurdles in the field of skin tissue-engineering. In this study I successfully developed prevascularized dermo-epidermal skin substitutes (vascDESS) for clinical application using human adipose-derived cells. For this I applied the stromal vascular fraction (SVF) derived from adipose tissue containing endothelial and mesenchymal cells, which are able to spontaneously develop into a mature and functional microvascular network *in vitro*. Of note, the SVF is relatively abundant and accessible in comparison to other adult autologous cell sources and can be used intraoperatively after tissue harvest, without *in vitro* expansion.

The peculiarity of the endothelial cell fraction of the SVF is, however, that it can only be maintained in a suitable 3D culture system, whereas it is rapidly lost on cell culture plastic (in 2D culture). I managed to establish appropriate *in vitro* conditions by integrating the SVF into a previously developed tissue-engineered, hydrogel-based, dermo-epidermal skin graft. The *de novo* microvascular plexus, developing under these circumstances, demonstrated a great similarity to normal human capillaries, exhibiting a lumen, pericyte coverage, and organotypic microstructures, such as a basal lamina, "peg-and-socket" junctions, pseudopodia, caveolae, pinocytotic vesicles, and complex intercellular junctions.

Using the *in vitro* prevascularization approach, I was able to considerably accelerate the onset of blood perfusion in the skin substitutes after transplantation, which resulted in several positive effects in comparison to non-prevascularized transplants:

1) the absence of shrinkage resulting in an enlarged transplant size,
2) increased collagen type I deposition,
3) increased cell proliferation in both dermis and epidermis,
4) minimal expression of typical wound healing markers, such as CK16 and CK17,
5) rapid establishment of epidermal homeostasis.

These results confirm that *in vitro* prevascularization greatly improves the integration, cell survival, and all the functional properties of the skin substitutes *in vivo*. In particular, the significantly reduced contraction of vascDESS may mean a major clinical improvement. Graft contraction is especially dramatic in young patients, namely in the areas of the joints, which forces these patients to undergo repetitive, painful surgeries, and long hospitalization.

Optimizing *in vitro* culture conditions leads to a significantly shorter production time of human dermo-epidermal skin substitutes (chapter 4.2)

The main goal of the Tissue Biology Research Unit (TBRU) is to use engineered dermo-epidermal skin substitutes clinically in an autologous and permanent fashion to treat patients with acute and severe skin injuries. However, the main drawback of this was initially the relatively long production time of 3-4 weeks [89]. Therefore, in this study I aimed at optimizing the standard *in vitro* culture conditions to shorten the production time of the skin grafts.

I was able to establish a modified protocol with a significantly reduced incubation time of keratinocytes on the dermal template before transplantation, i.e. from 14 to 6 days. The obtained results clearly indicate that only 2-3 layers of keratinocytes were sufficient to induce a near normal, mature epidermis after transplantation. Moreover, I observed that cultivation of keratinocytes on dermal skin templates for longer than 6 days *in vitro* did not result in an improvement of skin barrier properties, epidermal stratification or maintenance of the stem cell compartment.

To conclude, we were able to markedly shorten the total *in vitro* culture time from 21 to 12 days *in vitro*, a finding that has an important clinical impact on the treatment of burned patients suffering from skin defects.

"Trooping the colour" - Restoring the original donor skin color by addition of melanocytes to bioengineered skin analogs (chapter 4.3)

Matching skin pigmentation has a paramount cosmetic impact after skin grafting. Even more importantly is sufficient skin protection against ultraviolet (UV) radiation. Hence, one of the major future plans of the TBRU is to tissue-engineer pigmented skin substitutes containing melanocytes to restore skin pigmentation or to treat severe skin disorders such as vitiligo. However, for the approval by the federal regulatory authority (Swissmedic) and initiation of phase I clinical trials, those skin substitutes need to undergo respective preclinical research. For this purpose initial *in vivo* studies were performed using the immuno-incompetent rat model.

We added human melanocytes in different ratios to the epidermal compartment of dermo-epidermal skin analogs. Interestingly, the skin color production was independent of the original number of melanocytes added to the constructs, since any deviation from the physiological 1:5 ratio of melanocytes to keratinocytes in the basal layer, did not result in any

measurable “color” difference. Moreover, we observed that for the physiological restoration of skin pigmentation it is crucial that all three cell types - keratinocytes, melanocytes, and fibroblasts originate from the same donor skin.

Analysis of blood and lymph vascularization patterns in tissue-engineered human dermo-epidermal skin analogs of different pigmentation (chapter 4.4)

In this study I addressed another crucial issue, namely the ingrowth of blood and lymphatic vessels into human dermo-epidermal skin substitutes after transplantation. As our initially generated skin grafts are still lacking engineered blood and lymphatic capillaries, they are entirely dependent on the ingrowth of the patient’s vessels. If this process is insufficient, the long-term performance and survival of the engineered transplants will be negatively affected. To assess this, I investigated the blood and lymphatic vessel patterns in light- and dark-pigmented skin substitutes at 3, 8 and 15 weeks after transplantation.

Interestingly, all transplants were entirely vascularized already three weeks after, transplantation, whereas they still lacked the presence of lymphatic vessels. Overall my study demonstrated distinct blood vessel densities between the early (8 weeks) and late (15 weeks) healing stages after transplantation. Of note, similar differences were not seen with regard to lymph vessel ingrowth, as a comparable lymphatic vessel density was observed at 8 and 15 weeks after transplantation, respectively.

It can be concluded that the establishment of a rapid vascular supply within the transplanted skin has the highest priority with regard to immediate graft take and long-term survival, and therefore occurs earlier than lymphatic vessel ingrowth. Previous reports showed that lymphatic regeneration across scar tissues is severely impaired due to reduced lymphatic endothelial cell proliferation and abnormal lymphatic microarchitecture [46-47].

These findings are particularly important with regard to our planned clinical application of laboratory engineered skin substitutes. It appears tenable that a competent blood and lymphatic vessel supply will also develop when our skin substitutes are autologously transplanted onto human patients.

Tissue-engineered dermo-epidermal skin analogs exhibit *de novo* formation of a near natural neurovascular link 10 weeks after transplantation (chapter 4.5)

In this study I investigated how the host-derived innervation is guided into the transplanted human tissue-engineered skin analogs. I expected the *de novo* formation of a typical neurovascular link and asked the question if nerve ingrowth occurs alongside host blood or lymphatic vessels.

As mentioned above the growth dynamics of blood capillaries on the one hand, and lymphatic capillaries on the other hand, are fundamentally different. We have shown previously that a vascular network can be spontaneously established by neovascularization as early as three weeks post-transplantation. However, reasonable innervation of the dermal compartment is present only after eight weeks [54]. Certainly, early vascularization of a transplanted skin analog by capillaries and larger blood vessels is crucial to ensure sustained graft take and long-term survival and has therefore the highest physiological "priority" regarding the establishment of host structures within the transplanted tissue. In contrast, lymphatic vessels and nerve fibers are not indispensable for graft survival during the early stage after transplantation.

I could convincingly demonstrate that 10 weeks after transplantation a *de novo* formed neurovascular link was present in the dermal compartment with a typical alignment between blood vessels and nerve fibers as seen in typical neurovascular links. On the other hand, such a relationship could not be demonstrated between lymphatic vessels and nerve fibers in this setting.

All experimental studies presented in this thesis describe crucial requirements to make the clinical application of tissue-engineered autologous human skin grafts feasible. I was able to essentially improve the *in vitro* production process and characterize distinct *in vivo* regeneration steps in our preclinical studies.

6. REFERENCES

[1] Klar AS, Guven S, Biedermann T, Luginbuhl J, Bottcher-Haberzeth S, Meuli-Simmen C, et al. Tissue-engineered dermo-epidermal skin grafts prevascularized with adipose-derived cells. Biomaterials. 2014;35:5065-78.

[2] Pontiggia L, Klar A, Bottcher-Haberzeth S, Biedermann T, Meuli M, Reichmann E. Optimizing in vitro culture conditions leads to a significantly shorter production time of human dermo-epidermal skin substitutes. Pediatr Surg Int. 2013;29:249-56.

[3] Bottcher-Haberzeth S, Klar AS, Biedermann T, Schiestl C, Meuli-Simmen C, Reichmann E, et al. "Trooping the color": restoring the original donor skin color by addition of melanocytes to bioengineered skin analogs. Pediatric Surgery International. 2013;29:239-47.

[4] Klar A, Böttcher-Haberzeth S, Biedermann T, Schiestl C, Reichmann E, Meuli M. Analysis of blood and lymph vascularization patterns in tissue-engineered human dermo-epidermal skin analogs of different pigmentation. Pediatric Surgery International. 2014;30:223-31.

[5] Biedermann T, Klar AS, Bottcher-Haberzeth S, Schiestl C, Reichmann E, Meuli M. Tissue-engineered dermo-epidermal skin analogs exhibit de novo formation of a near natural neurovascular link 10 weeks after transplantation. Pediatr Surg Int. 2013.

[6] Gurtner GC, Werner S, Barrandon Y, Longaker MT. Wound repair and regeneration. Nature. 2008;453:314-21.

[7] Freinkel RK, Woodley D. The biology of the skin. New York: Parthenon Pub. Group; 2001.

[8] Haass NK, Smalley KS, Li L, Herlyn M. Adhesion, migration and communication in melanocytes and melanoma. Pigment Cell Res. 2005;18:150-9.

[9] Passeron T, Coelho SG, Miyamura Y, Takahashi K, Hearing VJ. Immunohistochemistry and in situ hybridization in the study of human skin melanocytes. Exp Dermatol. 2007;16:162-70.

[10] Tobin DJ, Bystryn JC. Different populations of melanocytes are present in hair follicles and epidermis. Pigment Cell Res. 1996;9:304-10.

[11] Borovansky J, Riley PA. Melanins and melanosomes : biosynthesis, biogenesis, physiological, and pathological functions. Weinheim: Wiley-Blackwell; 2011.

[12] Girolomoni G, Caux C, Lebecque S, Dezutter-Dambuyant C, Ricciardi-Castagnoli P. Langerhans cells: still a fundamental paradigm for studying the immunobiology of dendritic cells. Trends Immunol. 2002;23:6-8.

[13] Lacour JP, Dubois D, Pisani A, Ortonne JP. Anatomical mapping of Merkel cells in normal human adult epidermis. Br J Dermatol. 1991;125:535-42.

[14] Simpson CL, Patel DM, Green KJ. Deconstructing the skin: cytoarchitectural determinants of epidermal morphogenesis. Nat Rev Mol Cell Biol. 2011;12:565-80.

[15] Watt FM. Role of integrins in regulating epidermal adhesion, growth and differentiation. EMBO J. 2002;21:3919-26.

[16] Blanpain C, Fuchs E. Epidermal homeostasis: a balancing act of stem cells in the skin. Nat Rev Mol Cell Biol. 2009;10:207-17.

[17] Rochat A, Kobayashi K, Barrandon Y. Location of stem cells of human hair follicles by clonal analysis. Cell. 1994;76:1063-73.

[18] Watt FM, Hogan BLM. Out of Eden: Stem cells and their niches. Science. 2000;287:1427-30.

[19] Jones PH, Harper S, Watt FM. Stem cell patterning and fate in human epidermis. Cell. 1995;80:83-93.

[20] Kaiser HW, Ness W, Jungblut I, Briggaman RA, Kreysel HW, O'Keefe EJ. Adherens junctions: demonstration in human epidermis. J Invest Dermatol. 1993;100:180-5.

[21] Green KJ, Gaudry CA. Are desmosomes more than tethers for intermediate filaments? Nat Rev Mol Cell Bio. 2000;1:208-16.

[22] Fitzpatrick TB, Freedberg IM. Fitzpatrick's dermatology in general medicine. 6th ed. New York: McGraw-Hill, Medical Pub. Division; 2003.

[23] Tinkle CL, Pasolli HA, Stokes N, Fuchs E. New insights into cadherin function in epidermal sheet formation and maintenance of tissue integrity. P Natl Acad Sci USA. 2008;105:15405-10.

[24] Perez-Moreno M, Jamora C, Fuchs E. Sticky business: orchestrating cellular signals at adherens junctions. Cell. 2003;112:535-48.

[25] Niessen CM. Tight junctions/adherens junctions: basic structure and function. J Invest Dermatol. 2007;127:2525-32.

[26] Anderson JM, Van Itallie CM, Fanning AS. Setting up a selective barrier at the apical junction complex. Current Opinion in Cell Biology. 2004;16:140-5.

[27] Fuchs E. Keratins and the skin. Annu Rev Cell Dev Biol. 1995;11:123-53.

[28] Schweizer J, Bowden PE, Coulombe PA, Langbein L, Lane EB, Magin TM, et al. New consensus nomenclature for mammalian keratins. J Cell Biol. 2006;174:169-74.

[29] Kasza KE, Rowat AC, Liu JY, Angelini TE, Brangwynne CP, Koenderink GH, et al. The cell as a material. Current Opinion in Cell Biology. 2007;19:101-7.

[30] Sorrell JM, Caplan AI. Fibroblast heterogeneity: more than skin deep. Journal of Cell Science. 2004;117:667-75.

[31] Breitkreutz D, Koxholt I, Thiemann K, Nischt R. Skin basement membrane: the foundation of epidermal integrity--BM functions and diverse roles of bridging molecules nidogen and perlecan. Biomed Res Int. 2013;2013:179784.

[32] Marionnet C, Pierrard C, Vioux-Chagnoleau C, Sok J, Asselineau D, Bernerd F. Interactions between fibroblasts and keratinocytes in morphogenesis of dermal epidermal junction in a model of reconstructed skin. Journal of Investigative Dermatology. 2006;126:971-9.

[33] Marinkovich MP, Keene DR, Rimberg CS, Burgeson RE. Cellular origin of the dermal-epidermal basement membrane. Dev Dyn. 1993;197:255-67.

[34] Fleischmajer R, Schechter A, Bruns M, Perlish JS, Macdonald ED, Pan TC, et al. Skin Fibroblasts Are the Only Source of Nidogen during Early Basal Lamina Formation in-Vitro. Journal of Investigative Dermatology. 1995;105:597-601.

[35] Timpl R, Brown JC. Supramolecular assembly of basement membranes. Bioessays. 1996;18:123-32.

[36] Kruegel J, Miosge N. Basement membrane components are key players in specialized extracellular matrices. Cell Mol Life Sci. 2010;67:2879-95.

[37] Aumailley M, Bruckner-Tuderman L, Carter WG, Deutzmann R, Edgar D, Ekblom P, et al. A simplified laminin nomenclature. Matrix Biol. 2005;24:326-32.

[38] Boer A, Nischal KC. Www.derm101.com: A growing online resource for learning dermatology and dermatopathology. Indian J Dermatol Ve. 2007;73:138-40.

[39] Ohmori S, Kurata K. Experimental studies on the blood supply to various types of skin grafts in rabbits using isotope P32. Plast Reconstr Surg Transplant Bull. 1960;25:547-55.

[40] Clemmesen T, Ronhovde DA. Restoration of the blood-supply to human skin autografts. Scand J Plast Reconstr Surg. 1968;2:44-6.

[41] Zarem HA, Zweifach BW, Mcgehee JM. Development of Microcirculation in Full Thickness Autogenous Skin Grafts in Mice. American Journal of Physiology. 1967;212:1081-&.

[42] Capla JM, Ceradini D, Tepper OM, Callaghan MJ, Bhatt KA, Galiano RD, et al. Skin graft vascularization involves precisely regulated regression and replacement of endothelial cells through both angiogenesis and vasculogenesis. Plastic and Reconstructive Surgery. 2006;117:836-44.

[43] Yan A, Avraham T, Zampell JC, Aschen SZ, Mehrara BJ. Mechanisms of lymphatic regeneration after tissue transfer. PLoS One. 2011;6:e17201.

[44] Paavonen K, Puolakkainen P, Jussila L, Jahkola T, Alitalo K. Vascular endothelial growth factor receptor-3 in lymphangiogenesis in wound healing. Am J Pathol. 2000;156:1499-504.

[45] Nogami M, Hoshi T, Arai T, Toukairin Y, Takama M, Takahashi I. Morphology of lymphatic regeneration in rat incision wound healing in comparison with vascular regeneration. Leg Med (Tokyo). 2009;11:213-8.

[46] Warren AG, Slavin SA. Scar lymphedema: fact or fiction? Ann Plast Surg. 2007;59:41-5.

[47] Avraham T, Clavin NW, Daluvoy SV, Fernandez J, Soares MA, Cordeiro AP, et al. Fibrosis Is a Key Inhibitor of Lymphatic Regeneration. Plastic and Reconstructive Surgery. 2009;124:438-50.

[48] Young B, Woodford P, O'Dowd G, Wheater PR. Wheater's functional histology : a text and colour atlas. 6th edition. / ed.

[49] Carmeliet P, Tessier-Lavigne M. Common mechanisms of nerve and blood vessel wiring. Nature. 2005;436:193-200.

[50] Carmeliet P. Blood vessels and nerves: Common signals, pathways and diseases. Nature Reviews Genetics. 2003;4:710-20.

[51] Glebova NO, Ginty DD. Growth and survival signals controlling sympathetic nervous system development. Annu Rev Neurosci. 2005;28:191-222.

[52] Marko SB, Damon DH. VEGF promotes vascular sympathetic innervation. Am J Physiol-Heart C. 2008;294:H2646-H52.

[53] Biedermann T, Klar AS, Bottcher-Haberzeth S, Schiestl C, Reichmann E, Meuli M. Tissue-engineered dermo-epidermal skin analogs exhibit de novo formation of a near natural neurovascular link 10 weeks after transplantation. Pediatr Surg Int. 2014;30:165-72.

[54] Biedermann T, Bottcher-Haberzeth S, Klar AS, Pontiggia L, Schiestl C, Meuli-Simmen C, et al. Rebuild, restore, reinnervate: do human tissue engineered dermo-epidermal skin analogs attract host nerve fibers for innervation? Pediatric Surgery International. 2013;29:71-8.

[55] Makita T, Sucov HM, Gariepy CE, Yanagisawa M, Ginty DD. Endothelins are vascular-derived axonal guidance cues for developing sympathetic neurons. Nature. 2008;452:759-63.

[56] Honma Y, Araki T, Gianino S, Bruce A, Heuckeroth RO, Johnson EM, et al. Artemin is a vascular-derived neurotropic factor for developing sympathetic neurons. Neuron. 2002;35:267-82.

[57] Larrivee B, Freitas C, Suchting S, Brunet I, Eichmann A. Guidance of vascular development: lessons from the nervous system. Circ Res. 2009;104:428-41.

[58] Long JB, Jay SM, Segal SS, Madri JA. VEGF-A and Semaphorin3A: modulators of vascular sympathetic innervation. Dev Biol. 2009;334:119-32.

[59] Chauvet S, Burk K, Mann F. Navigation rules for vessels and neurons: cooperative signaling between VEGF and neural guidance cues. Cell Mol Life Sci. 2013;70:1685-703.

[60] Gentile P, Orlandi A, Scioli MG, Di Pasquali C, Bocchini I, Cervelli V. Concise Review: Adipose-Derived Stromal Vascular Fraction Cells and Platelet-Rich Plasma: Basic and Clinical Implications for Tissue Engineering Therapies in Regenerative Surgery. Stem Cell Transl Med. 2012;1:230-6.

[61] Locke M, Windsor J, Dunbar PR. Human adipose-derived stem cells: isolation, characterization and applications in surgery. ANZ J Surg. 2009;79:235-44.

[62] Guven S, Karagianni M, Schwalbe M, Schreiner S, Farhadi J, Bula S, et al. Validation of an automated procedure to isolate human adipose tissue-derived cells by using the Sepax(R) technology. Tissue Eng Part C Methods. 2012;18:575-82.

[63] Mitchell JB, McIntosh K, Zvonic S, Garrett S, Floyd ZE, Kloster A, et al. Immunophenotype of human adipose-derived cells: temporal changes in stromal-associated and stem cell-associated markers. Stem Cells. 2006;24:376-85.

[64] Harada Y, Yamamoto Y, Tsujimoto S, Matsugami H, Yoshida A, Hisatome I. Transplantation of freshly isolated adipose tissue-derived regenerative cells enhances angiogenesis in a murine model of hind limb ischemia. Biomed Res. 2013;34:23-9.

[65] World Health Organization. Violence and Injury Prevention Team. Facts about injuries : preventing global injuries. Geneva: World Health Organization; 2001.

[66] Peck MD, Kruger GE, van der Merwe AE, Godakumbura W, Ahuja RB. Burns and fires from non-electric domestic appliances in low and middle income countries Part I. The scope of the problem. Burns. 2008;34:303-11.

[67] Gurtner GC, Werner S, Barrandon Y, Longaker MT. Wound repair and regeneration. Nature. 2008;453:314-21.

[68] Bottcher-Haberzeth S, Biedermann T, Reichmann E. Tissue engineering of skin. Burns. 2010;36:450-60.

[69] Falanga V. Wound healing and its impairment in the diabetic foot. Lancet. 2005;366:1736-43.

[70] Tannous ZS, Mihm MC, Jr., Sober AJ, Duncan LM. Congenital melanocytic nevi: clinical and histopathologic features, risk of melanoma, and clinical management. J Am Acad Dermatol. 2005;52:197-203.

[71] Schiestl C, Stiefel D, Meuli M. Giant naevus, giant excision, eleg(i)ant closure? Reconstructive surgery with Integra Artificial Skin (R) to treat giant congenital melanocytic naevi in children. J Plast Reconstr Aes. 2010;63:610-5.

[72] Herndon DN, Barrow RE, Rutan RL, Rutan TC, Desai MH, Abston S. A Comparison of Conservative Versus Early Excision - Therapies in Severely Burned Patients. Annals of Surgery. 1989;209:547-53.

[73] Andreassi A, Bilenchi R, Biagioli M, D'Aniello C. Classification and pathophysiology of skin grafts. Clin Dermatol. 2005;23:332-7.

[74] Berman B, Viera MH, Amini S, Huo R, Jones IS. Prevention and management of hypertrophic scars and keloids after burns in children. Journal of Craniofacial Surgery. 2008;19:989-1006.

[75] Barbour JR, Schweppe M, O SJ. Lower-extremity burn reconstruction in the child. J Craniofac Surg. 2008;19:976-88.

[76] Loss M, Wedler V, Kunzi W, Meuli-Simmen C, Meyer VE. Artificial skin, split-thickness autograft and cultured autologous keratinocytes combined to treat a severe burn injury of 93% of TBSA. Burns. 2000;26:644-52.

[77] Meuli M, Raghunath M. Tops and flops using cultured epithelial autografts in children. Pediatric Surgery International. 1997;12:471-7.

[78] Gobet R, Raghunath M, Altermatt S, MeuliSimmen C, Benathan M, Dietl A, et al. Efficacy of cultured epithelial autografts in pediatric burns and reconstructive surgery. Surgery. 1997;121:654-61.

[79] Pontiggia L, Biedermann T, Meuli M, Widmer D, Bottcher-Haberzeth S, Schiestl C, et al. Markers to evaluate the quality and self-renewing potential of engineered human skin substitutes in vitro and after transplantation. J Invest Dermatol. 2009;129:480-90.

[80] Klar AS, Bottcher-Haberzeth S, Biedermann T, Schiestl C, Reichmann E, Meuli M. Analysis of blood and lymph vascularization patterns in tissue-engineered human dermo-epidermal skin analogs of different pigmentation. Pediatr Surg Int. 2013.

[81] Fistarol SK, Itin PH. Disorders of pigmentation. J Dtsch Dermatol Ges. 2010;8:187-201; quiz -2.

[82] Auger FA, Gibot L, Lacroix D. The pivotal role of vascularization in tissue engineering. Annu Rev Biomed Eng. 2013;15:177-200.

[83] Kaully T, Kaufman-Francis K, Lesman A, Levenberg S. Vascularization--the conduit to viable engineered tissues. Tissue Eng Part B Rev. 2009;15:159-69.

[84] Ko HC, Milthorpe BK, McFarland CD. Engineering thick tissues--the vascularisation problem. Eur Cell Mater. 2007;14:1-18.

[85] Supp DM, Supp AP, Bell SM, Boyce ST. Enhanced vascularization of cultured skin substitutes genetically modified to overexpress vascular endothelial growth factor. J Invest Dermatol. 2000;114:5-13.

[86] Montano I, Schiestl C, Schneider J, Pontiggia L, Luginbuhl J, Biedermann T, et al. Formation of human capillaries in vitro: the engineering of prevascularized matrices. Tissue Eng Part A. 2010;16:269-82.

[87] Marino D, Luginbuhl J, Scola S, Meuli M, Reichmann E. Bioengineering dermo-epidermal skin grafts with blood and lymphatic capillaries. Sci Transl Med. 2014;6:221ra14.

[88] Muller AM, Mehrkens A, Schafer DJ, Jaquiery C, Guven S, Lehmicke M, et al. Towards an intraoperative engineering of osteogenic and vasculogenic grafts from the stromal vascular fraction of human adipose tissue. Eur Cell Mater. 2010;19:127-35.

[89] Biedermann T, Pontiggia L, Bottcher-Haberzeth S, Tharakan S, Braziulis E, Schiestl C, et al. Human Eccrine Sweat Gland Cells Can Reconstitute a Stratified Epidermis. Journal of Investigative Dermatology. 2010;130:1996-2009.

7. ABBREVIATIONS

BSA	Bovine serum albumin
CD	Cluster of differentiation
CK	Cytokeratin
DAPI	4',6-diamidino-2-phenylindole
DESS	Dermo-epidermal skin substitutes
DMEM	Dulbecco's Modified Eagle Medium
FCS	Fetal calf serum
FdA	Fluorescein diacetate
FITC	Fluorescein iso-thiocyanate
H&E	Haematoxylin & Eosin
PBS	Phosphate buffered saline
PE	Phosphate buffered saline
TBSA	Total body surface area
TBRU	Tissue Biology Research Unit
TE	Tissue engineering
TRITC	Tetramethyl rhodamine iso-thiocyanate

8. CURRICULUM VITAE

Personal Data

Name	**Agnieszka Klar**
Date of birth	**09. Januar 1983**
Place of birth	**Poland**

Education

2009 – present **PhD study**

University Zürich, Switzerland
Tissue Biology Research Unit, Department of Surgery, University Children's Hospital Zurich, Switzerland

2007 – 2009 **Master of Biological Sciences**

University of Konstanz, Department of Biology, Germany
Elective major: Pharmacology and Immunology
Master thesis: *Development of novel immunotherapies against tumor-specific antigen NY-ESO-1.* Supervision Prof. Dr. C. Renner

2004 – 2007 **Bachelor of Biological Sciences**

University of Konstanz, Department of Biology, Germany
Elective major: Pharmacology and Immunology
Bachelor thesis: *Knockdown of mitochondrial proteins involved in apoptosis.* Supervision Prof. Dr. A. Wendel

2002 – 2004 **Education to Pharmacy Technician**

Medical College of Further Education, Poland

1998 – 2002 **Matura, foreign languages and biology focus**

High School, Poland

Presentations and Posters

November 2013 **XXVI International Symposium on Pediatric Surgical Research**

Capetown, South Africa

Oral presentation: *Analysis of blood and lymph vascularization patterns in tissue-engineered human dermo-epidermal skin analogs of different pigmentation*

August 2013 **General Assembly on Training Multidisciplinary scientists for Tissue Engineering and Regenerative Medicine (MultiTERM)**

Basel, Switzerland

Oral presentation: *Development of prevascularized dermo-epidermal skin grafts*

June 2013 **World Congress Tissue Engineering International & Regenerative Medicine Society (TERMIS)**

Istanbul, Turkey

Oral presentation: *Engineering pre-vascularised dermo-epidermal skin grafts for clinical application*

Jan.-February 2013 **Gordon Conference: Vascular Cell Biology**

Ventura, USA

Poster Presentation: *Engineering prevascularized dermo-epidermal skin grafts for clinical application*

September 2012 **XXV International Symposium on Pediatric Surgical Research**

London, United Kingdom

Oral presentation: *Accelerating in vitro culture of human dermo-epidermal skin substitutes reduces waiting time for patients.*

May 2011 **Mid-Term Review European Program on Training Multidisciplinary scientists for Tissue Engineering and Regenerative Medicine (MultiTERM)**

Uppsala, Sweden

Oral presentation: *Engineering of pre-vascularised autologous dermo-epidermal skin grafts*

Others

October 2012 **FZK Meeting**

Zürich, Switzerland
Participant

August 2011 **6th World Congress on Pediatric Burns**

Zürich, Switzerland
Participant

June 2010 **Skin *in vitro***

Frankfurt, Germany
Participant

9. PUBLICATIONS

Included in the thesis

Klar AS, Güven S, Biedermann T, Böttcher-Haberzeth S, Meuli-Simmen C, Meuli M, Martin I, Scherberich A, and Reichmann E. Tissue-engineered dermo-epidermal skin grafts prevascularized with adipose-derived cells. *Biomaterials, 2013, 35(19):5065-5078*

Klar AS[#], Pontiggia L[#], Böttcher-Haberzeth S, Biedermann T, Meuli M, and Reichmann, E. Optimizing *in vitro* culture conditions leads to a significantly shorter production time of human dermo-epidermal skin substitutes. *Pediatr Surg Int., 2013, 29(3):249-56*

Bottcher-Haberzeth S, **Klar AS,** Biedermann T, Schiestl C, Meuli-Simmen C, Reichmann E, and Meuli M. Trooping the color": restoring the original donor skin color by addition of melanocytes to bioengineered skin analogs. *Pediatr Surg Int., 2013, 29(3):239-47*

Klar AS[#], Böttcher-Haberzeth[#], Biedermann T, Schiest C, Reichmann E, and Martin Meuli. Analysis of blood and lymph vascularization patterns in tissue-engineered human dermo-epidermal skin analogs of different pigmentation. *Pediatr Surg Int., 2014, 30(2):223-31*

Klar AS[#], Biedermann T[#], Böttcher-Haberzeth S, Schiestl C, Reichmann E, abd Martin Meuli. Tissue-engineered dermo-epidermal skin analogs exhibit *de novo* formation of a near natural neurovascular link 10 weeks after transplantation. *Pediatr Surg Int., 2014, 30(2):165-72*

Other publications

Pontiggia L, Biedermann T, Böttcher-Haberzeth S, Oliveira C, Braziulis E, **Klar AS**, Meuli-Simmen C, Meuli M, and Reichmann, E. (2013). *De novo* epidermal regeneration using human eccrine sweat gland cells: higher competence of secretory over absorptive cells. *J Invest Dermatol., 2014, doi: 10.1038/jid.2014.30*

Böttcher-Haberzeth S[#], Biedermann T[#], **Klar AS**, Pontiggia L, Rac J, Nadal D, Schiestl C, Reichmann E, Meuli M. Tissue engineering of skin: human tonsil-derived mesenchymal cells can function as dermal fibroblasts. *Pediatr Surg Int., 2014, 30(2):213-22*

Kisiel M, **Klar AS**, Martino MM, Ventura M, and Hilborn J. Evaluation of injectable constructs for bone repair with a subperiosteal cranial model in the rat. *PLoS One, 2013, 8(8): e71683.*

Kisiel M, **Klar AS**, Ventura M, Buijs J, Mafina MK, Cool SM, Hilborn J. Complexation and sequestration of BMP-2 from ECM mimetic hyaluronan gel for improved bone formation. *PLoS One, 2013, 8(10): e78551.*

Zimmermann AK, Imig J, **Klar AS**, Renner CR, Korol D, Fink D, Stadlmann S, Singer G, Knuth A, Moch H, Caduff R. Expression of MAGE-C1/CT7 and selected cancer/testis antigens in ovarian borderline tumours and primary and recurrent ovarian carcinomas. *Virchows Archiv, 2013, 462(5):565-574*

In preparation

Klar AS, Güven S, Simen-Meuli C, Meuli M, Martin I, Scherberich A[#], Reichmann E[#]. A direct comparison of the vasculogenic potential of adipose- and peripheral blood- derived endothelial progenitor cells

Luginbühl J, Marino D, Hartmann F, **Klar AS**, Scola S, Meuli M, Reichmann E. Bioengineered blood and lymphatic capillaries instruct the scar-less remodelling of dermo-epidermal skin substitutes

Böttcher-Haberzeth S[#], Biedermann T[#], **Klar AS**, Widmer D, Schiestl C, Neuhaus K, Meuli M, and Reichmann E. Pigmented dermo-epidermal skin substitutes in a long term *in vivo* assay

Biedermann T[#], Böttcher-Haberzeth S[#], **Klar AS**., Pontiggia L, Weber A, Schiestl C, Reichmann E, and Meuli M. Influence of human palmar fibroblasts on pigmentation of dermo-epidermal skin substitutes *in vivo*

Sun W, Sun Y, **Klar AS**, Geutjes PJ, Veltien A, Lemmers-van de Weem B, Reichmann E, Heerschap A, Oosterwijk E. Pre-vascularized hybrid scaffolds for urogenital tissue engineering

10. CONTRIBUTIONS

I contributed to the following publications as indicated:

Tissue-engineered dermo-epidermal skin grafts prevascularized with adipose-derived cells

Experimental outline

Performance of experiments

Figures

Manuscript writing

Optimizing in vitro culture conditions leads to a significantly shorter production time of human dermo-epidermal skin substitutes

Transplantation of dermo-epidermal substitutes

Modulation of the pre-incubation time of fibroblasts in DESS: effect on graft take *in vivo* (Figure 2C)

Variation of the incubation time of keratinocytes on the dermal substitutes before transplantation: effect on graft take and stratification *in vivo* (Figure 4B)

Effect of air–liquid interface cultivation of DESS on graft take and stratification *in vivo* (Figure 5A, C, D, F)

Arrangement of figures 2, 4, 5

"Trooping the color": restoring the original donor skin color by addition of melanocytes to bioengineered skin analogs

Assistant, surgical procedure of skin substitute transplantation

Human keratinocyte, melanocyte, and fibroblast isolation and cultivation (Figure 1-6)

Melanocyte position in light and dark tissue engineered skin analogs 8 weeks after transplantation. Processing and staining of transplanted grafts (Figure 3)

Analysis of blood and lymph vascularization patterns in tissue-engineered human dermo-epidermal skin analogs of different pigmentation

Experimental outline

Performance of experiments

Figures

Manuscript writing

Tissue-engineered dermo-epidermal skin analogs exhibit de novo formation of a near natural neurovascular link 10 weeks after transplantation

Assistant, surgical procedure of skin substitute transplantation (Figure 1-4)

Evaluation of blood, lymphatic vessel, and nerve fiber distribution in normal rat back skin. Processing and staining of rat skin (Figure 1)

Evaluation of host blood and lymphatic vessel distribution as well as host innervation in human tissue engineered skin analogs 10 weeks after transplantation. Processing and staining of transplanted grafts (Figure 2)

Evaluation of host innervation relating to host vascularization. Processing and staining of transplanted grafts (Figure 3)

Evaluation of host innervation relating to host lymphatic vessels in human tissue-engineered skin analogs 10 weeks after transplantation. Processing and staining of transplanted grafts (Figure 4)

Arrangement of figures 1-4

11. ACKNOWLEDGEMENTS

I would like to gratefully and sincerely thank my supervisor, Prof. Dr. Ernst Reichmann for his understanding, encouragement, and advice he has provided throughout my PhD time in the TBRU. I would also like to thank for giving me the opportunity of doing my PhD studies in such an interesting field.

I would like to thank Prof. Dr. Beat Schäfer for supervising my PhD thesis and Prof. Dr. Lukas Sommer, and Prof. Dr. Ivan Martin for being a committee member of my PhD thesis.

Many thanks to PD. Dr. Arnaud Schrberich and Dr. Sinan Güven for their scientific support and grateful help during my secondment in Basel.

Great thanks to all present and former members of the TBRU for their scientific support, stimulating suggestions, and friendship throughout my PhD studies.

I would like to thank my family and all my friends.

This work was financially supported by the Clinical Research Priority Program (CRPP) of the Faculty of Medicine of the University of Zurich to E.R., by the EU-FP7 project EuroSkinGraft (FP7/2007-2013: grant agreement No. 279024 to E.R.), by the EU-FP7 (MultiTERM, grant agreement No. 238551 to E.R.), and by the Swiss National Science Foundation (Grant No. 310030-120432 and 310030-138519 to A.S.). We are particularly grateful to the Foundation Gaydoul and the sponsors of "DonaTissue" (Thérèse Meier, Robert Zingg) for their generous financial support and interest in our work.